Dissertation

PhD-Thesis

TOWARDS A BETTER UNDERSTANDING OF NON-HEMATOPOIETIC STEM AND PROGENITOR CELL BIOLOGY AND FUNCTION

submitted by

Andreas Reinisch, MD

for the Academic Degree of a

Doctor of Philosophy

(Ph.D.)

at the

Medical University of Graz

Stem Cell Research Unit (SCRU)

Department of Hematology, Univ. Clinic of Internal Medicine

under supervision of

PD Dr. Dirk Strunk

2010

TABLE OF CONTENTS

1 Acknowledgements 5
2 Zusammenfassung 6
3 Summary 8
4 Glossary 9
5 Abbreviations 11
6 Introduction 14
6.1 Introduction to regenerative medicine 14
6.2 The hematopoietic “SC niche” concept as a basis for mesenchymal and endothelial progenitor cell isolation and use. 19
6.3 Multipotent mesenchymal stromal / stem cells (MSCs) 21
6.4 Endothelial progenitor cells (EPCs) 25
6.5 Goals of the thesis 27
7 Materials and Methods 28
7.1 Collection of umbilical cord blood and peripheral blood 28
7.2 Preparation of pooled human platelet lysate (pHPL) 28
7.3 Preparation of cell culture medium 29
7.4 Culture of UCB-MSCs 30
7.4.1 MSC Isolation 30
7.4.2 MSC large-scale expansion 30
7.4.3 MSC long-term expansion 31
7.4.4 CFU-F assay 31
7.5 Culture of peripheral blood and cord blood-derived ECFCs 31
7.5.1 ECFC isolation 31
7.5.2 ECFC large-scale expansion 32
7.5.3 ECFC colony assay 32
7.6 Cell phenotype determination 33
7.6.1 Flow cytometry 33
7.6.2 Histology, immune cytochemistry and immune histochemistry 35
7.7 Cell function 36
7.7.1 MSC differentiation 36
7.7.2 Hematopoietic support 37
7.7.3 Network formation 37

7.7.4 Immune modulation 38
7.7.4.1 Modulation by UCB-MSCs 38
7.7.4.2 Modulation by UCB-ECFCs 38
7.8 Genomic stability of ECFCs 39
7.9 Telomere measurements 40
7.9.1 Telomere length 40
7.9.2 Telomerase activity 41
7.10 Multiplex growth factor analysis 41
7.11 Animal experiments 42
7.12 *In vivo* SC imaging 43
7.12.1 Progenitor cell labeling 44
7.12.2 SPIO uptake visualisation and quantification 44
7.12.3 Transmission Electron Microscopy 45
7.12.4 MRI phantoms 46
7.12.5 MR image aquisistion 46
7.13 Statistical analysis 47
8 Results 48
8.1 UCB-MSC propagation 48
8.2 Long-term expansion 50
8.3 UCB-MSC functionality 52
8.4 Recovery of ECFCs from peripheral blood and large-scale propagation in an animal protein-free humanized system 57
8.5 Preserved ECFC phenotype, proliferation, progenitor hierarchy and genomic stability after large-scale expansion and cryopreservation 64
8.6 ECFC function after humanized large-scale propagation *in vitro* and *in vivo* 73
8.7 Progenitor cell imaging 82
8.8 Vascular and osteogenic regeneration models 86
9 Discussion 90
9.1 pHPL can replace FBS during progenitor cell isolation and expansion 90
9.2 Umbilical cord blood as a source for non-hematopoietic progenitor cells 91
9.3 ECFC-based vascular regeneration 93
9.4 Development of novel organ regeneration models 96
9.5 MRI-based cell tracking 97
10 Literature 100
11 Declaration 117
12 Appendix I ..... 118+

13 Appendix II ..... 119+

14 Appendix III ..... 120+

15 Appendix IV ..... 121+

1 Acknowledgements

I would like to take the opportunity to thank all people that were directly or indirectly involved to accomplish this thesis.

First and foremost I want to thank my boss, group leader, supervisor, mentor and friend PD Dr. Dirk Strunk for guiding me through the last years. I'm very greatful for his intellectual support, the many, many hours of sitting together, discussing results and planning new experiments.

I would like to show my gratitude to Prof. Dr. Werner Linkesch and Prof. Dr. Gottfried Dohr for their help and critical comments as members of my Thesis Committee and for reviewing the thesis.

I want to say "Thank you" to all lab members who accompanied me through my scientific life and shared all their knowledge and experience with me. Beyond their help in scientific questions they provided the right environment and working climate for a young medical student. Our coffee chats, lab breakfasts, lunch breaks were always welcome and essential distractions to handle the busy working days during my thesis. Thank you: Eva Rohde, Katharina Schallmoser, Christina Bartmann, Daniela Thaler, Nici Hofmann, Margaretha Frühwirth, Monica Farrell, Claudia Url, Anna Ortner, Nathalie Liechtenstein, Birgit Feilhauer, Daniela Blattl.

Moreover I thank my friends who accepted my frequent excuses of being unavailable for spare time activities and nevertheless were always there for bringing diversion into my life.

Many thanks to my parents who supported me continuously and uncondionally.

Finally I want to acknowledge my girlfriend Stefanie Flattinger for her love and patience. Her presence was the energy that always recharged my batteries. Thank you Schatz for being there whenever I needed you.

2 Zusammenfassung

Regenerative Medizin ist ein neuartiges Therapiekonzept beruhend auf der Idee geschädigte Organe und Gewebe aktiv zu regenerieren. Im Falle einer Zelltransplantation können die verabreichten Zellen entweder direkt, vor Ort, die geschädigten Zellen ersetzen oder unterstützend für lokale Reperaturprozesse wirken. Die Umsetzung dieser einfach klingenden Idee, Stamm- und Vorläuferzellen für die Behandlung von diversen Erkrankungen herzunehmen, ist bisher hauptsächlich daran gescheitert, dass grundlegende Voraussetzungen für einen klinischen Einsatz nicht erfüllt werden konnten.

Zu diesen Voraussetzungen zählen neben einer effizienten Herstellung von Stammzelltransplantaten in passender Qualität und Quantität auch das Vorhandensein geeigneter präklinischer Modelle, um die Funktionalität der hergestellten Transplantate testen zu können. Zusätzlich bedarf es bildgebender Methoden, die es erlauben die verabreichten Zellen im Körper des Menschen nachzuverfolgen. Solche Methoden könnten wesentlich zur Effizienzsteigerung bestehenden Transplantationsprotkolle beitragen.

Diese Arbeit beschäftigte sich hauptsächlich mit der Herstellung von zellulären Tranplantaten in entsprechender Quantiät und Funktionalität. Die geringe Anzahl von nicht blutbildenten Stamm- und Vorläuferzellpopulationen im menschlichen Organismus machen eine Vermehrung dieser Zellen für klinische Einsätze notwendig.

Wir konnten Protokolle zur Isolation und Vermehrung von endothelialen Kolonie-bildenten Vorläuferzellen und multipotenten mesenchymalen Stromazellen entwickeln. Zusätzliche konnte die Verwendung von Nabelschnurrestblut als Alternativquelle für die Herstellung von klinisch einsetzbaren Stammzelltransplantaten etabliert werden.

Xenogenes fetales Kälberserum wurde als Quelle für Wachstumsfaktoren durch hochwirksames humanens Plättchenlysat in der Zellkultur ersetzt. Somit wird das Risiko für eine mögliche Immunisierung durch artfremde Proteine und die Übertragung von tierischen Krankheitserregern reduzieren. Durch geeigneter Testverfahren konnte ein Erhalt der Zellfunktion unter tierproteinfreien Zellkulturbedingungen bestätigt werden. Im Tiermodell waren diese Zellen nach

subkutaner Gabe fähig durchblutete menschliche Gefäße und reifen menschlichen Knochen zu bilden.

Weiters wurden superparamagnetische Eisenoxidparitkel für die Markierung von Stamm- und Progenitorzellen getestet, um deren Verteilung im Körper mittels optimierter Magnetresonanztomographie-basierender, bildgebender Verfahren zu analysieren und somit eine ideale Grundlage zur Verbesserung bestehender regenerativmedizinischer Transplantationsprotokolle zu schaffen.

Die Ergebnisse dieser Arbeit sollen dazu beitragen neue Verfahren der Stamm- und Progenitorzelltransplantation zur Organregeneration zu entwickeln.

3 Summary

The basic concept of regenerative medicine is a curative treatement of diseases through transplantation of cells that bear the potential to regenerate damaged tissue by direct cell replacement or by supportive functions. Nevertheless this straightforward idea of simply transplanting stem and progenitor cells to cure patients partly struggles because basic prerequistes needed to reach this ambiguous goal have so far not been able to be fulfilled. These prerequists include the efficient production of stem cell transplants in sufficient quality and quantity, availability of preclinical models to test transplant functionality and appropriate methodologies to evaluate cell fate early after application that subsequently can help to modulate and improve transplantation protocols.

This study mostly deals with production of cellular transplants in appropriate quantity and functionality. The scarcity of stem and progenitor cell populations that are primarily used for the purpose of regenerative medicine is the reason that these cells have to be expanded *in vitro* before use**.** We developed GMP-compliant protocols for isolation and propagation of non-hematopoietic progenitor cells including endothelial colony-forming progenitor cells and multipotent mesenchymal stromal cells. Human umbilical cord blood has been employed as an alternative source to produce virtually pure cell transplants for putative clinical applications. Xenogenic fetal bovine serum was replaced by highly efficient human pooled platelet lysate as a new source for growth factors and reduces risk of animal pathogen transmission, xeno-immunisation therefore facilitating clinical applicability. Progenitor cells, cultured under fully humanized conditions, were highly functional *in vitro* and were capable of forming human tissue including perfused vessels and mature bone when transplanted into immune deficient mice *in vivo*.

To track these cells *in vivo,* superparamagnetic iron oxid nanoparticles were used for cellular labeling and magnetic resonance imaging strategies were optimized to allow for high resolution single cell imaging.

Results obtained should help to develop new procedures of stem and progenitor cell transplantation for organ regeneration

4 Glossary

Stem cell: A cell that has self-renewal capacity and can give rise to one or more mature cell lineages under appropriate conditions.

Progenitor Cell: A cell capable of proliferation that differentiates into progeny of one specific lineage.

Multipotency: Differentiation capacity into more than 3 lineages that belong to the same germ layer.

Pluripotency: Differentiation capacity into lineages of more than one germ layer.

Multipotent mesenchymal stromal / stem cells (MSCs): Non-hematopoietic proliferating cells of mesodermal origin, that are capable of differentiating into more than 3 mesodermal lineages (including, e.g., osteoblasts, chondrocytes, adipocytes, pericytes, smooth muscle cells/myocytes) *in vitro* as well as *in vivo.*

Hematopoiesis: The commitment and differentiation process that leads from a hematopoieitic stem cell to the formation of mature cells of all 7 major blood cell lineages (erythrocytes, platelets, myeloid cells [granulocytes, monocytes], lymphoid cells [B and T cells, NK cells])

Hematopoietic stem cell niche: Distinct microenvironment within the BM, providing the ideal place for HSC self renewel and maintainance.

Hematopoietic stem cells (HSCs): Immature, self-renewing cells, located in distinct SC niches within BM, capable of long term (throughout the whole life) blood and immune system reconstitution upon transplantation into primary and even secondary recipients. *One donor can share SCs with several recipients.*
In mice defined as: blood cell lineage-marker (**l**in) negative, **s**ca-1 positive, c-**k**it positive cells (LSK)

In humans CD34 and/or CD133 alone or in combination are used to identify HSCs. These markers can not differentiate between true HSCs and HPCs. Therefore, the term **HSPCs (hematopoietic stem and progenitor cells)** has been introduced to describe mixed HSC and HPC populations.

Hematopoietic progenitor cells (HPCs): Highly proliferating cells without self-renewing capacity that are able to provide short-term but no long-term reconstitution upon transplantation. HPCs can be devided into a myeloid and lymphoid subtype. In humans, HPCs are phenotypically indistinguishable from HSCs so far.

Endothelial progenitor cells (EPCs): Cells with proliferative potential that are thought to be responsible for vessel integrity and can contribute to neovasculogenesis and tumor vessel formation. The term EPC is frequently misused for non-proliferating cells of hematopoietic origin (CFU-Hill, CACs).

Colony-forming unit Hill (CFU-Hill): Cellular clusters of monocytes and T-cells that are formed *in vitro* after 2-4 days under defined culture conditions. Formerly these cell clusters were called CFU-EC.Their frequency of 5-28 colonies per mL of peripheral blood is inversely correlated to the Framingham score predicting cardiovascular disease risk (Hill et al., 2003).

Circulating angiogenic cells (CACs): Myeloid cells (mostly monocytes) that can be isolated from peripheral blood under defined angiogenic culture conditions. CAC number is evaluated on day 4 by microscopy (cells per high power field) and is also associated with cardiovascular disease risk. These cells do not display colony formation, do not proliferate and can not form vessels *in vivo.*

Endothelial colony-forming progenitor cells (ECFCs): Circulating and/or vessel wall-derived, non-hematopoietic, proliferating, colony-forming cells. ECFCs are prototype endothelial progenitor cells of mesodermal origin that are capable of generating functional endothelial lineage progeny. ECFCs can form stable vessels upon transplantation *in vivo*.

5 Abbreviations

7-AAD	7-Aminoactinomycin D
bFGF	basic Fibroblast Growth Factor
BLI	Bioluminiscence Imaging
BM	Bone Marrow
BOECs	Blood Outgrowth Endothelial Cells
CACs	Circulating Angiogenic Cells
CAR cells	CXCL12-Abundant Reticular cells
CF-4	fou- layered Cell Factory
CFSE	Carboxyfluorescein Succinimidyl Ester
CFU-EC	Colony-Forming Unit - Endothelial Cell
CFU-F	Colony-Forming Unit - Fibroblast
CGH	Comparative Genomic Hybridization
CPDs	Cummulative Population Doublings
CT	Computed Tomography
CVD	Cardiovascular Disease
DAB	Diaminobenzidine
DAPI	4',6-Diamidino-2-Phenylindole
DMEM	Dulbecco's Modified Eagle Medium
DMSO	Dimethylsulfoxide
DNA	Desoxyribonucleic Acid
ECFCs	Endothelial Colony Forming Progenitor Cells
ECs	Endothelial Cells
EDTA	Ethylenediaminetetraacetic Acid
EGF	Epidermal Growth Factor
EGM	Endothelial Growth Medium
EPCs	Endothelial Progenitor Cells
FACS	Fluorescence-Activated Cell Sorting / Scanning
FBS	Fetal Bovine Serum
FSC	Forward Scatter
FFPE	Formalin-Fixed Paraffin-Embedded
fpVCT	flat panel Volume Computed-Tomography

GM-CSF	Granulocyte/Macrophage Colony-Stimulating Factor
GvHD	Graft versus Host Disease
H&E	Hematoxylin and Eosin
HA/TCP	Hydroxyapatite/Tri-calcium Phosphate
HMVECs	Human Microvascular Endothelial Cells
HPCs	Hematopoietic Progenitor Cells
HPP	High Proliferative Potential
HSCs	Hematopoieitc Stem Cells
HSCTx	Hematopoietic Stem Cell Transplantation
HSPCs	Hematopoietic Stem and Progenitor Cells
HUVECs	Human Umbilical Vein Endothelial Cells
IBMX	3-Isobutyl-1-Methylxanthine
IGF	Insulin-like Growth Factor
IND	Investigational New Drug
ISCT	International Society for Cellular Therapy
LCA	Leukocyte Common Antigen (CD45)
LMP	Low Melting Point
LPP	Low Proliferative Potential
MAPCs	Mulitpotent Adult Progenitor Cells
MCAM	Melanoma Cell Adhesion Molecule
MEM	Minimum Essential Medium
MI	Myocardial Infarction
MIAMI cells	Marrow-Isolated Adult Mulitlineage-Inducible cells
MNCs	Mononuclear Cells
MRI	Magnetic Resonance Imaging
MS	Multiple Sclerosis
MSCA-1	Mesenchymal Stem Cell Antigen-1
MSCs	Multipotent Mesenchymal Stromal / Stem Cells
NC	Nucleated Cells
PB	Peripheral Blood
PBS	Phosphate Buffered Saline
PCR	Polymerase Chain Reaction
PDs	Population Doublings

PDGF	Platelet-Derived Growth Factor
PECAM	Platelet Endothelial Cell Adhesion Molecule
PET	Positron Emission Tomography
PHA	Phytohemagglutinin
pHPL	pooled Human Platelet Lysate
PI	Propidium Iodine
PNA	Peptide Nucleic Acid
PRP	Platelet Rich Plasma
RPMI	Rosswell Park Memorial Institute
RT	Room Temperature
SC	Stem Cell
SDF-1	Stromal Derived Factor-1
SPECT	Single Photon Emission Computed Tomography
SPIOs	Superparamagnetic Iron Oxid Particles
SSC	Side Scatter
TGF	Transfoming Growth Factor
TRAP	Telomeric Repeat Amplification Protocol
T1DM	Type 1 Diabetes Mellitus
UCB	Umbilical Cord Blood
UC	Umblical Cord
VCAM	Vascular Cell Adhesion Molecule
VEGFR-2	Vascular Endothelial Growth Factor Receptor-2
VSELs	Very Small Embryonic-like Cells
vWF	von Willebrand Factor

6 Introduction

6.1 Introduction to regenerative medicine

Regenerative stem cell therapy is a novel concept in modern medicine based on the assumption that different types of stem and progenitor cells can regenerate damaged organs, improve their functions or even cure diseases. More than 50 years ago the first attempts in regenerative **s**tem **c**ell (SC) therapy were made by transplanting **b**one **m**arrow (BM), a source rich in **h**ematopoietic **s**tem and **p**rogenitor **c**ells (HSPCs), to regenerate the blood and immune system (Thomas et al., 1957). Since then, extensive basic research and increasing clinical experience has led to the current comprehensive knowledge about HSPCs. The relatively high content of HSPCs within the BM (0.1-1.0% of **n**ucleated **c**ells [NC]) and sufficient harvesting made it possible to transplant HSPCs without *in vitro* expansion. The rather invasive BM harvesting procedure, formerly used as a preferred method of collecting these cells for transplantation, was subsequently almost replaced by blood cell aphaeresis based on the fact that chemotherapy or cytokine treatment can induce HSPC mobilization into the **p**eripheral **b**lood (PB). Due to the regular clinical use of HSPCs and the limited knowledge about their non-hematopoieitic counterparts the terms SC transplantation and **h**ematopoietic **SC t**ransplantation (HSCTx) have been used for years almost as an equivalent.

More recent studies have provided evidence for the existence of non-hematopoietic immature progenitor cell populations within the BM capable of maintaining the stromal and vascular HSPC-mircoenvironment and regenerating tissue (Friedenstein et al., 1966, Rafii et al., 1994, Asahara et al., 1999).

Generally adult stem and progenitor cells can be subdivided into (1) hematopoietic and a (2) non-hematopoietic fractions. The latter includes **m**ultipotent **m**esenchymal **s**tromal/stem **c**ells (MSCs) and **e**ndothelial **c**olony-**f**orming progenitor **c**ell (ECFCs). The tissue regenerative potential and additional properties as immune modulation and vessel regeneration attributed to MSCs and ECFCs made them attractive candidates for cellular therapy based regenerative medicine purposes.

After initial successful applications (Horwitz et al., 1999, Koc et al., 2000, Le Blanc et al., 2004) many cinical trials have been initiated to study the therapeutic effects of non-hematopoietic cell transplantation. Although it was thought to be beneficial for treating a variety of different disease entities, the overall outcome for patients receiving this therapy seems to be limited. Success rates in clinical trials are low and promising early results turned out to be irreproducible in larger cohorts (Le Blanc et al., 2008, Matoba et al., 2008).
Possible explanations for the low efficiency may include the use of inappropriate cell types, insufficient quality and quantity of applied cells, limited delivery of the cells to the target organ, sub-optimal timing of the transplantation after the disease onset, wrong application mode and others.

Because of the scarcity of both cell types within BM and PB (1 in 1,000-10,000 NCs within BM, < 1 in 1 x 10^6 NCs within PB) (Reinisch et al., 2009), *in vitro* cell expansion is a prerequisite for their therapeutic applicability. The production of transplants containing the required quantity of cells with conserved functions constitutes the primary hurdle which mainly hinders more frequent use of MSCs and ECFCs. Currently, most investigators refer their applied cell quantity for non-hematopoietic regeneration to numbers established in the field of HSCTx. In hematology the application of transplants containing 1-2 x 10^6 $CD34^+$ HSPCs per kilogram body weight of the recipient regularly results in sufficient engraftment (Bender et al., 1992, Haas et al., 1994, Shpall et al., 1998, Serke and Johnsen, 2001). Direct application of MSCs and ECFCs without *ex vivo* propagation is limited by the low frequency of 1 in 1,000-10,000 cells within BM. Other primary sources like PB or UCB contain even lower amounts of less than 1 in 1 x 10^6 cells (Lin et al., 2000, Kogler et al., 2004, Reinisch et al., 2007, Reinisch et al., 2009).
Elaborate *ex vivo* expansion is necessary to reach the required large cell numbers that are currently estimated to be required (i.e., 200 million cells for a 100 kg recipient, if 2 million cells per kg body weight are considered to be ideal). Proper dose finding studies to determine optimal cell quantity for non-hematopoietic regenerative therapies are mandatory in future.

Reasons why current expansion protocols for MSC or ECFC propagation are not yet optimally suited for comprehensive testing or application of these products as an **i**nvestigational **n**ew **d**rug (IND) are mainly due to two limiting factors:

First, current expansion protocols depend on the presence of animal proteins, like selected lots of **f**etal **b**ovine **s**erum (FBS) within the culture medium and/or animal-derived matrix proteins for coating of tissue culture surfaces. Because their use carries the risk of pathogen transmission together with the possibility of xeno immunization (Selvaggi et al., 1997, Mackensen et al., 2000, Tuschong et al., 2002, Sakamoto et al., 2007, Sundin et al., 2007), reduction or replacement of xenogenic protein content would be benefical. Based on the assumption that FBS is essential for successful cell propagation, attempts to reduce FBS protein content were made mainly by incubation of cell cultures with serum free medium or medium supplemented with human serum prior to application (Kuznetsov et al., 1997a, Kuznetsov et al., 2000, Spees et al., 2004). Doucet et al. recently demonstrated that growth factors derived from human platelets can replace FBS in cultures of MSCs under laboratory scale conditions (Doucet et al., 2005). We and others adapted this approach and established different protocols for MSC propagation without FBS (Lange et al., 2007, Mannello and Tonti, 2007, Reinisch et al., 2007, Schallmoser et al., 2007b) by using **p**ooled **h**uman **p**latelet **l**ysate (pHPL) as an alternative.

Second, most protocols start with elaborate enrichment methods including density gradient separation or cell-sorting. Omitting these procedures that further diminish the amount of starting material needed would result in higher final cell yield within shorter time periods.

A major drawback of regenerative medicine and cellular therapy approaches is the lack of cell tracking and subsequent little knowledge regarding the behavior of the transplanted cells *in vivo*. The possibility to visualize the applied cells and to track their location and migration would provide a tool to evaluate efficacy and efficiency of cell-based therapies. So far, it has been impossible to predict the homing capacity and hence the efficiency of different cellular therapies early after injection. Non invasive continuous monitoring of the transplanted cells using appropriate imaging modalities would offer a tremendous advantage to evaluate treatment effect by providing information about the number of cells that home to the target organ.

Documenting the lesion targeting efficiency of different cell populations under various transplantation settings could optimize SCTx protocols regarding cell dose, best application mode and ideal timing. *In vivo* cell imaging could help to distinguish active processes of SC engraftment from unspecific cell trapping events and finally will elucidate the exact time course and the mechanism of SC homing. Suitable cell tracking modalities could eventually improve treatment strategies in regenerative medicine or may even help to find the reasons for poor success rates.

Appropriate *in vivo* imaging techniques include (1) non-radioactive **m**agnetic **r**esonance **i**maging (MRI), (2) X-ray-based **c**omputed **t**omography (CT), (3) radioisotope using **s**ingle **p**hoton **e**mission **c**omputed **t**omography (SPECT) and **p**ositron **e**mission **t**omography (PET) and (4) optical imaging approaches using fluorescence and bioluminescence **(Table 1).**

All methods have in common the fact that they strictly depend on a suitable cell labeling to enable tracking within the body. By tagging appropriate contrast agents to cells they become visible using the corresponding imaging technique (e.g. ^{111}In is clinically used for leucocyte szintigraphy). The requirements for the labels as well as for the imaging modality are considerable in a human setting and thus experience with *in vivo* stem cell imaging is minimal. A major criterion for the label, particularly if used with stem and progenitors cells, is lack of genetic modification or perturbation of the target cells that possibly hampers the regenerative functions. Therefore reporter gene assays combined with optical imaging or nuclear medicine may not be applied for clinical assessment of cellular therapies. Radioisotope labeling is limited through its poor spatial resolution and the risk of genetic alterations to the cells. Tracking cells labeled with exogenous applied fluorescent tags is further restricted by the short penetration depth of fluorescent light. Additionally the optimal stem cell label should loose minimal amounts of label through proliferation or transfer to non-targeted cells to allow for long term imaging and detection of small cell numbers, ideally single cells.

Although each imaging modality has advantages as well as disadvantages, MRI is considered to be best suited for human applications because of its unlimited penetration depth and high soft tissue contrast **(Table 1)**.

Labeling cells with **s**uper **p**aramagnetic **i**ron **o**xide nanoparticles (SPIOs, **Table 5**) allows for the detection of the cells using MRI and can provide a first step towards determining the clinical outcome of cellular transplants.

Table 1: Comparison of different imaging modalities.

Technique	MRI	CT	PET	SPECT	Fluor. imaging	BLI
Resolution	10-100µm	25-50µm	1-5mm	1-5mm	2-3mm	2-3mm
Depth	No limit	No limit	No limit	No limit	<1cm	1cm
Imaging Agents	Gd^{3+}, Mn^{2+}, Fe^{2+}, Fe^{3+}	Iodine	^{18}F, ^{11}C, ^{15}O, ^{4}Cu	^{99m}Tc, ^{111}In, ^{123}I	GFP, NIR dyes	Luciferins
Current relevance for SCT	Yes	Yes	No*	No*	No**	No**
Limitations	Long acquisition time	Lack of cell labeling, radiation	Radiation*	Radiation*	Depth**	Depth**
Detection threshold (cell number)	Single cells	Not addressed	Metabolism dependent	>10,000	Single cells	~1,000

(modified from Arbab & Frank, Regen.Med. (2008))

Abbrev.: MRI: Magnetic Resonance Imaging; CT: Computed Tomography; PET: Positron Emission Tomography; SPECT: Single Photon Emission Computed Tomography; BLI: Bioluminescence Imaging; SCT: Stem Cell Therapy; Gd^{3+}: Gadolininum; Mn^{2+}: Manganase, Fe^{2+}: Iron; F: Fluorine, C: Carbon, O: Oxygen; Cu: Copper; Tc: Technetium; In: Indium; I: Iodine; GFP: Green fluorescent protein; NIR: Near Infrared

* mainly because of the risk of DNA damage due to radioactive tracers

** mainly because of limited penetration depth that hampers clinical applicablility in humans

6.2 The hematopoietic "SC niche" concept as a basis for mesenchymal and endothelial progenitor cell isolation and use.

Research on adult stem cells began more than half a century ago, when scientists discovered that the BM contains transplantable HSPCs (Till and Mc, 1961). These cells built the basis for the continuous, life-long replenishment of the complete blood cell differentiation hierarchy. HSCs have self-renewing capacity and by dividing asymmetrically, HSCs proliferate without losing their immature, undifferentiated state. HSCs were the first tissue-specific stem cells to be isolated prospectively (Spangrude et al., 1988) and are the best studied subset within the adult stem cell pool. Human HSPCs are characterized by the expression of several markers including CD34 (Civin et al., 1984, Majdic et al., 1994), AC133 (Prominin) (Yin et al., 1997), CD90 (Thy-1) (Murray et al., 1995) and VEGFR-2 (**v**ascular **e**ndothelial **g**rowth **f**actor **r**eceptor-**2**, KDR, [kinase insert domain containing receptor]) (Ziegler et al., 1999). Unfortunately all of these surface epitopes are not HSPC specific and thus combinations of several markers are necessary for detailed HSPC characterization. Recently the Weissman lab described a novell hierarchy of HSPCs in **u**mbilical **c**ord **b**lood (UCB) based on the expression of CD34, CD90 and CD45RA (Majeti et al., 2007). Since 1957 (Thomas et al., 1957) HSCs have been used in transplantations to treat a variety of hematologic and non-hematologic malignancies.

In addition to HSPCs, BM contains a heterogeneous population of non-hematopoietic cells **(Figure 1)**. In 1978 Schofield hypothesized the presence of cells in the vicinity of the HSC in the BM that have the ability to directly or indirectly regulate HSC behavior and number. These cells provide the structural components of physically discrete microenvironments within the BM and built the basis for the BM SC niche concept (Schofield, 1978).

A hematopoiesis supportive microenvironment has been identified at the (1) endosteal SC niche, the cellular interface between the marrow cavity and its surrounding bony structures as well as (2) in close proximity to the BM sinusoids and adjacent mesenchymal cells, a region called vascular SC niche. Both the "endosteal SC niche" and "vascular SC niche" contain immature progenitor cells. MSCs

constitute the progenitors for osteoblasts, chondroblasts and fat cells. The main function attributed to MSCs is to provide stromal support for the maintenance and differentiation of blood-forming stem cells. The exact functions of ECFCs representing an immature cell population within BM-sinusoids are currently not known.

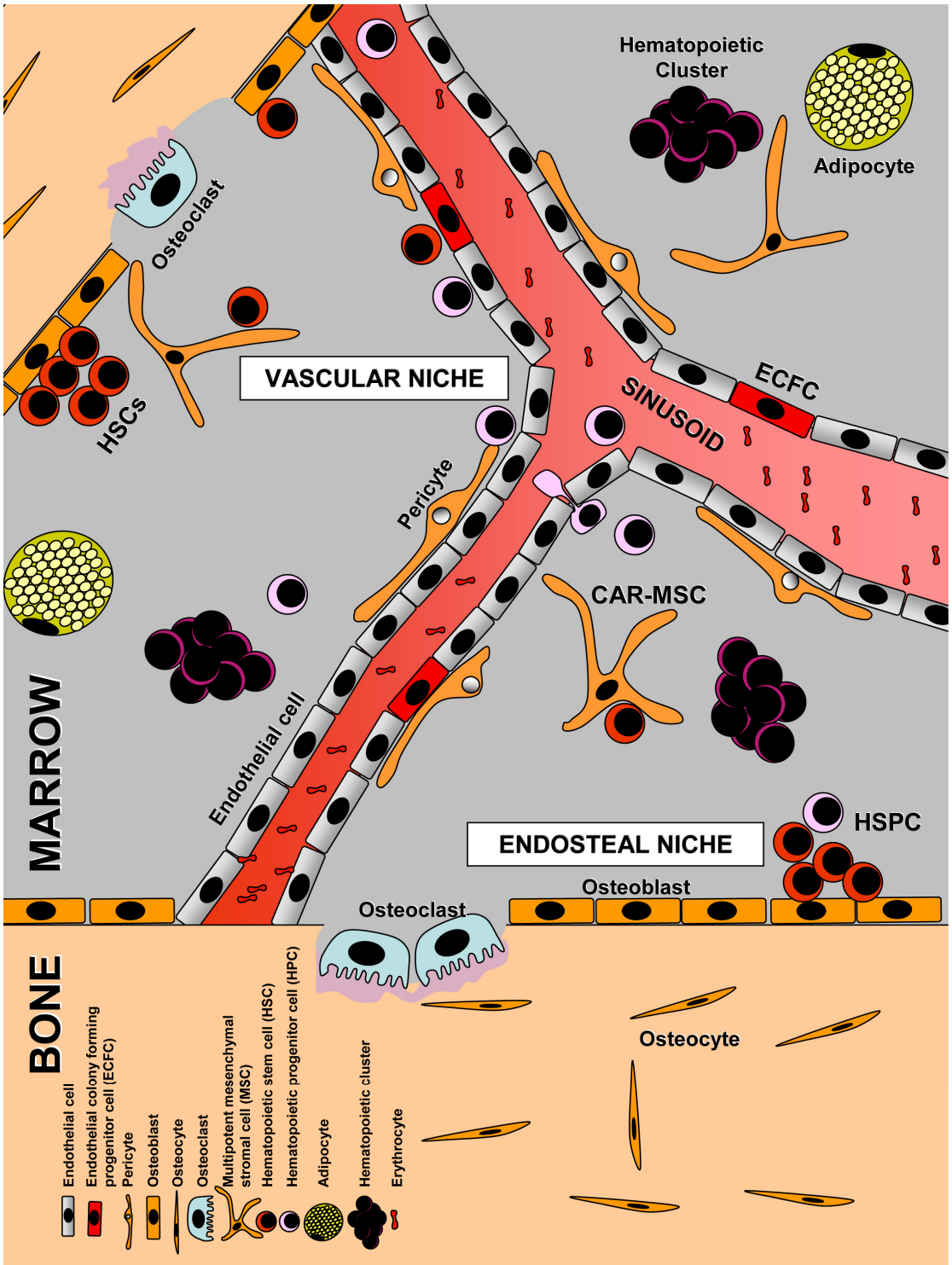

Figure 1. Cartoon of BM SC niches

Cartoon depicting the endosteal bone marrow stem cell niche with osteoblasts (orange rectangular cells) and adjacent hematopoietic stem cells (HSCs, red, round cells) and hematopoietic progenitor cells (HSPCs, pink, round cells). Endothelial cell-lined (grey, rectangular cells), blood containing sinusoids surrounded by pericytes (orange, adjacent to vessels) and CXCL12-abundant reticular multipotent mesenchymal stromal cells (CAR-MSCs, orange) represent the vascular bone marrow stem cell niche. A minor fraction of the endothelial cells, termed endothelial colony forming progenitor cells has an immature phenotype (ECFCs, red). Osteoclasts (light blue cells) resorb bone material.

6.3 Multipotent mesenchymal stromal / stem cells (MSCs)

Bone-forming osteoblasts, chondroblasts and probably also fat cells within the BM, are important players in the hematopoietic SC niche physiology. Early experiments suggested that HSC are enriched close to the bone surface, a site called endosteum (Gong, 1978). More sophisticated approaches with genetically modified mice provided evidence of the important role of osteoblast subsets on the regulation the of HSC pool (Calvi et al., 2003, Zhang et al., 2003, Stier et al., 2005).

Osteoblasts are derived from a common mesenchymal progenitor. The theory of the existence of such a mesenchymal stem or progenitor cell within the BM can be traced back to early experiments showing that transplantation of BM to ectopic locations can result in regeneration of bone including marrow (Tavassoli and Crosby, 1968). The successful isolation of the immature progenitor cells responsible for that phenomenon was first conducted by Friedenstein and coworkers as early as in the late 1960s and early 1970s. This group provided evidence for the existence of an immature fibroblastoid, non-hematopoietic cell type within the BM capable of (1) forming colonies when flushed out of the marrow (**c**olony **f**orming **u**nit-**f**ibroblast, CFU-F) and (2) forming bone and transferring hematopoietic microenvironment *in vivo* when transplanted subcutaneously into mice (Friedenstein et al., 1966, Friedenstein et al., 1968, Friedenstein et al., 1974). Friedenstein called these cells osteogenic or BM stromal stem cells. Later on others renamed this population mesenchymal stem cells or MSCs (Caplan, 1991).

MSCs are isolated through their ability to adhere to plastic surfaces and in addition to their bone forming capacity these cells can be differentiated *in vitro* into other

mesodermal lineages including cartilage and fat (Prockop, 1997, Pittenger et al., 1999). Based on the differentiation along these three lineages (bone, cartilage, fat) scientists tend to call MSCs multipotent, although multipotent cells should give rise to more than 3 cell types representing differentiation within one germ layer. Following these strict definitions, only MSCs isolated in the Prockop lab can be defined as multipotent by differentiating towards at least 4 mesodermal lineages including myogenic differentiation in addition to osteo-, chondro- and adipogenic differentiation (Prockop, 1997) **(Table2)**.

Table 2. Differentiation capacity of various BM-derived MSC types.

GERM LAYER	MESODERM							ECTO	ENDO
LINEAGE	Osteo	Chondro	Adipo	Myo	Fibro	Endothelial	Hemato	Neuro	Endodermal
Prockop et al. : **MSCs**	+	+	+	+	n.a.	n.a.	n.a.	n.a.	n.a.
Pittenger et al.: **MSCs**	+	+	+	n.a.	n.a.	n.a.	n.a.	n.a.	n.a.
Reyes et al.: **MAPCs**	+	+	+	+	+	+	n.a.	+	+ (hep)
Kucia et al.: **VSELs**	n.a.	n.a.	n.a.	+ (cardio)	n.a.	n.a.	n.a.	+	+ (panc)
D`Ippolito et al.: **MIAMI**	+	+	+	n.a.	n.a.	n.a.	n.a.	+	+ (panc)

Abbreviations: ECTO: Ectoderm; ENDO: Endoderm; Osteo: osteogenic; Chondro: chondrogenic; Adipo: adipogenic, Myo: myogenic; Fibro: fibroblastoid; Hemato: hemtopoietic; Neuro: neurogenic; cardio: cardiomyogenic; hep: hepatogenic; panc: pancreatic; n.a.: not analyzed; +: positively tested

Over the years investigators have isolated diverse populations derived from the BM-MSC pool, by using different methods. “**M**ultipotent **a**dult **p**rogenitor **c**ells” (MAPCs), “**m**arrow-**i**solated **a**dult **m**utilineage **i**nducible cells” (MIAMI) and “**v**ery **s**mall **e**mbryonic-**l**ike stem cells” (VSELs) represent immature types of MSCs and were thought to have even increased differentiation potential and the ability to cross lineage boundaries to give rise to cells of different germ layers (Reyes et al., 2001, Jiang et al., 2002, D'ippolito et al., 2004, Kucia et al., 2006) **(Table2)**. The *in vivo* relevance of all these different populations is still an open question.

To set common standards characterizing MSCs, the **I**nternational **S**ociety for **C**ellular **T**herapy (ISCT) has defined minimum criteria in addition to plastic adherence including the ability to differentiate along osteogenic, adipogenic and chondrogenic lineage as well as a certain immune phenotype. At least 95% of the cells within a MSC population should be positive for CD105, CD73, CD90 and less than 2% of cells should lack the expression of CD45, CD34, CD14 or CD11b, CD79α or CD19 and HLA-DR. (Dominici et al., 2006)

Our knowledge about MSCs is mainly based on the characterization of cultured cells. However, little is known about their anatomic localization and phenotypic characteristics *in vivo* due to the absence of specific and unique markers that would allow for in situ identification of MSCs. Crisan et al. have demonstrated that MSCs are mainly located in close proximity to vessels and resemble pericyte phenotype *in vivo* (Crisan et al., 2008). These data provoked speculations about the possibility that all MSCs are pericytes (Caplan, 2008).

Other recently identified stromal cells, located between the endosteal region and the BM vasculature, also resemble MSCs and may have additional fundamental roles in HSC regulation and biology. Because these reticular cells produce large amounts of the chemokine CXCL12 (SDF-1, **s**tromal **d**erived **f**actor 1), they were named CAR-cells (**C**XCL12 **a**bundant **r**eticular cells) (Sugiyama et al., 2006). Sacchetti et al. demonstrated that CD146 (**m**elanoma **c**ell **a**dhesion **m**olecule, MCAM) identifies a population of MSCs that is similar to CAR-cells *in vivo* and can generate bone and hematopoietic microenvironment when transplanted subcutaneously together with supporting osteoinductive **h**ydroxy**a**patite/**t**ri-**c**alcium **p**hosphate particles (Sacchetti et al., 2007).
Other surface epitopes like Stro-1 (Simmons and Torok-Storb, 1991), CD106 (**v**ascular **c**ell **a**dhesion **m**olecule-1, VCAM-1) (Gronthos et al., 2003), CD49a (α-1 Integrin), CD271 (low affinity nerve growth factor receptor), MSCA-1 (**m**esenchymal **s**tem **c**ell **a**ntigen-1, frizzeled-9, clone W8B2) were also investigated to prospectively enrich for MSCs in the BM (Buhring et al., 2007).
MSCs represent a potential therapeutic tool due to their intrinsic properties of (1) differentiating into mature mesodermal lineages upon appropriate extrinsic signals,

their (2) immune modulatory and (3) hematopoietic support functions (Horwitz et al., 2005, Delorme B et al., 2006, Dominici et al., 2006). Since the first successful transplantations of MSCs for enhancing HSPCs engraftment (Koc et al., 2000) and treating of acute **g**raft-**v**ersus-**h**ost-**d**isease (GvHD), (Le Blanc et al., 2004) and osteogenesis imperfecta (Horwitz et al., 1999) they have been in the focus of developments towards a wide array of cellular regenerative therapies. Additional MSC use ranges from tissue engineering to application of MSCs as suppliers for cytokines and growth factors that can lead to an increase of local angiogenesis and inhibition of scar formation and fibrosis (Caplan, 2005). Additionally these cells can support hematopoietic engraftment when co-infused with HSCs (Koc et al., 2000, Lazarus et al., 2005) and are capable of suppressing the immune system in case of GvHD or autoimmune diseases like Crohn's disease or **m**ultiple **s**clerosis (MS) (Uccelli et al., 2008).

The rather invasive BM harvesting procedure and the fact that the presence of MSCs is not a unique feature of BM initiated the search for alternative MSC sources. Although BM is the tissue most extensively studied, the existence of non-hematopoietic stem and progenitors outside the BM has recently also been demonstrated. Tissues that allow for successful MSC isolation include UCB (Erices et al., 2000, Mareschi et al., 2001, Bieback et al., 2004, Kogler et al., 2004, Reinisch et al., 2007), adipose tissue (Gronthos et al., 2001, Zuk et al., 2002, Kern et al., 2006), **u**mbilical **c**ord (UC) (1987, Romanov et al., 2003, Wang et al., 2004, Sarugaser et al., 2005, Lu et al., 2006, Reinisch and Strunk, 2009), placenta (Miao et al., 2006) and amniotic fluid (In 'T Anker et al., 2003).

6.4 Endothelial progenitor cells (EPCs)

A second key player within the non-hematopoieitic compartment of the BM is the vasculature and recent data provide evidence that this anatomical location, distant from the endosteal area, might represent another SC niche with distinct functions (Arai et al., 2004, Kiel et al., 2005, Kiel et al., 2007). There is a known close relationship between hematopoietic and endothelial lineages. During embryonic development the vasculature has a crucial role in regulation of HSCs (Choi et al., 1998, Jaffredo et al., 1998, De Bruijn et al., 2002, Eilken et al., 2009). Many HSCs reside adjacent to the BM vascular system mainly consisting of arterioles, venules and enlarged capillary like structures called BM sinusoids. These sinusoids represent the "gates" for all incoming and outgoing cells in the BM.

A small fraction within the vessel-lining **e**ndothelial **c**ells (ECs) is considered to be responsible for (1) maintaining integrity of existing vessels and (2) formation of new vessels (Ingram et al., 2005b), a process called "neovasculogenesis". These unique characteristics indicate that this immature cell has to be capable of proliferation and differentiation to generate mature endothelial lineage progeny, hence resembling a vascular tissue specific stem or progenitor cell.

Although the term EPC was first introduced by Asahara and colleagues, describing $CD34^+$-enriched blood-borne cells as "circulating EPCs" (Asahara et al., 1997) a major breakthrough towards a better understanding of vascular progenitor cell biology was the identification of **b**lood **o**utgrowth **e**ndothelial **c**ells (BOECs) and ECFCs in human blood (Solovey et al., 1997, Lin et al., 2000, Ingram et al., 2004, Ingram et al., 2005b). BOECs and ECFCs completely lack the expression of CD45 (**l**eukocyte **c**ommon **a**ntigen, LCA), in clear contrast to the cells described in the seminal work by Asahara that contained a complex mixture of hematopoietic $CD45^+$ as well as $CD45^-$ cell types (Asahara et al., 1997). The colony-like mixed cell clusters derived from these putative EPCs *in vitro* were later interpreted as **c**olony-**f**orming **u**nits of **EC**s (CFU-EC) (Hill et al., 2003). The true nature of these *in vitro* generated cell clusters was recently redefined by clonal analysis showing their unambiguous hematopoietic origin (Case et al., 2007, Timmermans et al., 2007, Yoder et al., 2007). The composition of these colony-like structures was shown to result from a functional cross-talk between T cells and monocytes *in vitro* (Rohde et al., 2007,

Hirschi et al., 2008). Based on these findings the term CFU-EC was renamed as CFU-Hill.

Because ECFCs emerge later (after 2-4 weeks) in culture compared to CFU-Hill and other so-called **c**irculating **a**ngiogenic **c**ells (CACs) of hematopoietic origin (Vasa et al., 2001b), ECFCs have been called “late outgrowth EPCs”. The term “early outgrowth EPCs” has been used for CFU-Hill and CACs that appear after 3-4 days in culture (Gulati et al., 2003, Hur et al., 2004, Yoon et al., 2005).

These cells although different compared to ECFCs regarding their origin and phenotype appear to have pro-angiogenic activity (Rafii and Lyden, 2003, Grunewald et al., 2006, Jin et al., 2006, Hirschi et al., 2008, Kovacic et al., 2008) and might play a central role in vascular homeostasis, repair and tumor neo-angiogenesis (Folkman, 2002, Khakoo and Finkel, 2005). Nevertheless their hematopoietic origin together with the lack of proliferative potential strongly argues against a true endothelial progenitor phenotype. The direct contribution of these BM-derived, non-ECs to neo-vessel formation including the integration into the endothelial layer is still a matter of debate (Lyden et al., 2001, Carmeliet, 2003, Rafii and Lyden, 2003, Ruiz De Almodovar et al., 2006, Schatteman et al., 2007, Gao et al., 2008, Hirschi et al., 2008, Purhonen et al., 2008).

It is meanwhile accepted knowledge that ECFCs represent the true endothelial progenitor cell. In contrast to CFU-Hill and CACs, ECFCs show robust proliferation *in vitro* and profound vessel formation capacity *in vivo.* These unique properties make them attractive candidates for vascular regenerative therapy (Melero-Martin et al., 2007, Yoder et al., 2007).

6.5 Goals of the thesis

The goals of this project were (1) to test the feasibility and applicability of FBS-free cell culture methods on alternative MSC sources such as human UCB or human umbilical cord and furthermore (2) to translate the use of pooled HPL as a humanized growth factor substitute for ECFC cultures. (3) After the establishment of the technology to propagate MSCs and ECFCs for experimental and therapeutic application with self-made GMP-compliant pHPL (Reinisch et al., 2007, Schallmoser et al., 2007a, Rohde E et al., 2008b, Schallmoser et al., 2008, Reinisch et al., 2009), cell functionality should be tested *in vitro* and *in vivo.* (4) As it is of critical importance to localize and track cells after application *in vivo,* imaging modalities including MRI should be employed and suitable magnetic contrast agents (SPIOs) should be tested to reach sufficient cell labeling that allows cell visualisation. Subsequent optimization of MRI protocols on a phantom *in vitro* will provide the basis for comprehensive cell tracking studies *in vivo*. (5) Furthermore, both progenitor populations will be used to develop model systems for non-invasively monitoring the spatial and temporal distribution of applied cells.

7 Materials and Methods

Experiments and results that were not completely conducted by myself are designated and coworkers are explicitly mentioned.

7.1 Collection of umbilical cord blood and peripheral blood

(UCB collection was performed by midwives or study nurses from the Department of Gynecology and Obstetrics, Medical University of Graz)

UCB from term pregnancies was collected immediately after delivery in 50mL tubes (Falcon) preloaded with preservative-free heparin (250 U/tube; Biochrom AG, Berlin, Germany; www.biochrom.de). Cells were counted using a Sysmex KX 21 hematology analyzer (Sysmex America Inc., Mundelein, IL; www.sysmex.com).
Steady-state venous PB was obtained from healthy volunteers (max. 4 x 6 mL; 4 male, 2 female; age 26-50 years) and patients with cardiovascular disease (CVD; 1 x 6 mL, 4 male, 3 female, age 45-86). A maximum volume of 24 mL PB per volunteer or CVD-patient, respectively, was collected in 6 mL vacuette tubes preloaded with 108 IU/6mL of preservative-free sodium heparin (Greiner Bio-One GmbH, Kremsmünster, Austria, www.gbo.com). Blood samples were obtained after written informed consent in accordance with the declaration of Helsinki. The study protocols were approved by the institutional review board of the Medical University of Graz (protocol numbers 19-252 ex 07/08 and 18-243 ex 06/07)

7.2 Preparation of pooled human platelet lysate (pHPL)

(performed by PD Dr. Katharina Schallmoser and MTA Claudia Url, Stem Cell Research Unit [SCRU], Univ. Clinic of Blood Group Serology and Transfusion Medicine, Medical University of Graz)

HPL was prepared as described (Schallmoser et al., 2007a). Briefly, whole blood (450 ± 45 mL) was collected after informed consent from random donors fulfilling the

Austrian law requirements for blood donation. Red blood cells and plasma were separated automatically from the buffy coat fraction and transferred into satellite containers (Compomat G3, NPBI, Amsterdam, Netherlands). The **p**latelet **r**ich **p**lasma (PRP) was subjected to inline filtration for leukocyte depletion (PALL Autostop, Pall, Dreieich, Germany). Testing for sterility was routinely performed and the PRP was frozen at -30°C for platelet fragmentation. After thawing at 37°C, at least ten units of platelet lysate were pooled to avoid individual donor variations and the HPL pool was frozen again in aliquots at -30°C until use (Schallmoser et al., 2007a, Schallmoser and Strunk, 2009).

7.3 Preparation of cell culture medium

The α-modified **m**inimum **e**ssential **m**edium (α-MEM , M4526; Sigma-Aldrich; St. Louis; MO, USA; www.sigmaaldrich.com) was supplemented with 100 U/mL Penicillin and 100 µg/mL Streptomycin, 2 mM L-Glutamine (all Sigma;) and either 10% preselected FBS (Hyclone, Logan, UT, USA) or 10% pHPL as described (Bartmann et al., 2007a, Schallmoser et al., 2007a, Schallmoser and Strunk, 2009). To avoid platelet gel formation, two U/mL preservative-free Heparin (Biochrom AG) were added to the supplemented α-MEM before pHPL addition.

Endothelial **g**rowth **m**edium (EGM) was prepared by supplementing endothelial cell basal medium (EBM-2) with “single quots” (aliquots containing hydrocortisone, human **e**pidermal **g**rowth **f**actor [EGF], **v**ascular **e**ndothelial cell **g**rowth **f**actor [VEGF], human **b**asic **f**ibroblast **g**rowth **f**actor [bFGF], R3 **i**nsulin-**l**ike **g**rowth **f**actor-1 [IGF-1], and ascorbic acid in concentrations predefined by the producer, all Lonza, Walkersville, MD; www.lonzabioscience.com). The EGM was heparinized with 10 U/mL of preservative-free Heparin (Biochrom AG) before adding 10% pHPL, 2mM L-Glutamine, 100 U/mL penicillin and 100 µg/mL Streptomycin (all Sigma)

7.4 Culture of UCB-MSCs

7.4.1 MSC Isolation

UCB mononuclear cells (UCB-MNCs) were recovered from the interface obtained by density gradient centrifugation (Ficoll-Paque^{TM}-PLUS, StemCell Technologies Inc., Vancouver, Canada, www.stemcell.com). Cell number and viability were determined from the mean of four measurements with a hemocytometer. The MNCs were washed twice with phosphate buffered saline (PBS) before plating in tissue culture flasks (Corning Inc., Acton, MA, USA) with a density of 1 x 10^6 MNC/cm^2 directly in supplemented α-MEM (Sigma). Non-adherent cells were removed by complete medium change after 2-3 days. The cultures were fed twice weekly. MSC colonies of at least 50 cells (one to three per UCB) in primary cultures were trypsinized (0.25% trypsin/1mM **e**thylene**d**iamine**t**etraacetic **a**cid [EDTA], 1-5 min, 37°C; Sigma) after 15-25 days and reseeded without counting into three new flasks. After first passage, cells were grown until reaching confluence. On days 12 to 16, first passage cells were harvested and counted before aliquots were cryopreserved, kept in liquid nitrogen and re-thawed for experimental and preclinical expansion experiments. Whenever indicated UCB-MSCs cultured in our experiments in FBS-supplemented medium are called UCB-MSC^{FBS} and UCB-MSCs cultured in pHPL-supplemented medium are called UCB-MSC^{HPL} throughout this thesis.

7.4.2 MSC large-scale expansion

For clinical scale expansion, 3 x 10^5 MSC derived from first passage cultures were seeded in α-MEM/10% pHPL or α-MEM/10% FBS with a compromise seeding density of 30/cm^2 on 1 m^2 culture area in four four-layered **c**ell **f**actories (CF-4; Nalge Nunc International, Naperville, IL, USA, www.nuncbrand.com) and cultured to reach confluence as previously established (Schallmoser et al., 2007a). Cultures were maintained by thirty percent medium change twice weekly and MSCs were harvested on days 13 to 15 by trypsinisation. A cartoon summarizing the expansion strategy is shown in **Figure 2**.

7.4.3 MSC long-term expansion

MSCs were further propagated at very low seeding density (1/cm^2) in tissue culture flasks (Corning) to evaluate the long-term growth kinetics in FBS- and pHPL-supplemented α-MEM at the clonal level. Estimated total MSC yield and **c**umulative **p**opulation **d**oublings (CPDs) were calculated for a total of 7 passages (14 ± 2 days per passage).

7.4.4 CFU-F assay

CFU-F assays were performed to evaluate the clonal expansion capacity of MSCs (Bartmann et al., 2007a). For optimal counting of colonies, MSCs were seeded at 1/cm^2 in duplicates in 150 cm^2 culture dishes (Corning) for two weeks, washed, fixed with Aceton/Methanol (3:2 parts v/v, 15 minutes, on ice; Merck, Darmstadt, Germany, www.merck-chemicals.com) and air dried. After re-hydration for 10 minutes with de-ionized water, colonies were visualized with Harris´ Hematoxylin staining (10-12 minutes; Merck). Colonies consisting of ≥ 50 cells were counted using a SZX 12 stereo microscope (Olympus, Hamburg, Germany, www.olympus.de) (Bartmann et al., 2007a).

7.5 Culture of peripheral blood and cord blood-derived ECFCs

7.5.1 ECFC isolation

Cell culture was initiated within less than two hours after blood collection. Except in initial titration experiments, any manipulation of freshly obtained cells such as red blood cell lysis or density gradient centrifugation was strictly avoided in ECFC cultures to minimize cell loss. Heparinized blood was directly diluted in EGM-2 in a 1:4 to 1:10 ratio of PB : supplemented medium depending on the culture vessel size (e.g., 5 mL blood plus 20 mL EGM-2 per T75 vented cap cell culture flask; Corning). Depending on the volume, whole UCB was diluted 1:5 to 1:2. Non-adherent cells were removed after overnight culture at 37°C, 5% CO2 in humidified atmosphere by

washing three to six times with excess pre-warmed 37°C PBS before adding new pre-warmed 37°C EGM-2. Thereafter, the medium was replaced three times weekly until a visible outgrowth of cobblestone-type colonies appeared.

7.5.2 ECFC large-scale expansion

Primary culture-derived ECFCs were seeded in 500 mL EGM-2 per CF-4 (Nunc) in two CF-4s per ECFC donor at a maximum seeding density of 100 ECFCs/cm^2 corresponding to 2.5 x 10^5 ECFCs/CF-4 and cultured at 5% CO_2, 37°C, 95% air humidity in a clean room. Large scale ECFC cultures were maintained by replacing 200 mL of medium with new pHPL-supplemented EGM-2 twice weekly until cells reached near confluence. After 11 to 25 days, ECFCs were harvested using 0.25% trypsin/1mM EDTA (70 mL per CF-4, 1-5 min, 37°C; Sigma). Nucleated cell numbers were determined using a hemocytometer as the mean of four measurements and viability by trypan blue exclusion. Viability was simultaneously measured by adding **7**-**a**mino-**a**ctinomycin **D** (7-AAD; Becton Dickinson, Franklin Lakes, NJ; www.bdbiosciences.com) exclusion with a four colour FACSCalibur® instrument equipped with a 488 nm argon ion laser and a 635 nm red diode laser (BD) post harvest and post cryopreservation. For cryopreservation, cells were washed in PBS and resuspended to a concentration of 0.5 to 5.0 x 10^6/mL in a pre-cooled (0°C) cryosolution containing EGM-2/10% pHPL with 10% v/v **di**m**e**thyl **s**ulf**o**xide (DMSO, Cryosure, WAK Chemie Medical GmbH, Steinbach, Germany; www.wak-chemie.net) (Baxter Oncology, Deerfield, IL; www.baxter.com) in cryotubes (Nunc). Freezing was performed using a computer-controlled freezer (Sylab Ice Cube 1810, Neupurkersdorf, Austria, www.sylab.at) and cryopreserved cells were stored in liquid nitrogen.

7.5.3 ECFC colony assay

In preliminary experiments, serial dilutions were analyzed in triplicate to determine endothelial colony frequency in established ECFC populations. These pilot colony assays revealed optimum countable colonies starting from a seeding density of 10

ECFCs/cm^2 **(Figure 9A)**. Colony assays were initiated with ECFCs in a density of 10 cells/cm^2. After 10 and 14 days cultures were washed three times with PBS, fixed with Acetone/Methanol for 15 minutes (3:2 parts v/v, 0°C; Merck), air dried and rehydrated for 10 minutes with deionized water before Harris´ Hematoxylin staining (10-12 minutes; Merck). To allow for a precise colony enumeration, all colonies were documented using digital imaging with a DP12 camera connected to a SZX 12 stereo microscope (Olympus). Exact cell number per colony was analyzed by using ImageJ software (http://rsbweb.nih.gov). Briefly, normal **j**oint **p**hotographic **e**xperts **g**roup format (*.jpg) or **t**agged **i**mage **f**ile **f**ormat (*.tif) files were set to 8 bit gray scale, the background was subtracted and the colour threshold was adjusted to get an ideal display of the cells. Subsequently, particles of a size between 15 and 2,000 pixels^2 were counted as single cells. The accuracy of resulting cell number was compared to microscopic counting in at least 10 colonies per plate (Reinisch and Strunk, 2009). **L**ow **p**roliferative **p**otential (LPP) and **h**igh **p**roliferative **p**otential (HPP) colonies were defined, as published, as colonies comprising of 51 to 500 and >500 cells, respectively, at day 14 **(Figure13)** (Ingram et al., 2004, Ingram et al., 2005b).

7.6 Cell phenotype determination

7.6.1 Flow cytometry

Flow cytometry was performed to test for reactivity with anti-human **m**onoclonal **a**nti**b**odies (mAbs) HLA-DR, CD13, CD14, CD19, CD31, CD34, CD45, CD73 (all BD), CD90 (BeckmanCoulter, Inc., Fullerton, CA; www.beckmancoulter.com), CD105 (Caltag Laboratories; Burlingame; www.caltag.com), CD144, VEGF-Receptor 2 (KDR; R&D Systems, Minneapolis, MN; www.rdnsystems.com) HLA-ABC (Harlan Sera-Lab, Leicestershire, UK; www.harlaneurope.com), CD133 (Milteny Biotec, Bergisch Gladbach, Germany; www.miltenybiotec.com) CD144 (Bender MedSystems GmbH, Vienna, Austria; www.bendermedsystems.com) and CD146 (Chemicon International, Temecula, CA; www.chemicon.com) **(Table 3)**. Briefly, cells were washed after trypsinization and blocked with 10% v/v sheep serum as described (Bartmann et al., 2007b). Cell suspensions were then stained for 25 minutes at 4°C

with directly fluorochrome conjugated mouse anti-human mAbs. Appropriate negative control isotype matched Abs (BD) were used in the same concentration as the testing antibodies. Data from a minimum of 10,000 viable 7-AAD-excluding cells was acquired. List mode files were analyzed with CellQuest™ Pro, Paint-A-Gate Pro® software (BD) or FlowJo software (Tree Star Inc., Ashland, OR; www.flowjo.com).

Table 3. Flow Cytometry antibody list

AG	Synonyme	Conjug.	Clone	Isotype	Conc.	Dilut.	Comp.	Ordering No.
control	isotype	FITC	X40	IgG1	50 µg/mL	1:100	BD	345815
control	isotype	FITC	X39	IgG2a	50 µg/mL	1:25	BD	349051
control	isotype	PE	X40	IgG1	50 µg/mL	1:30	BD	345816
control	isotype	PE	2735	IgG2b	50 µg/mL	1:80	BD	555743
control	isotype	PE	X39	IgG2a	50 µg/mL	1:5	BD	349053
control	isotype	APC	X39	IgG2a	100 µg/mL	1:100	BD	340473
CD3	UCHT-1	FITC	UCHT1	IgG1	100 µg/mL	1:100	Dako	F0818
CD14	Leu-M3; LPS-R	PE	MFP9	IgG2b	50 µg/mL	1:50	BD	345785
CD15	Leu-M1; Lex	FITC	MMA	IgM	100 µg/mL	1:50	BD	347423
CD19	Leu-12	PE	SJ25C1	IgG1	12,5 µg/mL	1:20	BD	345789
CD29	Integrin ß1 chain	APC	MAR4	IgG1	50µg/mL	1:100	BD	559883
CD31	PECAM-1	FITC	WM59	IgG1	50µg/mL	1:100	BD	555445
CD34	HPCA-2	PE	8G12	IgG1	25 µg/mL	1:20	BD	345802
CD34	HPCA-2	APC	8G12	IgG1	100 µg/mL	1:50	BD	345804
CD38	Leu-17	PE	HB-7	IgG1	12,5 µg/mL	1:20	BD	345806
CD45	HLe-1; LCA, T200	FITC	2D1	IgG1	50 µg/mL	1:50	BD	345808
CD45	HLe-1; LCA, T200	APC	HI30	IgG1	3 µg/mL.	1:5	BD	555485
CD56	NCAM	FITC	NCAM16.2	IgG2b	6 µg/mL	1:10	BD	345811
CD73	Ecto-5'-nucleotidase	PE	AD2	IgG1	6,25 µg/mL.	1:10	BD	550257
CD90w	Thy-1	FITC	F15.42	IgG1	25 µg/mL	1:50	Immunotech	1839
CD105	Endoglin	APC	SN6	IgG1	50 µg/mL	1:100	Caltag	MHCD10505
CD133	Prominin	APC	AC133	IgG1	11 µg/mL	1:20	Miltenyi	130-000-826
CD146	Muc-18, MCAM	FITC	P1H12	IgG1	1 mg/mL	1:1000	Chemicon	MAB16985F
HLA-ABC	MHC class I	FITC	W6/32	IgG2a	100 µg/ml	1:100	AbD Serotec	MCA81F
HLA-DR	MHC class II	FITC	L243	IgG2a	25 µg/mL	1:25	BD-IS	347363
VEGF-R2	KDR, FLK-1	PE	89106	IgG1	50 µg/mL	1:50	R&D	FAB357P

7.6.2 Histology, immune cytochemistry and immune histochemistry

(Histology was done in cooperation with Prof. Christine Beham-Schmid, Institute of Pathology, Medical University of Graz; IHC was performed by Nicole A. Hofmann, MSc, Stem Cell Research Unit, [SCRU], Medical University of Graz)

Matrigel plugs were excised, and immediately fixed in 4% neutral bufferd formaldehyde (Sigma) for 24 hours. Dehydrated samples were embedded in paraffin and sectioned. In the case of bone development, tissue was decalcified after fixation using EDTA. 2-4µm sections were stained with Hematoxylin and Eosin (H&E) for microscopic evaluation of vessel or bone formation.

Immune cytochemistry and immune histochemistry was performed to detect reactivity with mouse anti-human Abs CD34 (clone 581, BD), CD31 (JC70A), Vimentin (V9), and **v**on **W**illebrand **f**actor (vWF, F8/86, all Dako, Glostrup, Denmark, www.dako.com) in titrated individual concentrations accompanied by appropriately diluted and isotype matched controls **(Table 4)**. **F**ormalin-**fi**xed **p**araffin-**e**mbedded tissue (FFPE) sections were deparaffined in an incubator at 65°C for 40-60 minutes and rehydrated by decreasing alcohol incubation. Microwave treatment at 160W for 20 min in 10% target retrieval solution (Dako) was followed by endogenous peroxidase blocking through incubation in 3% H_2O_2 for 10 min. To reduce unspecific staining we blocked with Vector M.O.M. mouse Ig blocking reagent (Vector Laboratories, Inc., Burlingame, CA, www.vectorlabs.com) for 60 min and additionally with protein block serum-free (Dako) for 30 min. Sections were incubated with specific antibodies or controls for 30 minutes and reactivity was visualized with UltraVision LP large volume detection system HRP polymer (Thermo Fischer Scientific, Freemont, CA, www.labvision.com) and stained with Dako REAL DAB+ Chromogen (Dako) for 5 min following the manufacturer's instructions. Stained sections were counterstained with Harris´ Hematoxylin solution (Merck) for 20 seconds and mounted with mounting medium (Tissue Tek, Coverslipping Resin, Sakura Finetek USA Inc, Torrance, CA; www.sakuraus.com).

Table 4. Antibodies used for immune histochemistry and immune cytochemistry

AG	Conjug.	Clone	Species	Isotyp	Reactivity	Conc.	Dilution	Company	Ord. No.
IgG1	-	MOPC-31C	Mouse	IgG1	Isotype ctrl.	500 µg/mL	up to1:100	BD	557273
Vimentin	-	V9	Mouse	IgG1	Human	360 µg/mL	1:200	Dako	M0725
vWF	-	F8/86	Mouse	IgG1	Human	235 µg/mL	1:100	Dako	M0616
CD31	-	JC70A	Mouse	IgG1	Human	515 µg/mL	1:100	Dako	M0823
TER-119	biotin	TER-119	Rat	IgG2b	Mouse	500 ug/mL	1:100	BD	553672
CD146	-	N1238	Mouse	IgG1	Human	21 µg/mL	1:100	Novocastra	NCL-CD146
CD90	-	5E10	Mouse	IgG1	Human	500 µg/mL	1:250	BD	55593

7.7 Cell function

7.7.1 MSC differentiation

After clinical scale expansion, MSCs were cultured at a density of 5000 cells/cm^2 in T225 flasks (Corning) for 4 days in DMEM/nutrient mixture F-12 Ham (DMEM/Ham F12, Sigma, D8062), 10% FBS (Hyclone), 100 U/mL Penicillin and 100 µg/mL Streptomycin (Sigma) at 37°C, 5% CO_2, 90% air humidity, until they reached 90% confluence. After trypsinisation cells were seeded into 6-well plates to start the differentiation. For all differentiation protocols cells were cultured in the same basic medium (but with the different respective supplements) and were fed twice weekly by whole medium exchange.

To induce osteogenic differentiation, 90% confluent cells were incubated in DMEM/Ham F12/10% FBS supplemented with 0,1 µM dexamethason, 50 µg/mL L-ascorbic acid and 10 mM glycerophosphate disodium pentahydrate (all Sigma) for 10 days. For assessing osteogenic differentiation, alkaline phosphatase activity was assayed at day 10 by histochemical staining (alkaline phosphatase kit No.85, Sigma) following the manufacturer's instructions.

For adipogenic differentiation cells were grown in DMEM/Ham F12/10%FBS supplemented with 1 µM dexamethason, 100 µM indomethacin, 0,5 mM 3-**i**so**b**utyl-1-**m**ethyl**x**anthine (IBMX, all Sigma) and 10 µg/mL insulin (Novo Nordisk, Actrapid®, Bagsværd, Denmark, www.novonordisk.com) for 3 weeks. To visualize intracellular fat vacuoles cells were washed with PBS, fixed with formalin solution (4% w/v

formaldehyde, Sigma) for 10 minutes and stained with Oil Red O (0,5% stock solution in 2-propanol, 3:2 dilution in distilled water for staining) for 25 minutes.
To initiate chondrogenic differentiation cells were cultured in DMEM/Ham F12/10% FBS supplemented with 1 ng/mL **t**ransforming **g**rowth **f**actor-ß1 (TGF-ß1, R&D Systems) and 50 µg/mL L-ascorbic acid (Sigma). Production of mucopolysaccharides and glycosaminoglycans was verified after 21 days of chondrogenic induction by alcian blue staining. Cells were fixed with formalin solution (Sigma) for 10 minutes and stained with alcian blue (1% alcian blue in 3% acetic acid solution, pH 2.5) for 30 minutes

.

7.7.2 Hematopoietic support

Liquid cultures of MACS®-isolated $CD34^+$ UCB-MNCs (Miltenyi) were performed with and without a pre-established MSC feeder layer in 75 cm^2 flasks (Corning). Expansion medium consisted of RPMI-1640 (Sigma) supplemented with 10% FBS (Hyclone), 2 mM L-Glutamin (Sigma), 300 U/mL IL-3, 50 ng/mL Flt3-Ligand, 20 ng/mL SCF (all R&D Systems) and 800 U/mL **g**ranulocyte-**m**acrophage **c**olony-**s**timulating **f**actor (GM-CSF, Sandoz, Vienna, Austria, www.sandoz.at). Medium was changed twice during the 18-day expansion period. Cell number was measured by automated cell counting (CASY® TTC; Schaerfe-Systems, Reutlingen, Germany, www.casy-technology.com) and the non-adherent propagated cells were assayed for the presence of $CD34^+/CD38^+$ HPCs and $CD34^+/CD38^-$ HSCs by flow cytometry.

7.7.3 Network formation

In vitro vascular network formation was tested as previously described by seeding 7,500-10,000 large-scale expanded MSCs or ECFCs per 0.4 cm^2 well (Rohde et al., 2007). Briefly, cells were transferred into 16-well chamber slides (Lab-Tek®, Nunc) pre-filled with 50 µl Matrigel® (Chemicon) and cultured for 12-24 hours. In the case of vascular network preparation for MRI, 75,000-100,000 SPIO-labeled ECFCs were cultured in two-well chamber slides (Nunc). The vascular network formation was documented by acquiring video sequences at 30 minute intervals and covering a time

period of 24 hours with a cell observer (Zeiss, Maple Grove, MN; www.zeiss.com). Network branches were additionally photographically documented (Olympus IX51)

7.7.4 Immune modulation

7.7.4.1 Modulation by UCB-MSCs

MNCs were labeled with 1 µM 5(6)-**c**arboxy**f**luorescein diacetate N-**s**uccinimidyl **e**ster (CFSE; Sigma) for 15 min at 37°C. $3x10^5$ labeled MNCs were stimulated with 5µg/mL **p**hyto**h**em**a**gglutinin (PHA; Remel Inc, KS, USA, www.remelinc.com) in the absence or presence of different numbers of MSCs added together with the MNCs into 24-well plates (Corning) in RPMI-1640 (Sigma) supplemented with 10% FBS (Hyclone) and 2 mM L-Glutamin (Sigma). After four days MNCs were harvested, counted and consecutively assayed for loss of fluorescent intensity by flow cytometry to monitor proliferation (Muller et al., 2006).

7.7.4.2 Modulation by UCB-ECFCs

BM-MSC, used as a positive control and different UCB derived ECFCs were cultured until reaching confluence in 24 well plates at 37°C, 5% CO_2, 90% humidity. At confluence cell were treated with Mitomycin C (50 µg/mL, Sigma M4287) for 2 hours to block cell proliferation. After treatment cells were washed at least 4 times with pre-warmed medium to remove remaining Mitomycin C and finally fresh medium was added. Cells were cultured for 7 more days and proliferation inhibition was controlled visually through daily microscopy. MNCs were labeled with 2-4 µM CFSE (Sigma) for 15 min at 37°C. 1.5 x 10^5 labeled MNCs were stimulated with 5 µg/mL PHA (Remel) and cultured on the MSC or ECFC feeder layer in RPMI-1640 (Sigma) supplemented with 10% FBS (Hyclone) and 2 mM L-Glutamin (Sigma). Additionally, different ratios of MNC:MSC or MNC:ECFC were cultured simultaneously in 24-well plates (Corning) to study the direct effect of MSCs and ECFCs on MNC proliferation in suspension without using a feeder layer. After six days MNCs were harvested and consecutively assayed for loss of fluorescent intensity by flow cytometry to monitor proliferation

(Muller et al., 2006). At least 10,000 MNC cells were acquired on a FACS-Calibur instrument (BD) and subsequently analyzed by using proliferation analysis feature of FlowJo software (TriStar). Cell generations were calculated depending on the loss of fluorescence intensity in FL-1 channel.

7.8 Genomic stability of ECFCs

(array comparative genomic hybridization [array CGH] was performed by Anna C Obenauf, MSc; G-Banding was done by Karin Flicker, MSc, both Institute of Human Genetics, Medical University of Graz)

Metaphase chromosome spreads and karyotyping were performed according to standard laboratory procedures (Geigl et al., 2004). Briefly, PB- and UCB-derived ECFCs were grown in slide flasks. Proliferation status was evaluated by daily microscopy to find optimal conditions for colcemid incubation (3 drops of colcemid, 10µg/mL, for 3-8 hours, Invitrogen). After incubation, medium was removed and hypotonic treatment was performed with 0,075 M KCl for 20 min at room temperature. Subsequently, cells were fixed (5 minutes, ice cold methanol : acetic acid = 3:1), dried on a heating plate (37°C, humidified environment) and stained with Giemsa solution (4%). Images of metaphase spreads were taken (Leitz microscope, 100x objective) and cytovision software (Genetix GmbH, Dornbach, Germany; www.genetix.com) was used for karyotyping.

Array-CGH hybridization of ECFCs after large-scale expansion and in the course of long-term proliferation was performed and interpreted to determine the possible genomic alteration of cells expanded for four passages representing up to 37 population doublings and compared in selected samples to constitutional DNA. Array CGH was carried out using a whole genome oligonucleotide microarray platform (Human Genome CGH 44B Microarray Kit; Agilent Techologies, Santa Clara, CA; www.agilent.com). This array consists of approximately 43,000 60-mer oligonucleotide probes with a spatial resolution of 43 kb. Genomic DNA was prepared from cell lines following standard phenol chloroform extraction. As a reference DNA, commercially available male DNA was used (Promega, Madison, WI;

www.promega.com). Samples were labeled with the Bioprime array CGH genomic labeling system (Invitrogen) according to the manufacturer's instructions. Briefly, 500 ng test DNA and reference DNA were differentially labeled with dCTP-Cy5 or dCTP-Cy3 (GE Healthcare, Piscataway, NJ; www.ge.com). Further steps were performed according to the manufacturer's protocol (version 6.0). Slides were scanned using a microarray scanner (G2505B) and images were analyzed using CGH Analytics software 3.4.40 (both from Agilent) with the statistical algorithm ADM-2. Sensitivity threshold was 6.0 and the moving average window was set to 0.5. At least five consecutive clones had to be aberrant to be flagged by the software.

7.9 Telomere measurements

7.9.1 Telomere length

Telomere length was analyzed using a telomere **p**eptide **n**ucleic **a**cid (PNA) Kit/FITC (Dako) according to manufacturer's instructions with minor modifications. In short, for DNA denaturation, 2 x 10^6 cells were incubated for 10 minutes at 82°C either with hybridization solution containing telomere PNA probe or with hybridization solution only (mock sample). For hybridization, samples were placed overnight at room temperature (RT) in the dark. On the next day samples were washed twice and DNA-stained with propidium iodine (PI) for at least 2 hours at 2-8°C in the dark. Samples were analyzed on a FACSCalibur® instrument (BD) using FL1-H for FITC probe fluorescence and FL2-A/FL2-W for displaying DNA staining.

Cells in $G_{0/1}$- phase of the cell cycle were determined by FL2-A/FL2-W dot plot with gates set to exclude cells with more than one copy of the genome. At least 10,000 cells were acquired and subsequently analyzed for FL1-H signal using FlowJo-software. Mock hybridizations were used to determine auto-fluorescence of the cells. Auto-fluorescence signal was always set to the same value in FL1-H histogram (10^1 arbitrary fluorescence units) to minimize donor variations. Differences (delta FL1-H) between the autofluorescence and PNA probe-specific fluorescence signals in FL1-H were calculated.

7.9.2 Telomerase activity

(telomerase activity was analyzed by Anna C Obenauf, MSc, Institute of Human Genetics, Medical University of Graz)

Telomerase activity was assessed with a real-time PCR-based **t**elomeric **r**epeat **a**mplification **p**rotocol (TRAP) assay using a quantitative telomerase detection kit (Allied Biotech Inc., Ijamsville, MD; www.alliedbiotechinc.com) according to manufacturer's instructions. Briefly, cells were lysed with an appropriate amount of lysis buffer for adjusting 1000 cells/µl. A 7900HT Fast Real-Time PCR System (Applied Biosystems; Carlsbad, CA; www.appliedbiosystems.com) was used for experiment analysis. Double measurements were prepared and heat inactivated cell lysates served as a negative control. A standard curve with a TSR control template, provided in the kit, was generated.

7.10 Multiplex growth factor analysis

Aliquots of cell culture media before use (Start) and cell culture supernatants on the day of MSC or ECFC harvest (Harvest) were frozen at -70°C. Confluent MSCs were cultured under 1, 5 and 20% oxygen concentration for one week. Multiplex human growth factor detection kit (Beadlyte® Human Growth Factor Beadmates, Upstate, Lake Placid, NY, now: www.millipore.com) was used to measure the concentration of **p**latelet **d**erived **g**rowth **f**actor-AB/BB (PDGF-AB/BB) and VEGF in ECFC supernatants according to the manufacturer's instructions on a Luminex instrument (detection limit of 14 pg/mL for VEGF, 7 pg/mL for PDGF-AB/BB; Luminex Corporation, Austin, TX, www.luminexcorp.com).
VEGF content in MSC supernatant was evaluated by using **C**ytomatic **B**ead **A**rray on LSR II flow cytometer (CBA, BD). Aquired data were analyzed with FCAP software (BD).

7.11 Animal experiments

(nude mice experiments were performed together with Dr. Karl Kashofer, Institute of Pathology, Medical University of Graz)

Animal experiments were approved by the Animal Care and Use Committee at the Veterinary University of Vienna on behalf of the Austrian Ministry of Science and Research (**B**undes**m**inisterium for **W**issenschaft und **F**orschung, BMWF) according to the criteria published in the Guide for the Care and Use of Laboratory Animals by the National Institutes of Health (NIH publication 86-23, revised 1985).
8-10 week old highly immune-compromised mice ([1] nude mice, Hsd:Athymic Nude-Foxn1nu, Harlan, Indianapolis, IN; www.harlan.com; [2] NOG mice [NOD-SCID, IL2-receptor γ chain $^{-/-}$], NOD.Cg-Prkdc^{scid} Il2rg^{tm1Wjl}/SzJ, The Jackson Laboratory, Main, USA; www.jax.org) were used as recipients to almost exclude immune-mediated cell rejection. Mice were kept under **s**pecific **p**athogen **f**ree (SPF) conditions.
Different ratios of MSCs and ECFCs were combined and tested for their ability to generate subcutaneous vessel or bone. Both cell types were obtained after large scale expansion representing approximately 20 population doublings.To obtain stable vascular networks, ECFCs were mixed with allogeneic third party MSCs in a ratio of 20:80, resuspended in Matrigel® (Chemicon) and transplanted subcutaneously into the flank (Melero-Martin et al., 2007, Au et al., 2008). Matrigel plugs were generated by injecting 0.2mL of the human cell containing a final amount of $2x10^6$ cells per injection side. In another series of experiments, pure ECFCs without matrix and without stabilizing MSCs were diluted in PBS and injected subcutaneously. Application of MSCs and ECFCs in a ratio of 80:20 or MSCs applied without ECFCs was used to study MSC-mediated bone formation. Injections were performed under anesthesia of the mice. All mice were narcotized according the approval for animal handling (BMWF:-66.010/0082-II/10b/2009). Mice were observed for the indicated time periods of one to 20 weeks before euthanasia and excision of the generated vessel or bone containing tissue. After taking pictures, excised tissue was immediately fixed in neutral buffered 4% paraformaldehyde. If necessary bony tissue was decalcified in EDTA before embedding.

7.12 *In vivo* SC imaging

(fpVCT was performed together with PD Dr. Frauke Alves and DI Christian Dullin, Max Planck Institue [MPI] for Experimental Medicine, Medical University of Göttingen, Germany; µCT was performed together with Mag. Alexander Hofmeister, Core Facility Molecular Imaging, Center for Medical Research, Medical University of Graz)

For µCT and fpVCT analysis mice were narcotized by inhaling 2% isoflurane (Abbott, Forane®, UK, www.abbottuk.com) at a flow rate of 1.5 liter oxyen per minute in an induction chamber. At anesthesia mice were tranferred to the scanner and narcotisation was maintained. Native scans without contrast agents were performed on a preclinical scanner (µCT; Siemens Inveon, Siemens) and a non clinical prototype scanner equipped with two flat panel detectors (fpVCT; GE-Global Research, Niskayuna, NY, www.geglobalresearch.com) using standard protocols to detect bone formation. For contrast agent enhanced imaging on fpVCT 150µl iodine containing contrast agent per mouse (Isovist® 300; Bayer-Schering, Germany, www.diagnostic-imaging.bayerscheringpharma.de) was injected intraveneously via the tail veine 28 second before scanning was started. All fpVCT datasets were acquired using the same protocol: 1,000 views per rotation, 8 seconds of rotation per step, 360 used detector rows, 80 kVp and 100mA. Acquired data files were transformed to DICOM-files and analyzed with appropriate software.

To visualize bone growth, resorption and remodeling an osteo-integrating near infrared dye targeting hydroxyappatite (Osteosene^{750}, Visen Medical, USA, www.visenmedical.com) was applied intravenously at least 24 hours before imaging. Mice were anesthetized by 80 mg/kg ketamin hydrochlorid and 12 mg/kg xylazine (Sigma), applied intraperitoneally and fur was removed locally to avoid background fluorescence prior to the acquisition on an *in vivo* fluorescence imaging device (Maestro®, CRI, Germany, www.cri-inc.com).

7.12.1 Progenitor cell labeling

Resovist® (Bayer-Schering) and Endorem®(Guerbet, France, www.guerbet.de), both clinically applicable SPIOs **(Table 5),** were used for progenitor cell labeling. Cells were cultured in their appropriate medium until reaching confluence. Growth medium was replaced by fresh SPIO-containing medium (50-280 µg iron/mL) and cells were kept on regular culture conditions. Iron concentration within the labeling medium and labeling time were titrated to reach optimal labeling efficiency. To further enhance nanoparticle uptake, minor protocol modifications were made according to current puplications (Janic et al., 2009). Protamine sulfate (American Pharmaceutical Partners, Schaumberg, IL, www.appdrugs.com) a polycationic transfection agent containing more than 60% arginine was added to the cells in a concentration of 3 µg/mL together with SPIOs and serum-free RPMI-1640 medium was used for the first 15 minutes of labeling to exclude interactions between SPIO/protamin sulfate complexes and serum protein. After 15 minutes, equal volume of regular growth medium was added to the cultures and cells were further incubated for 24 hours.

Table 5. SPIOs use for progenitor cell labeling

Name	Producer	Fe-concentration in stem solution (mg/mL)	Mean hydrodynamic diameter (nm)	Core composition	Sheath composition
Resovist®	Bayer-Schering Germany	28	45-65	Fe_2O_3/Fe_3O_4	Carboxydextran
Endorem®	Guerbet France	12	80-150 Core: 50-75	Fe_2O_3/Fe_3O_4	Dextran

7.12.2 SPIO uptake visualisation and quantification

Single cell SPIO uptake was visualized using Prussian Blue staining and fluorescence microscopy. Cells were cultured either in small chamber slides, labeled and fixed with 4% formaldehyde (Sigma), or labeled cells were spun onto glass slide trypsinisation. For Prussian Blue staining, fixed cells were incubated with freshly

prepared staining solution containing 3% Potassium-Ferro-Cyanide mixed with equal amounts of 1% HCl for 10 minutes or until the iron particles were coloured blue. Cell nuclei were stained with nuclear fast red solution for 1-2 minutes and slides were mounted with appropriate mounting medium. A FITC-conjugated anti-dextran antibody (Stem Cells Technologies), binding the dextran sheath (see green mark in Table 5) of the applied nanoparticles was used for visualisation by fluorescence microscopy. Cell nuclei were counterstained using 4',6-**dia**midino-2-**p**heny**l**indole (DAPI) containing mounting medium (Vectorshield, Vector Labs). Pictures were taken on an Olympus BX51 upright microscopes equipped with a Color View III camera and Analysis B software (Olympus).

Flow cytometry was used for semi-quantitative evaluation of nanoparticle uptake. Enhanced cell granularity caused by intracellular SPIO accumulation was documented by comparing **s**ide **sc**atter properties (SSC-Height) of labeled cells and unlabeled controls. Cells were stained with an FITC-tagged anti-dextran antibody (Stem Cells Technologies) and fluorescence intensities were determined in FL-1 channel (FACSCalibur®, BD). Surface binding of dextran-containing nanoparticles (see green label in Table 5) or cytoplasmatic uptake was distinguished using cell permeabilization prior to Ab-staining (Fix and Perm, Invitrogen).

7.12.3 Transmission Electron Microscopy

(Performed together with Dr.Elisabeth Ingolic, Center for Electron Microscopy [FELMI], Graz University of Technology)

Sub-cellular SPIO distribution was investigated by transmission electron microscopy. Cells were fixed with 3% gluteraldehyde-cacodylate for one to 24 hours at 4°C, washed three times with 0.1 M sodium cacodylate buffer, fixed a second time with 1% osmium tetra oxide (OsO_4) for 2 hours at **r**oom **t**emperature (RT) and finally washed with distilled water. Fixed cells were re-suspended in 4% warm agarose and tranferred immediately to a glas slide for hardening. Once the agarosegel polymerized, small cubes were cut out and dehydrated with alcohol, propylene oxide and epon infiltration. After hardening in an epon mold for 48 hours at 60°C, the cell-agar pellets were sectioned and mounted on copper grids. The grids were stained in

1% uranyl acetate and lead citrate and specimens were imaged with a transmission electron microscope.

7.12.4 MRI phantoms

For evaluation of optimal labeling and determination of detection limits with MRI, we developed a phantom featured with properties that provide optimal human tissue comparable magnetic properties. Briefly, empty plastic balls (diameter: 4-7 cm) were filled with 1% **l**ow **m**elting **p**oint (LMP) agarose gel (Invitrogen) admixed with Gadolinium. Self-made metal cylinders were placed into the hardening agarose to leave space for cell placement. Equal amounts of cell suspension and 2% LMP agarose were resuspended to reach the final cell concentration in 1% LMP agarose. After gel formation and cylinder removal, cell suspensions were transferred into the left spaces, which were formed through cylinder removal.
For MRI of vascular networks, SPIO-labeled ECFCs were cultured on Matrigel (Millipore) in 2-well chamber slides (Nunc). After 24 hours of incubation, composite pictures of the formed networks were taken with a Zeiss microscope equipped with a motorized table to be capable of multi picture acquisition with subsequent aligning. Medium was removed and 1% LMP Agarose was put on top of the developed vascular network. For agarose polymerisation the panthoms were transferred to 4°C in the refrigerator.

7.12.5 MR image aquisistion

(Performed together with DI Clemens Diwoky and Prof. Rudolf Stollberger, Instiute for Medical Engineering, Graz University of Technology, MRI acquisition at 7T was tested together with Dr. Dieter Gross and Dr. Volker Lehmann, Bruker Biospin, Karlsruhe, Germany)

High resolution images at 3 and 7 Tesla (3T, 7T) systems were investigated and the impact of different field strength and gradient performance on the image quality was examined.

The scans were performed on a 3T Tim Trio (Siemens Medical, Germany, www.medical.siemens.com) clinical system with 38 mT/m gradient strength with a 18mm surface coil (Rapid Biomedical, Germany, www.rapidbiomed.com) and a 7T (Bruker BioSpin, Germany, www.bruker-biospin.com) system with maximum gradient performance of 1500 mT/m using a 25mm birdcage coil. After 2nd order shimming, 3D FLASH images were acquired with following parameters: 3T: 384x384 matrix, resolution 57x57x62 µm, TR/TE 200/14 ms, FA 20°, NSA 12; 7T: 384x384 matrix, resolution 57x57x78 µm, TR/TE 200/3.2 ms, FA 30°, NSA 4. A maximum intensity projection through the whole imaging volume was calculated in a postprocessing step performed with the use of ImageJ (NIH, USA).

7.13 Statistical analysis

Unless otherwise stated, data are shown as mean ± SEM. SPSS 15.0 software (SPSS Inc.; Chicago, IL; www.spss.com) for statistical analysis. After confirmation of normal distribution by Kolmogorov-Smirnov analysis ANOVA with Tukey's post hoc test was selected for further analysis. Homogeneity of variances was proofed by Levene Test. P-values < 0.05 were considered significant.

8 Results

The following results from the isolation, expansion and functional analysis of MSCs from human UCB have been published in:

Regenerative Medicine 2007 Jul;2(4):371-82.

Humanized system to propagate cord blood-derived multipotent mesenchymal stromal cells for clinical application.

See Appendix I

8.1 UCB-MSC propagation

A standardized procedure has been utilized to obtain MSCs from term UCB. Mean 3.5 ± 1.1 x 10^8 (range: 7.6 x 10^7 – 5.9 x 10^8) NC were recovered from 13 processed UCB samples. MSC cultures were successfully established in 6 of 13 samples (three with FBS- and three with pHPL-supplemented medium). A UCB sample volume > 40 mL correlated with a higher probability of successful outgrowth (p=0.018). We obtained a maximum of two to three colonies per UCB sample. Once established during 15-25 days of primary culture, UCB-MSCs from one flask were trypsinized and subsequently reseeded without counting for further expansion into three new flasks. After first passage (additional 14 days of culture), we obtained 2.4 ± 1.3 x 10^6 UCB-MSC^{HPL} and 3.2 ± 1.9 x 10^6 UCB-MSC^{FBS}. 3 x 10^5 UCB-MSC from each of the six MSC samples after primary passage were seeded for clinical scale expansion on one m^2 growth area (30 UCB-MSCs/cm^2; **Figure 2**).

We recovered 2.7 ± 1.8 x 10^8 UCB-MSC^{HPL} and 0.7 ± 0.2 x 10^8 UCB-MSC^{FBS} from clinical scale cultures. Results correspond to 8.5 ± 0.6 and 7.6 ± 0.2 population doublings over the 14 day culture period for UCB-MSC^{HPL} and UCB-MSC^{FBS},respectively **(Figure 3 A).**

Representative photographs of UCB-MSC cultures are shown in **Figure 3 B**.

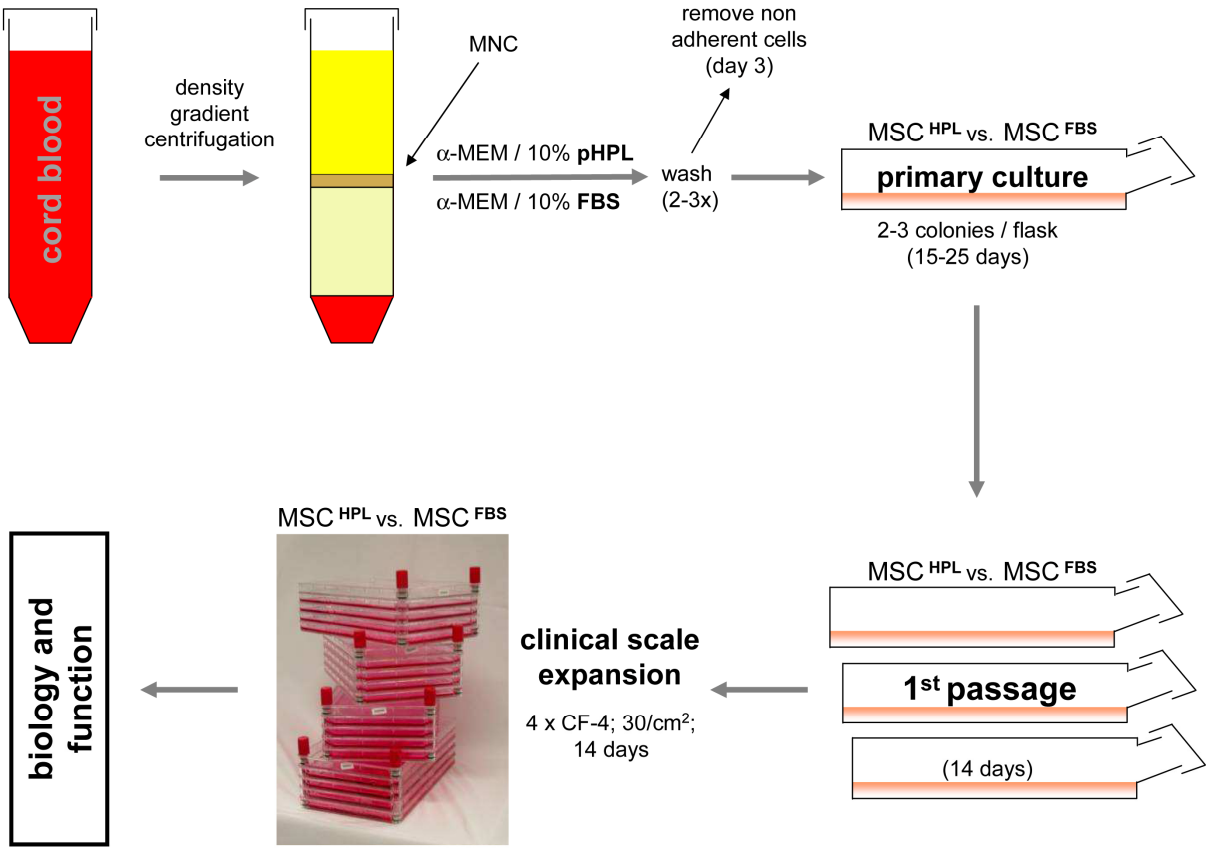

Figure 2. Three steps to clinical scale UCB-MSCs

The cartoon summarizes the essential steps for UCB-MSC culture. Primary culture was followed by a second expansion step (1st passage without MSC enumeration). 3 x 10^5 UCB-MSCs were seeded for the initiation of clinical scale expansions (third step).

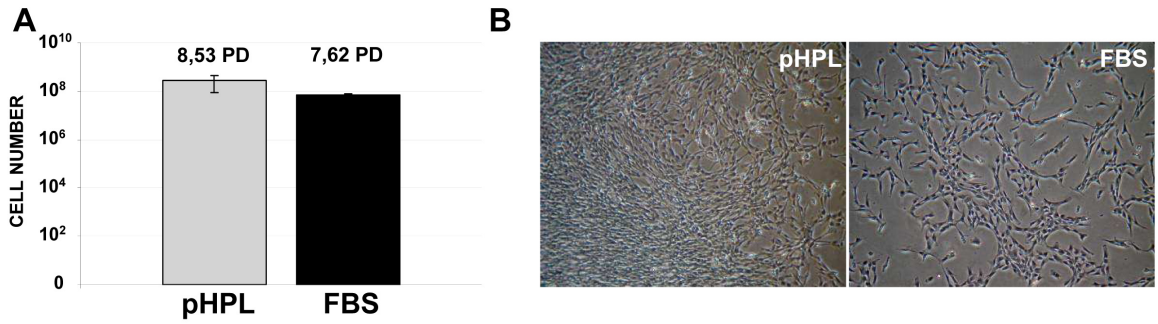

Figure 3: Growth characteristics of human MSC.

(A) Cell number and population doublings (PD) of UCB-MSC^{HPL} (grey bars) and UCB-MSC^{FBS} (black bars). Primary culture-derived UCB-MSCs were seeded with a density of 30/cm^2 for clinical scale expansion on 1m^2 culture area in 4 four-layered cell factories (CF-4). Mean ± SEM of three independent donors each per UCB-MSC^{HPL} and UCB-MSC^{FBS} are shown. (B) Representative picture (magnification: 40X) of UCB-MSC^{HPL} and UCB-MSC^{FBS} cultures.

These cells displayed a typical MSC immune phenotype without significant differences between UCB-MSC^{HPL} and UCB-MSC^{FBS} **(Figure 4)**.

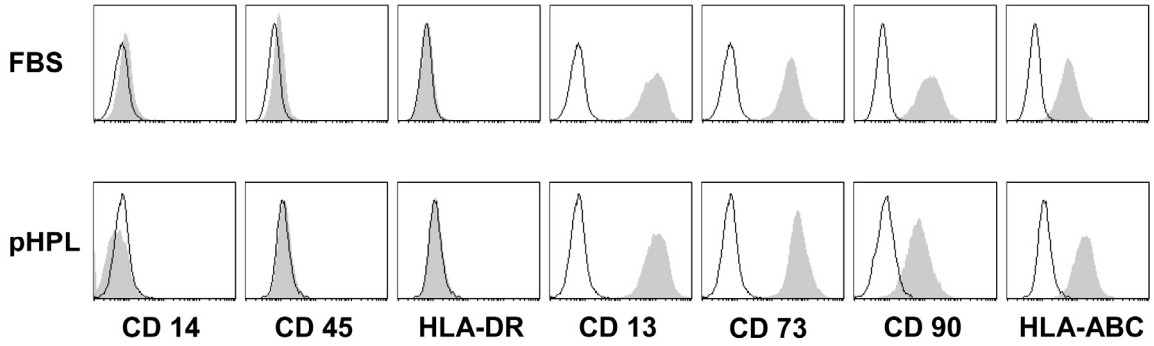

Figure 4: Representative immune phenotype of UCB-MSC.

The representative MSC marker profile was measured by flow cytometry. The grey filled histograms show mAb reactivity of UCB-MSC^{FBS} (upper panel) and UCB-MSC^{HPL} (lower panel). Black lines show the corresponding isotype control reactivity adjusted to mean fluorescence intensity (MFI) values of 10. One representative analysis of passage 2 UCB-MSCs is shown. No significant difference in marker expression has been found. Equal results were obtained with UCB-MSCs from 4 additional donors.

8.2 Long-term expansion

UCB-MSCs recovered after first passage were further cultured with a seeding density of 1/cm^2 for 5-6 additional passages to determine long term expansion yields in pHPL- and FBS-driven cultures. Rapid early MSC outgrowth was observed under both culture conditions. FBS was consistently more effective during later passages. Calculated cumulative cell yield was 4.7 ± 2.6 x 10^{14} UCB-MSC^{HPL} and 2.0 ± 1.6 x 10^{21} UCB-MSC^{FBS} **(Figure 5 A)**. Reduced proliferation in later passages was more pronounced in pHPL-supplemented cultures as evidenced also by dropping PDs (Figure 5 B). Cessation of proliferation over time was paralleled by reduction and final loss of CFU-F formation **(Figure 5 C-D).**

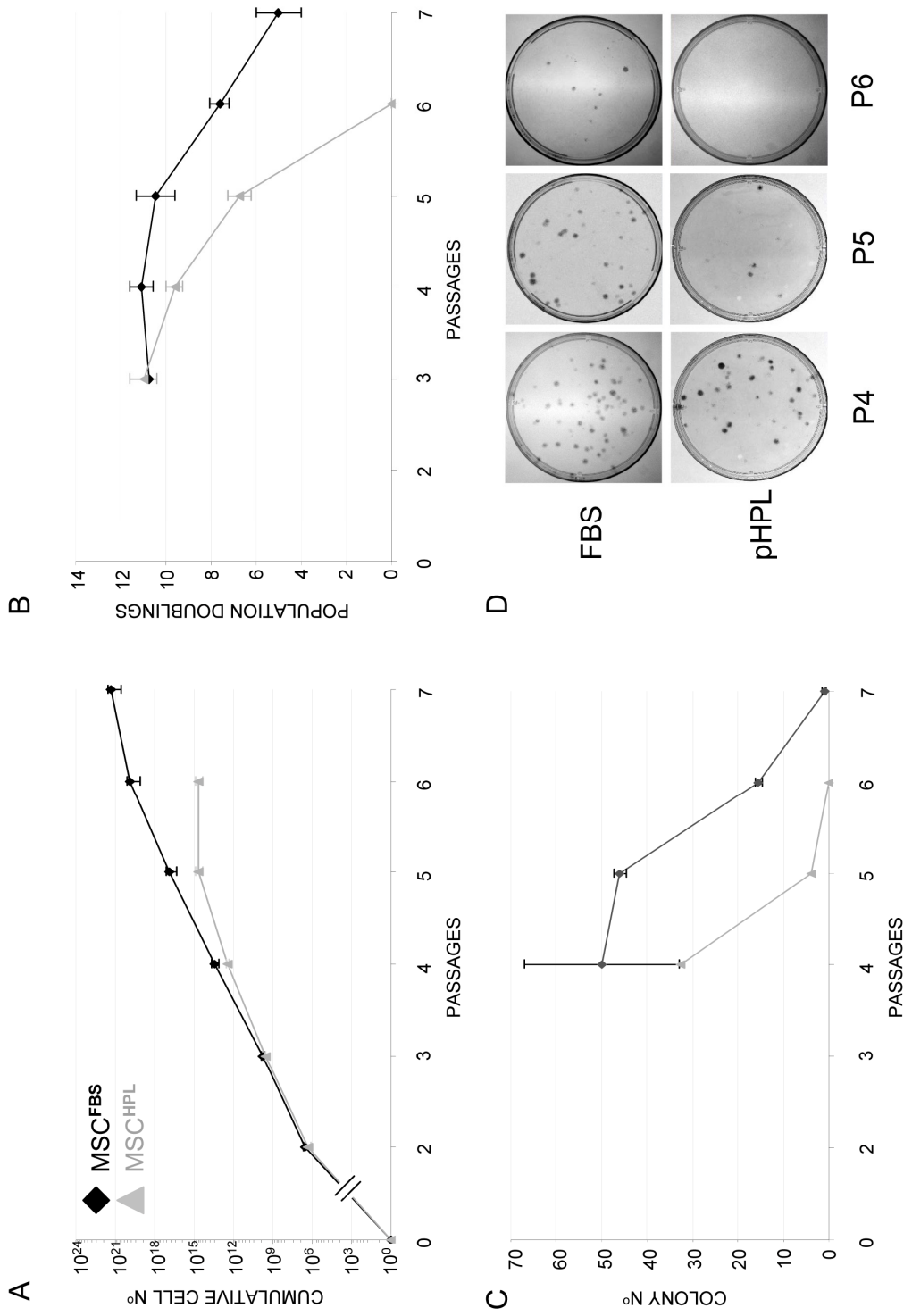

Figure 5. UCB-MSC long term expansion

(A) Mean ± SEM calculated cumulative number of UCB-MSCs recovered after low seeding density culture (1/cm2) with (▲) pHPL- or (♦) FBS-supplemented medium. **(B)** Population doublings over time. **(C)** CFU-F colony formation over time (n = 6). **(D)** Representative CFU-F of UCB-MSC^{HPL} and UCB-MSC^{FBS} cultures at defined passages are shown.

8.3 UCB-MSC functionality

To determine UCB-MSC differentiation potential, cells derived from clinical scale expansions were subjected to adipogenic, osteogenic and chondrogenic differentiation. Results obtained revealed that both UCB-MSC^{HPL} and UCB-MSC^{FBS} showed profound osteogenic and chondrogenic differentiation. UCB-MSCs propagated under both culture conditions showed only limited adipogenic differentiation **(Figure 6)**.

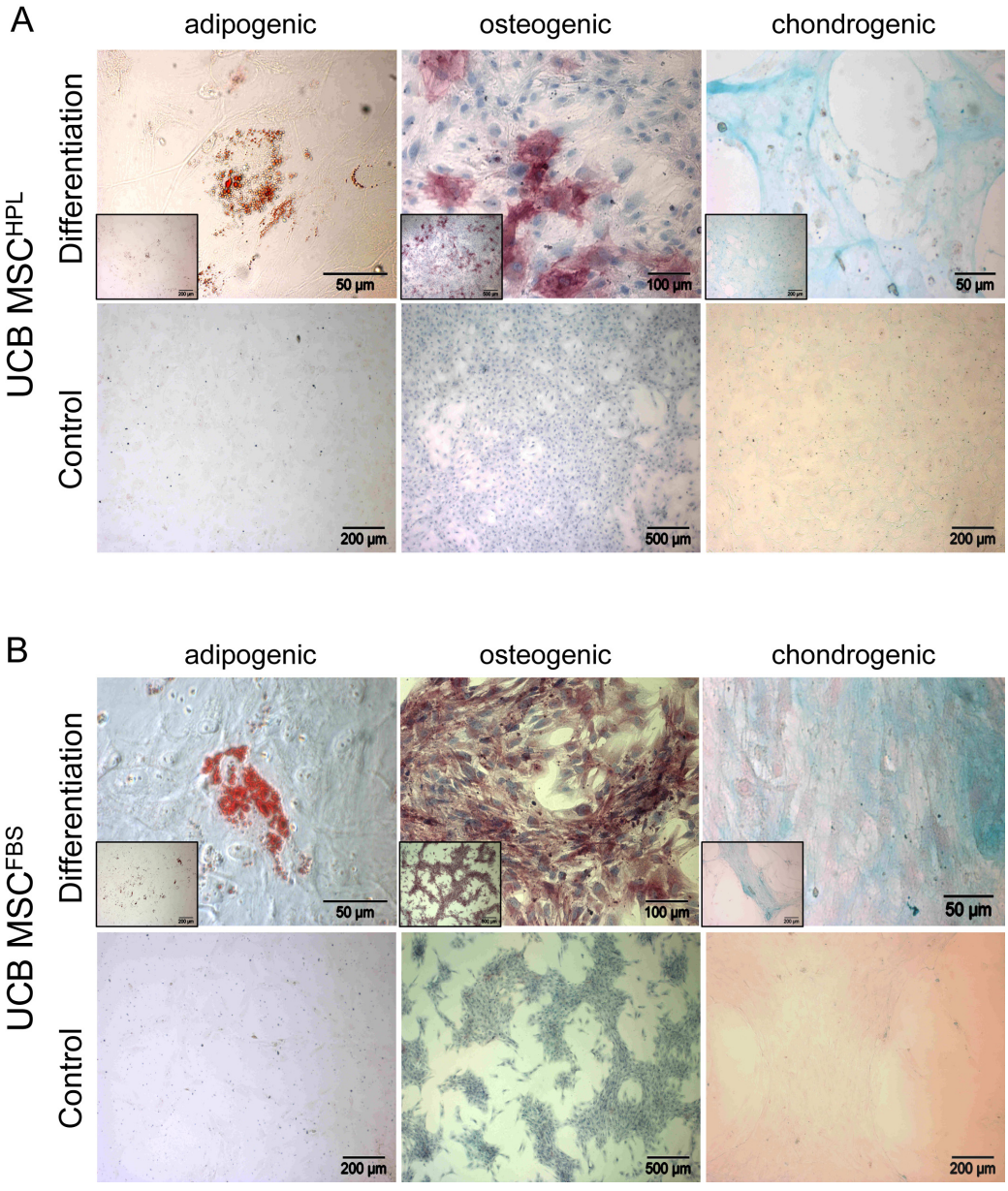

Figure 6: Adipogenic, osteogenic, and chondrogenic differentiation of UCB-MSCs.

(A) UCB-MSC^{HPL} as well as **(B)** UCB-MSC^{FBS} were induced to differentiate (upper rows) along adipogenic (left photographs, Oil Red O staining), osteogenic (middle photographs, Alkaline Phosphatase staining) and chondrogenic (right photographs, Alcian Blue staining) in comparison to the controls under appropriate stimulation (lower rows). Scale bars indicate magnification of photographs and high power inserts.

To further study the functionality of UCB-MSCs, three additional types of potency assays were performed. First, immune modulation was determined by culturing allogeneic CFSE-labeled MNCs in the absence or presence of UCB-MSCs. Control MNCs displayed stable CFSE label after four days of culture and an only minute increase in cell number from starting 3 x 10^5 to 4.2 ± 0.8 x 10^5/well. Addition of the mitogen PHA resulted in a four fold increase in mean cell number and an almost complete loss of CFSE label in the absence of MSCs. UCB-MSCs significantly inhibited mitogen induced MNC proliferation in a ratio of one MSC per ten MNCs ($p = 0.0007$ for UCB-MSC^{HPL} and $p = 0.03$ for UCB-MSC^{FBS}). UCB-MSCs^{HPL} were at least as efficient as UCB-MSCs^{FBS} ($p = 0.355$). At a 1:100 (MSC : MNC) ratio UCB-MSCs^{HPL} ($p = 0.0138$) but not UCB-MSCs^{FBS} ($p = 0.667$) significantly inhibited the PHA-induced MNC proliferation. UCB-MSCs did not induce proliferation of MNCs in the absence of PHA **(Figure 7)**.

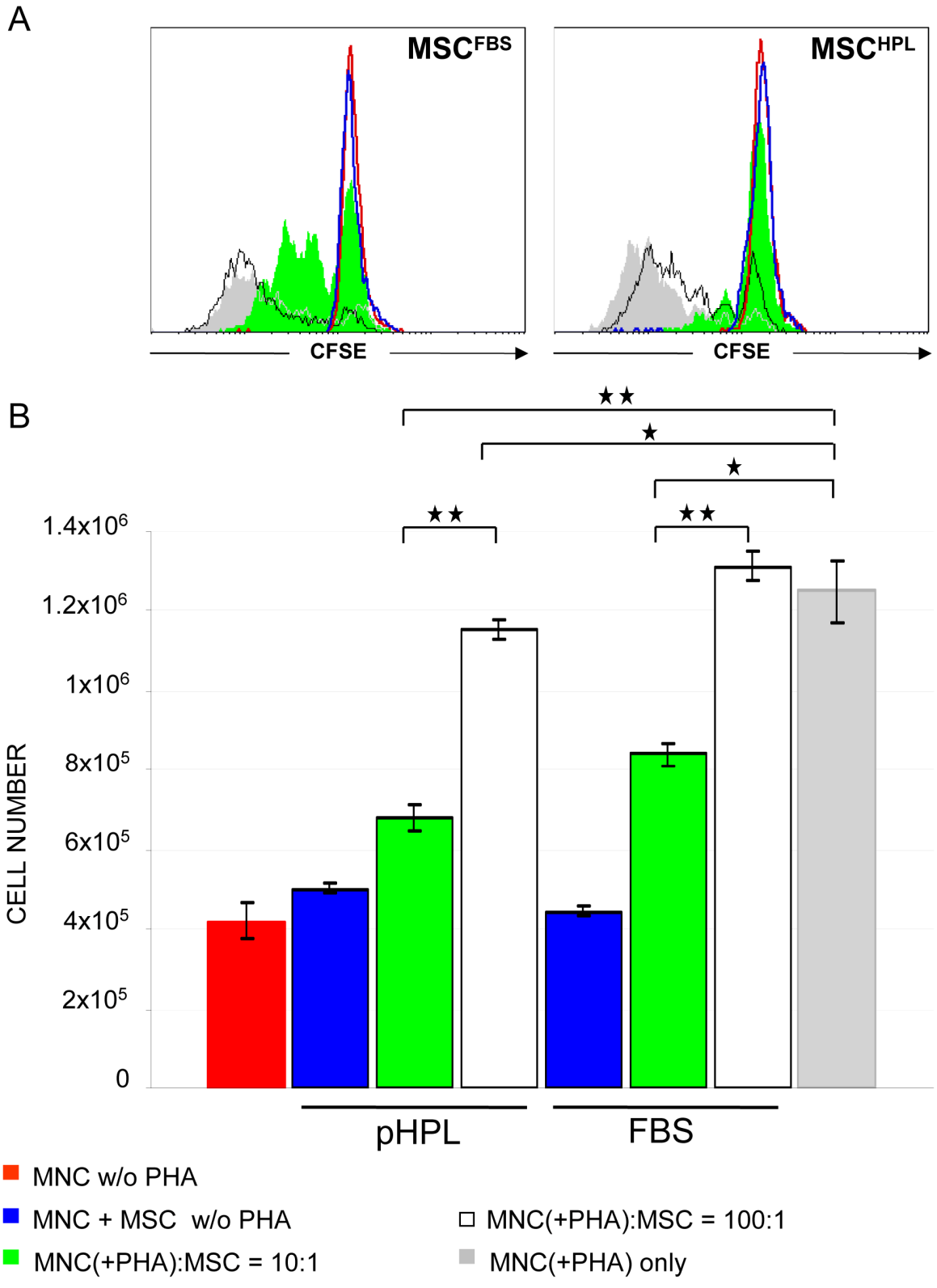
A
MSCFBS
MSCHPL
CFSE
CFSE
B
★★
★
★
★★
★★
1.4x10^6
1.2x10^6
1x10^6
8x10^5
6x10^5
4x10^5
2x10^5
0
CELL NUMBER
pHPL
FBS
MNC w/o PHA
MNC + MSC w/o PHA
MNC(+PHA):MSC = 10:1
MNC(+PHA):MSC = 100:1
MNC(+PHA) only

Figure 7. Immunemodulatory function of UCB-MSCs.

(A) Representative FACS histogram overlays. UCB-MSC^{HPL} (left overlay) or UCB-MSC^{FBS} (right overlay) were added in a 1:10 (3 x 10^4 MSCs to 3 x 10^5 MNCs/well; green filled histogram) or 1:100 (black line) ratio to test their influence on PHA (5 µg/mL) driven proliferation of allogeneic MNCs as monitored by CFSE expression. Mitogen stimulated MNCs without additional UCB-MSCs are shown in grey filled histograms with a grey line continuing over the green filled histograms. Red lines represent background proliferation without PHA stimulation. UCB-MSCs did not induce MNC proliferation (without PHA; blue line). **(B)** MNC proliferation (mean cell number ± SEM) of the same 5 groups and with the same color code as shown in **(A)**. Data were derived from co-culture pairs of MNCs from three different donors with two independent UCB-MSC^{HPL} (left) and two other UCB-MSC^{FBS} (right). Grey bars represent control cultures without UCB-MSCs. Red bars represent background MNC proliferation without PHA. Blue bars indicate lack of MNC proliferation in the presence of 10% UCB-MSCs without PHA. Significant differences are marked by asterisks (*$p < 0.05$ and **$p < 0.01$).

To measure the hematopoietic regulatory potential, sorted UCB-derived CD34$^+$ cells were stimulated with IL-3, Flt3-Ligand, SCF and GM-CSF in the absence or presence of MSCs. Cytokine-supplemented HSPC liquid cultures resulted in a 57-fold increase of **t**otal **n**ucleated **c**ells (TNCs) without UCB-MSCs compared to a mean 129-fold increase in the presence of UCB-MSC^{FBS} and 232-fold increase with UCB-MSC^{HPL}. UCB-MSC^{HPL} were slightly more efficient than UCB-MSC^{FBS} in stimulating proliferation of CD34$^+$ and CD34$^+$/CD38$^-$ cells **(Figure 8 A-D)**.

Third, vascular-like network formation of UCB-MSCs was evaluated in a matrigel-assay. Positive control UCB-derived ECFCs were capable to build three dimensional vascular-like networks within 12-24 h *in vitro*. UCB-MSC^{HPL} were at least as efficient as UCB-MSC^{FBS} in network formation, which may be related to a putative pericyte function **(Figure 8 E)**.

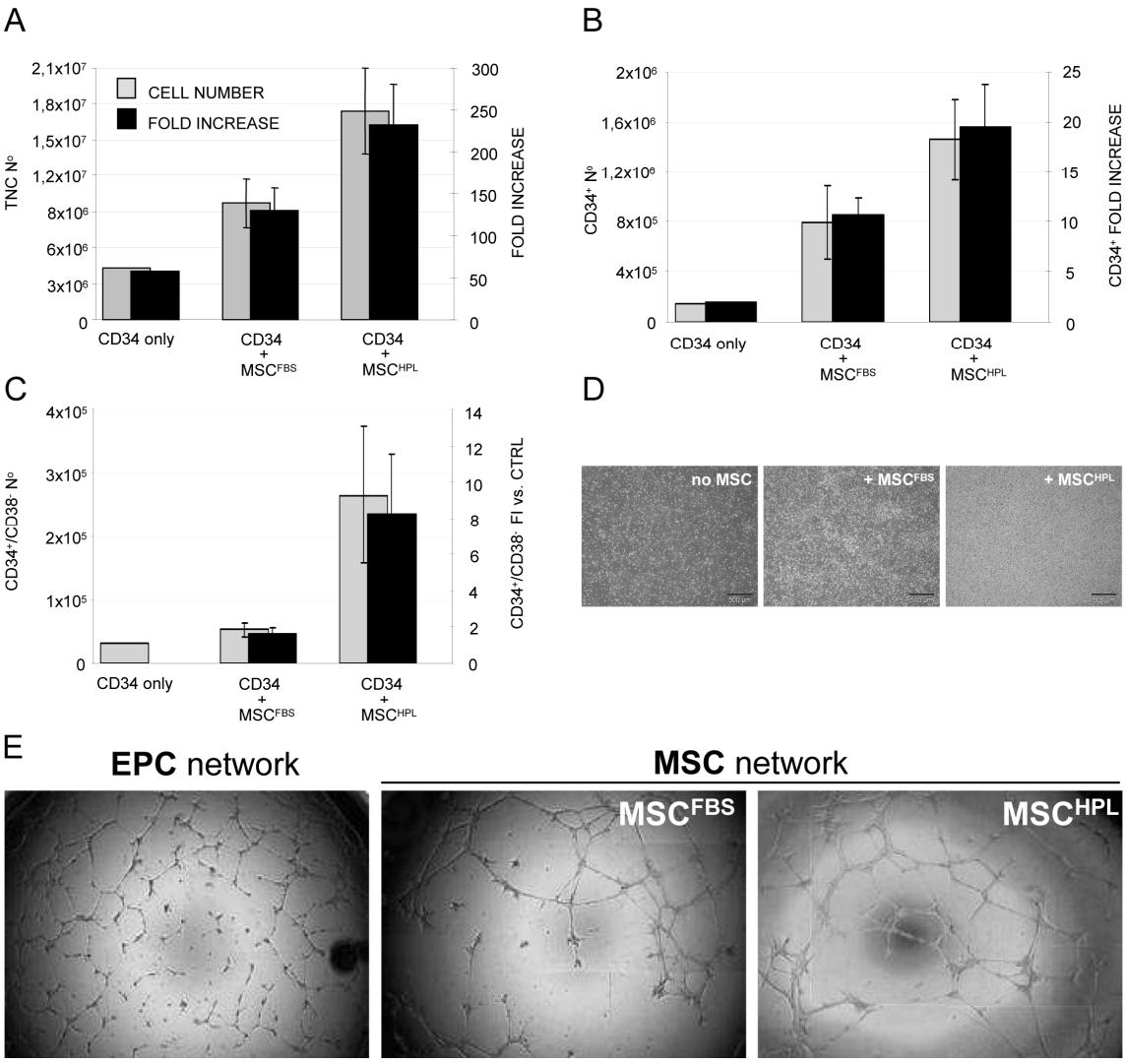

Figure 8. Hematopoietic and vascular support function.

(A) UCB-derived sorted $CD34^+$ cells were expanded in cytokine supplemented medium (RPMI-1640/10% FBS/GM-CSF/IL-3/SCF/Flt-3L) in the absence or presence of clinical scale expanded UCB-MSCs. Grey bars show harvested cell number and black bars show the fold increase of cell number compared to the starting $CD34^+$ cell number. **(B)** Harvested number of $CD34^+$ cells (grey bars) and fold increase (black bars) of $CD34^+$ cells after liquid culture with or without UCB-MSC support **(C)**. Harvested number (N°) of $CD34^+/CD38^-$ cells (grey bars) and fold increase (FI) of $CD34^+/CD38^-$ cells after liquid culture with UCB-MSC^{FBS} or UCB-MSC^{HPL} support compared to cytokine-supplemented liquid cultures in the absence of UCB-MSCs. (A-C, mean ± SEM of two independent expansions) **(D)** Representative culture appearance. **(E)** Two-dimensional vascular-like network formation by control UCB-derived endothelial colony forming progenitor cells (ECFCs) compared to UCB-MSC^{FBS} and UCB-MSC^{HPL}.

The results for translation of pHPL use to PB- and UCB-ECFC isolation, clinical-grade expansion, characterization and detailed *in vitro* as well as *in vivo* analysis of ECFCs have been published in:

Blood. 2009 Jun 25;113(26):6716-25. Epub 2009 Mar 25.

Humanized large-scale expanded endothelial colony-forming cells function *in vitro* and *in vivo*.

See Appendix II

8.4 Recovery of ECFCs from peripheral blood and large-scale propagation in an animal protein-free humanized system

The abandonment of animal-derived substitutes is considered to be a critical prerequisite for standardized clinical scale propagation of human cells intended for transplantation purposes (Rohde E et al., 2008a). Based on the previously demonstrated efficacy of animal serum-free large-scale clinical-grade propagation of MSCs from human BM and umbilical UCB, we hypothesized that endothelial lineage cells may also be propagated efficiently without animal serum (Reinisch et al., 2007, Schallmoser et al., 2007b, Schallmoser et al., 2008). In an initial set of experiments, we established that pHPL can replace FBS in standard cultures of established **h**uman **u**mbilical **v**ein **e**ndothelial **c**ells (HUVECs) and ECFCs derived from human UCB resulting in at least comparable colony outgrowth and proliferation **(Figure 9)**. Therefore, all subsequent experiments were performed in EGM supplemented with 10% pHPL.

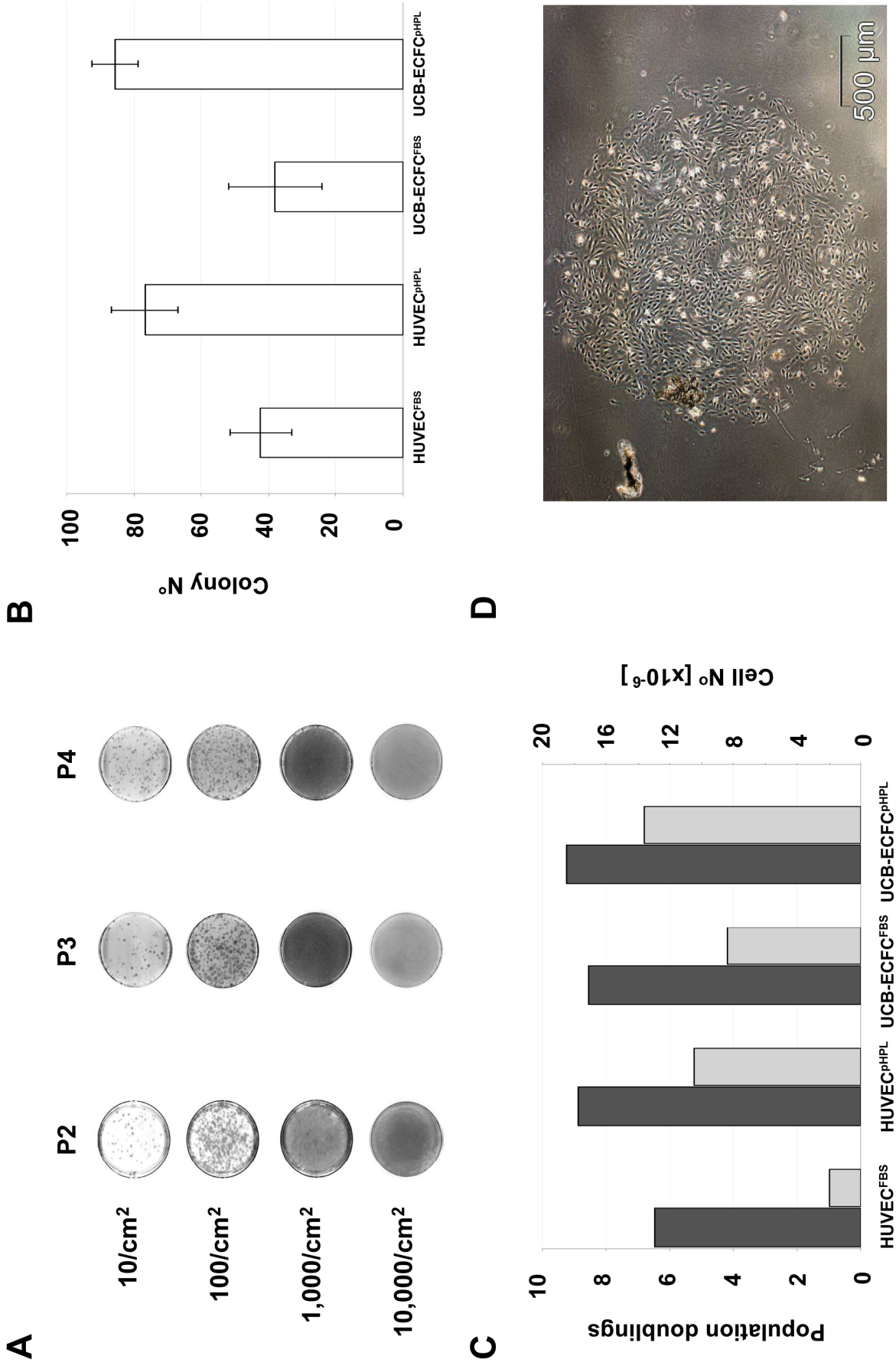
A
P2
P3
P4
10/cm²
100/cm²
1,000/cm²
10,000/cm²
B
Colony N°
0
20
40
60
80
100
HUVEC^FBS
HUVEC^pHPL
UCB-ECFC^FBS
UCB-ECFC^pHPL
C
Population doublings
0
2
4
6
8
10
Cell N° [x10⁻⁶]
0
4
8
12
16
20
HUVEC^FBS
HUVEC^pHPL
UCB-ECFC^FBS
UCB-ECFC^pHPL
D
500 µm

Figure 9. Animal serum-free culture, countability of endothelial colony density and cobblestone morphology of blood- and vessel-derived ECFCs.

(A) Serial ten-fold dilution experiment starting from 10,000 cells/cm^2 down to 10 cells/cm^2 of peripheral blood-derived ECFCs over 3 passages (P2, P3 and P4) in 55cm^2 culture plates with pooled human platelet lysate (pHPL) supplemented endothelial growth medium-2 (EGM-2).
10 cells/cm^2 (1st horizontal row) showing consistently separated colony density over the whole observation period. Plates with higher cell densities (2nd, 3rd and 4th row) were not countable even in higher electronic magnification of digitalized images due to an increasing degree of colony confluence with rising ECFC seeding density. **(B,C)** In another series of experiments, human umbilical vein endothelial cells (HUVEC) and umbilical cord blood-derived endothelial colony forming progenitor cells (UCB-ECFCs) were cultured as described under standard conditions in EGM-2/10% FBS (HUVEV^{FBS} & UCB-ECFC^{FBS}). For comparison, equal aliquots were cultured under animal serum-free conditions in EGM-2 supplemented with pooled human platelet lysate (pHPL) fully replacing FBS (HUVEV^{HPL} & UCB-EPC^{HPL}). **(B)** Colony number was determined in low density cultures (HUVEV^{FBS} & UCB-EPC^{FBS} vs. HUVEV^{HPL} & UCB-EPC^{HPL}). **(C)** Cell numbers (grey bars and right axis) and population doublings (black bars and left axis) are shown. **(D)** Global view on a typical medium – sized blood – derived ECFC colony at day 20 of primary culture. Magnification is indicated by scale bar insert.

In addition, standard procedures for EPC propagation strictly depend on coating the culture surface with matrix protein mostly of animal origin which may limit medical applicability (Solovey et al., 1997, Ingram et al., 2004, Melero-Martin et al., 2007, Rohde et al., 2007, Au et al., 2008). For that reason, we determined in a further step whether collagen coating is essential for the recovery of ECFCs. MNCs derived from the steady-state PB of six healthy volunteers were split and seeded onto either collagen-coated or uncoated tissue culture surfaces. The first colonies were detected after mean 9.4 ± 1.1 days in collagen-coated compared to 8.6 ± 0.5 days in uncoated cultures **(Figure 10A)**. No significant difference was observed in the number of colonies recovered under either condition (0.5 ± 0.2 versus 0.7 ± 0.4, **Figure 10B**). In a further series of experiments we tested whether density gradient separation of MNCs from PB was necessary to recover ECFCs. Seeding non separated whole blood which had just been diluted in EGM-2/10% pHPL on uncoated culture surface resulted in a delay in colony detection, but an almost eight fold significant rise in recovered ECFC colonies compared to MNC separation. We recovered a mean of 4.0 ± 0.8 colonies with typical cobblestone morphology per one milliliter of unseparated whole blood compared to less than one colony per milliliter after density

gradient separation. Reproducibility of this procedure was confirmed by propagating ECFCs from the same six volunteers in a technical replicate.

Based on previous experience with UCB-derived ECFCs propagated in conventional FBS-supplemented cultures (Rohde et al., 2006), we also succeeded in generating ECFCs under animal protein-free conditions from unseparated UCB in seven of seven samples. Because CVD represents the most important target for ECFC research and vascular regenerative therapy, unseparated PB from seven patients with stable CVD was utilized for ECFC recovery experiments as a proof of principle. First colonies were detected after mean 9.1 ± 5.6 days in uncoated cultures. The mean colony number of 2.6 ± 0.8 recovered per one mL did not show significant differences compared to the healthy control volunteers (4.0 ± 0.8, **Figure 10A,B**). Once established, colonies increased rapidly in size indicating a high proliferation rate **(Figure 10C-J)**. As a result, in six independent primary cultures a mean of 6.9 ± 2.8 x 10^4 oligoclonal ECFCs were harvested after 7-19 days of primary culture originating from one milliliter of normal unmanipulated PB. In comparison, a separate series of experiments was performed by seeding PB in six-well plates with a 10 cm^2 growth area to select for monoclonal colony growth by limited dilution. After primary culture, 3,000-38,000 ECFCs were harvested from four single ECFC clones from three donors after two weeks. For reasons of practicability, the scale-up for large-scale cultures was performed with oligoclonally-derived ECFCs available in higher quantity.

Based on previous experience with optimizing large-scale MSC expansion (Bartmann et al., 2007b, Reinisch et al., 2007, Schallmoser et al., 2007b, Schallmoser et al., 2008), we seeded oligoclonal ECFCs derived from 13 - 30 colonies from healthy volunteers after primary culture in a low density of 18 to 100 cells/cm^2 into two 2,528 cm^2 cell factories per culture sample. In four out of six cases we obtained > 1 x 10^8 ECFCs after 11-25 days of large-scale culture representing 7.6-10.2 population doublings. Two other cultures that were initiated from a starting cell density of 27 cells/cm^2 generated 2.7 x 10^7 and 3.4 x 10^7 after 25 and 20 days, respectively. Large-scale expansions of primary ECFCs (16-33 colonies) from three CVD patients did not show significant differences in final cell number compared to healthy volunteers **(Figure 10K).**

The highest long-term proliferation resulting in 36.8 ± 2.9 and 35.7 ± 2.4 cumulative population doublings was seen after long-term culture initiated with ECFC seeding densities of 10 and 100 cells/cm^2, respectively. Reduced proliferation was observed in long-term cultures initiated from more conventional seeding densities of 1,000 and 10,000 cells/cm^2 resulting in 31.4 ± 1.9 and 30.7 ± 2.2 cumulative population doublings, respectively **(Figure 10L)**. This indicates that the influence of cell seeding density on ECFC proliferation was preserved during long-term culture as previously observed for MSCs from human BM and UCB (Reinisch et al., 2007, Schallmoser et al., 2007b).

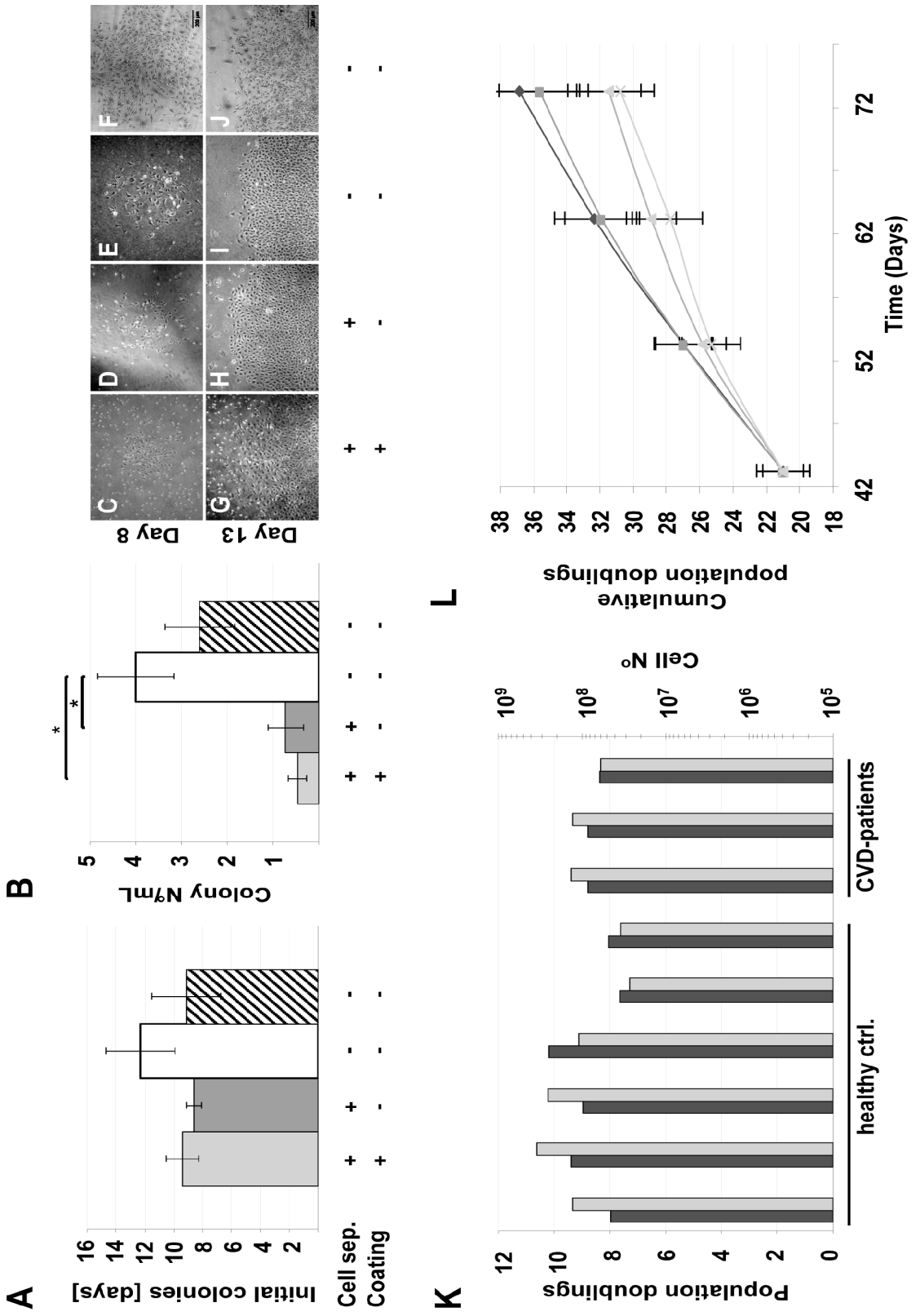
A
Initial colonies [days]
16
14
12
10
8
6
4
2
Cell sep.
Coating
+ + - -
+ - + -
B
Colony N°/mL
5
4
3
2
1
*
*
+ + - -
+ - + -
C D E F G H I J
Day 8
Day 13
+ + - -
+ - + -
K
Population doublings
12
10
8
6
4
2
0
healthy ctrl.
CVD-patients
Cell N°
10⁹
10⁸
10⁷
10⁶
10⁵
L
Cumulative population doublings
38
36
34
32
30
28
26
24
22
20
18
42
52
62
72
Time (Days)

Figure 10. ECFC recovery from human steady-state peripheral blood in an animal serum-free humanized system.

(A,B) Peripheral blood from healthy volunteers was density gradient-separated (**+**) to enrich for mononuclear cells (light grey) or immediately diluted (open bars) and seeded in EGM/10%pHPL in 75cm^2 cell culture flasks. Culture surfaces were coated (left light grey) with collagen only when indicated (**+**). Peripheral blood from patients with stable cardiovascular disease was also immediately diluted and seeded in EGM/10%pHPL (hatched bars). **(A)** The initial appearance of visible colonies was determined by daily culture observation. **(B)** Colony number was counted at the end of the primary 7-19-day culture period. Results are shown as mean ± SEM of six independent experiments. Asterisks denote statistically significant differences (*$p < 0.05$). **(C-J)** Representative early colonies (day 8) and parts of large expanded colonies (day 13) from healthy volunteers are depicted with 40x initial magnification corresponding to different recovery strategies as indicated. **(K)** Population doublings (dark grey) and expanded cell number (light grey bars) determined after large scale expansion of ECFCs from six healthy volunteers (healthy ctrl.) and three CVD patients are shown. **(L)** Cumulative population doublings (mean ± SD) as obtained during large scale expansion of ECFCs from six healthy volunteers after large scale expansion are shown. Large-scale expansion-derived cells bear a history of mean 21 population doublings before initiating long term culture at cell seeding densities of 10 (filled diamond), 100 (filled square), 1,000 (filled triangle) and 10,000 cells/cm^2 (x). Cells were reseeded during long term culture at indicated time points according to their initial seeding density.

8.5 Preserved ECFC phenotype, proliferation, progenitor hierarchy and genomic stability after large-scale expansion and cryopreservation

Proliferating ECFCs showed the typical cobblestone morphology of endothelial lineage cells (ECs) *in vitro* **(Figure 9D, Figure 10C-J).** Immune profiling by flow cytometry revealed the homogeneous reactivity of consistently more than 95% of the generated cells with monoclonal antibodies directed against human EC lineage marker molecules after large-scale expansion and before cryopreservation. Cultures contained less than 0.1% contamination with $CD45^+$ hematopoietic cells after large-scale propagation **(Figure 11A)**. Immune phenotype was unchanged after freezing, thawing and additional culture of cryopreserved ECFCs and was comparable to UCB-derived ECFCs, HUVECs and **h**uman **m**icro**v**ascular **EC**s (HMVECs) **(Figure 12)**. Immune cytochemistry confirmed CD144 (**v**ascular **e**ndothelial **c**adherin; [VE-Cadherin]) and CD146 (**m**elanoma and endothelial **c**ell **a**dhesion **m**olecule; [MCAM]) surface expression and demonstrated endothelial Weibel-Palade body-specific anti-von Willebrand factor and mesoderm-specific anti-vimentin antibody reactivities in appropriate subcellular localization as well as typical diffuse CD31 (**p**latelet-**e**ndothelial **c**ell **a**dhesion **m**olecule; [PECAM-1]) staining pattern **(Figure 11B-F)**. Isotpype control staining was negative in the concentration used in this experiment **(Figure 11G).**

Figure 11. Phenotypic characterization of large-scale expanded ECFCs.

(A) Representative flow cytometry histograms of ECFCs after humanized large-scale expansion showing reactivity with EC-expressed marker molecules (right shifted filled grey curves compared to black lined open curves of the appropriate isotype controls) and lack of reactivity with hematopoietic (CD14 and CD45) and stem cell-associated (CD90 and CD133) or activation (human leukocyte antigen class II type DR, HLA-DR) markers. (B-G) Representative cellular localization of (B) mesodermal cytoskeleton component Vimentin, (C) CD146/MCAM detected by prototype antibody P1H12, (D) CD144/VE-cadherin, (E) endothelial von Willebrand factor (vWF), (F) hematopoietic stem cell and vascular EC-specific CD31/PECAM-1, as compared to (G) one representative isotype control example. ECFCs were cryopreserved after large-scale expansion and thawed before seeding in chamber slides to obtain adherent cells for cytochemistry. Staining was done as specified. Brown color

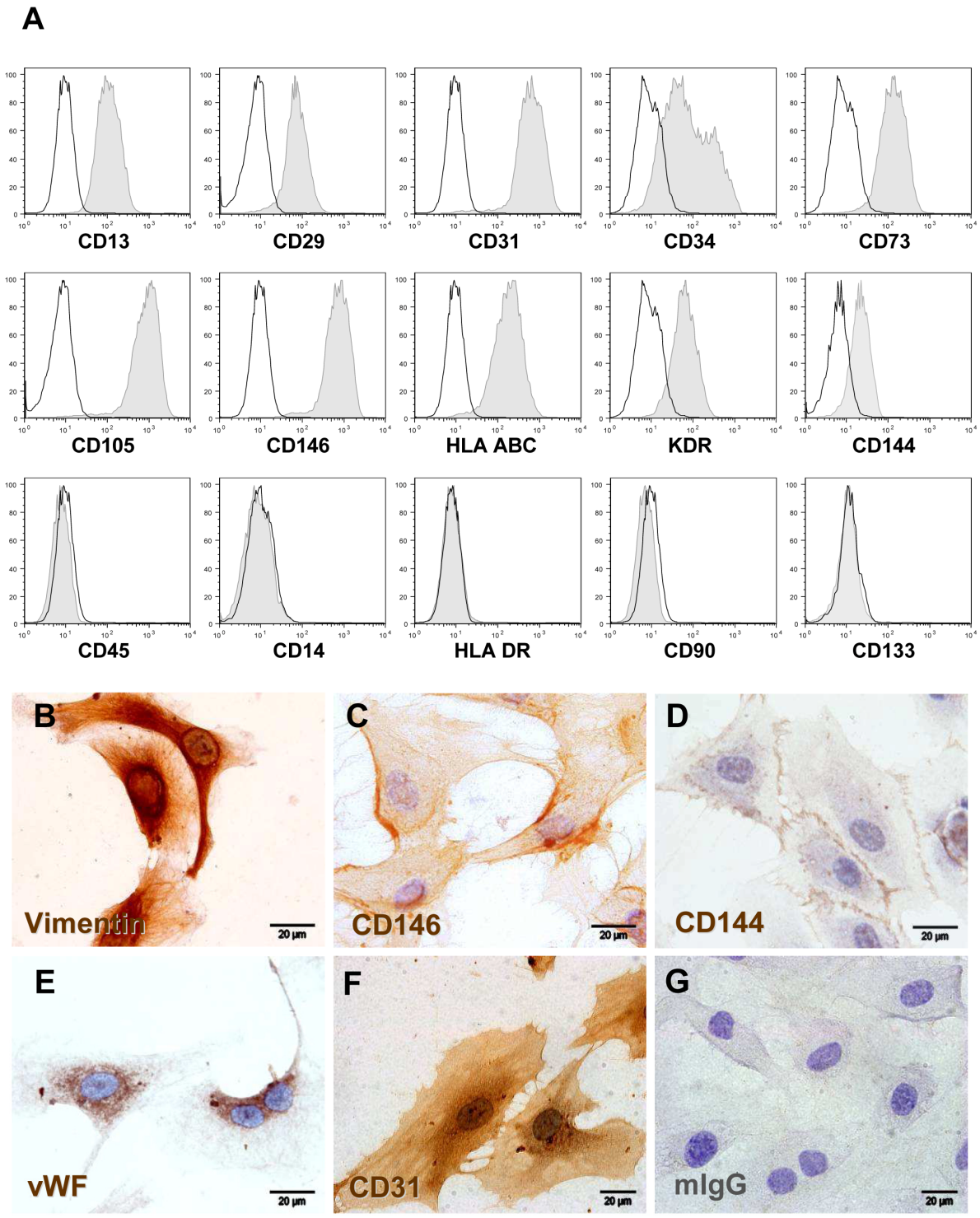

results from precipitation of the chromogen diaminobenzidine (DAB) mediated by antibody binding to the target molecule.

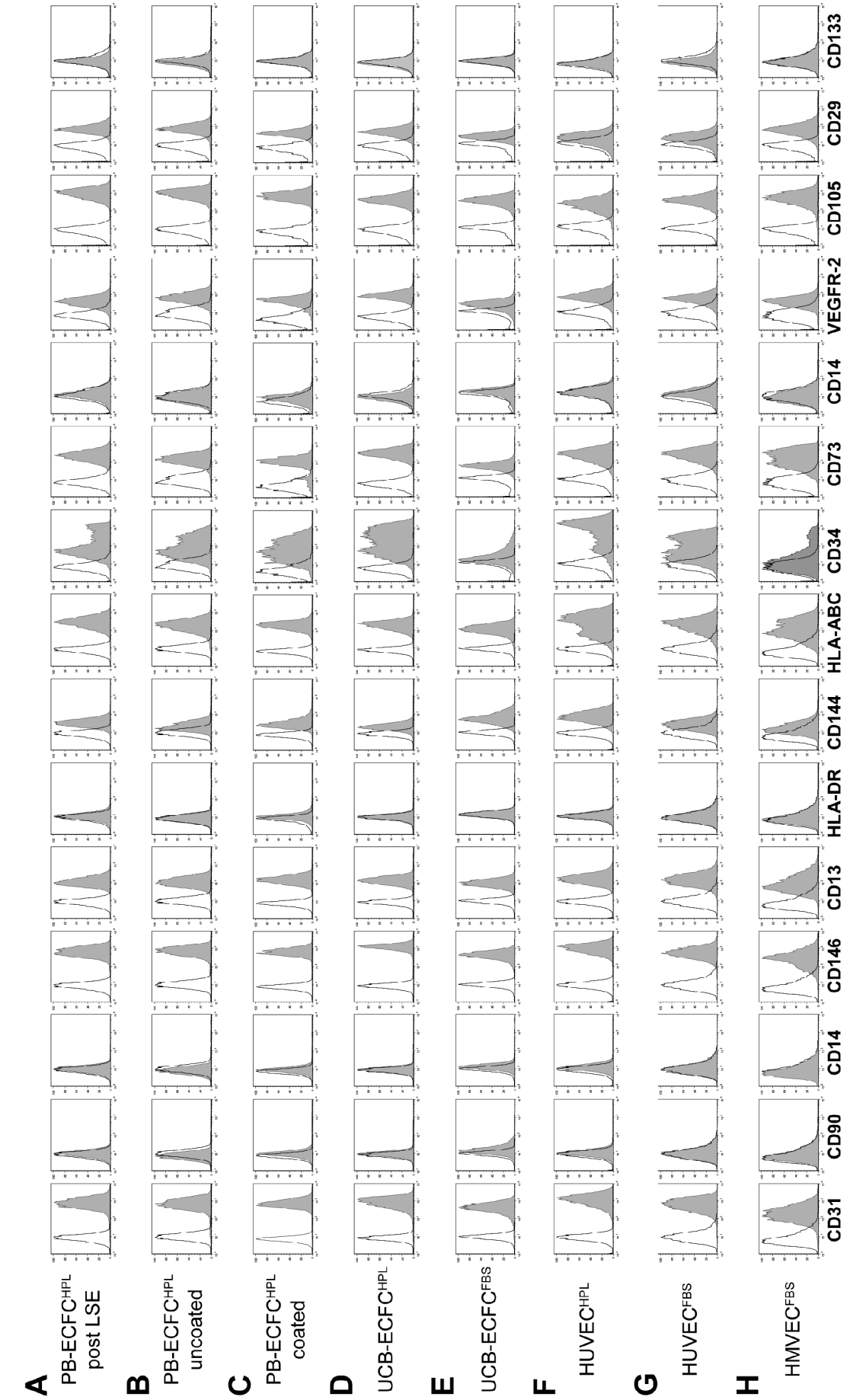
A
PB-ECFC^{HPL} post LSE
B
PB-ECFC^{HPL} uncoated
C
PB-ECFC^{HPL} coated
D
UCB-ECFC^{HPL}
E
UCB-ECFC^{FBS}
F
HUVEC^{HPL}
G
HUVEC^{FBS}
H
HMVEC^{FBS}
CD31
CD90
CD14
CD146
CD13
HLA-DR
CD144
HLA-ABC
CD34
CD73
CD14
VEGFR-2
CD105
CD29
CD133

Figure 12. Flow cytometry immune phenotyping of blood- and vasculature-derived ECFCs.

Flow cytometry was performed as described in the methods section to determine the immune phenotype of different types of ECFCs and ECs as indicated. Representative reactivity of monoclonal antibodies with endothelial lineage marker molecules (right shifted filled grey curves compared to black lined open curves of the isotype matched control antibody) CD31 (PECAM-1), CD146 (MCAM), CD13, CD144 (VE-Cadherin), HLA-ABC (human leucocyte antigen class I ABC), CD34, CD73, VEGF receptor type 2 (KDR), CD105 and CD29. No reactivity with hematopoietic marker CD45 (common leukocyte antigen) and CD14 (monocytes), activation marker HLA-DR or stem cell-associated markers CD90 and CD133. **(A-C)** Peripheral blood (PB)-derived ECFCs cultured in animal serum-free pooled human platelet lysate (pHPL)-supplemented EGM as described within this thesis **(A)** isolated under modified conditions (no coating, no cell separation) and analyzed after cryopreservation and thawing after large-scale expansion. **(B)** Immune phenotype of PB ECFCs isolated on uncoated or **(C)** collagen-coated culture vessel plastic. Direct comparison of the immune phenotype of umbilical cord blood-derived ECFCs (UCB ECFCs) with human umbilical vein endothelial cells (HUVECs) after culture **(D,F)** in the presence of pHPL as compared to **(E,G)** fetal bovine serum (FBS). **(H)** Flow cytometry of human microvascular endothelial cells (HMVECs) cultured under FBS conditions.

One hallmark of ECFC biology is the presence of a hierarchy of progenitor cells in any given ECFC population resulting in the appearance of colonies of different size and cell number under specific culture conditions *in vitro* (Ingram et al., 2004, Ingram et al., 2005b, Yoder et al., 2007, Hirschi et al., 2008). In initial experiments, we noted that colony number and total cell recovery were higher than expected under our optimized culture conditions with pHPL replacing FBS compared to published data (Solovey et al., 1997, Ingram et al., 2004). To test for long-term colony formation, culture products after subsequent passages were diluted in ten-fold serial dilution steps starting from 10,000 down to 10 ECFCs/cm^2. Results revealed countable colony frequencies only in assays initiated with 10 ECFCs/cm^2 **(Figure 9A)**. To determine clonogenicity, endothelial colonies derived from the cryopreserved cells of six donors after large-scale propagation were subjected to a precise colony analysis after large-scale expansion using ImageJ software (Reinisch and Strunk, 2009). We found that the entire hierarchy of low and high proliferative potential (LPP and HPP) (Ingram et al., 2004) progenitors was maintained in all samples. As expected, large HPP colonies matured during the final culture phase between d10-d14 at the expense of smaller ones **(Figure 13A)**.

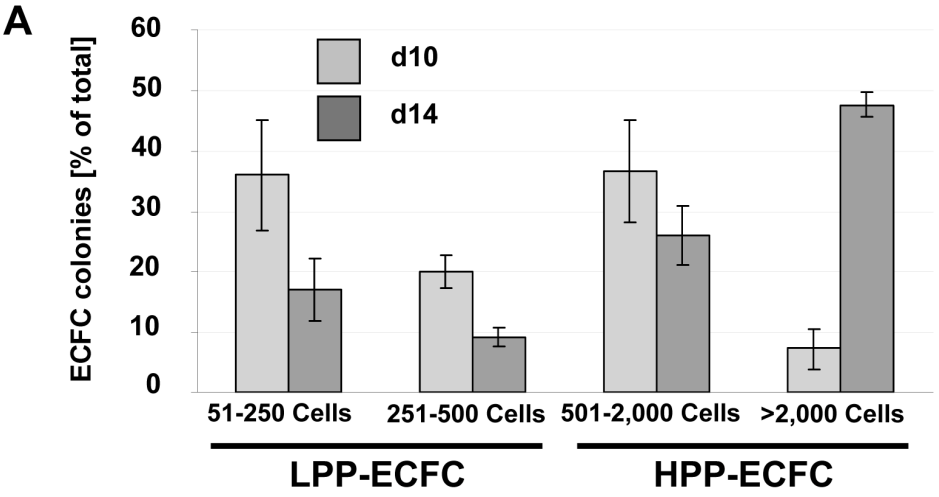
A
ECFC colonies [% of total]
60
50
40
30
20
10
0
d10
d14
51-250 Cells
251-500 Cells
501-2,000 Cells
>2,000 Cells
LPP-ECFC
HPP-ECFC

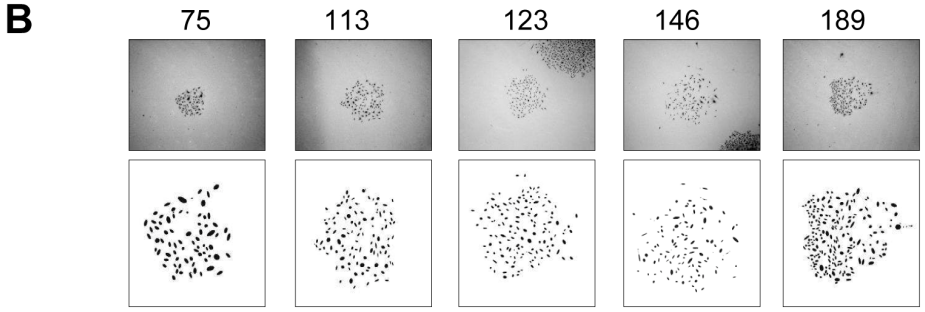
B
75
113
123
146
189

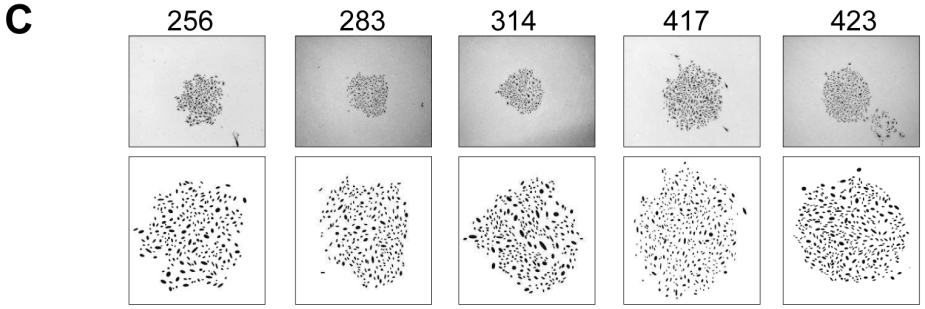
C
256
283
314
417
423

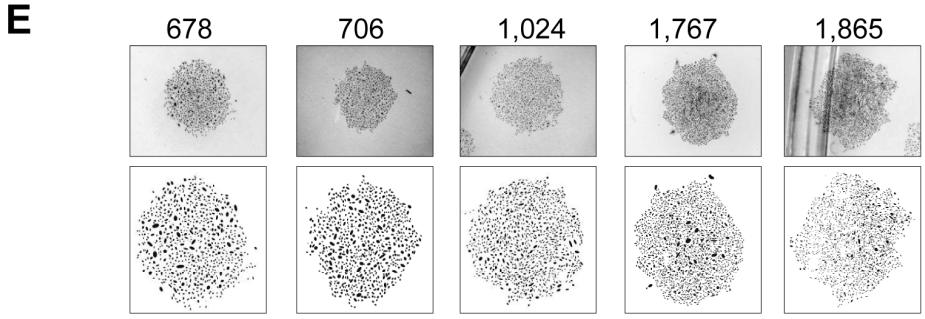
E
678
706
1,024
1,767
1,865

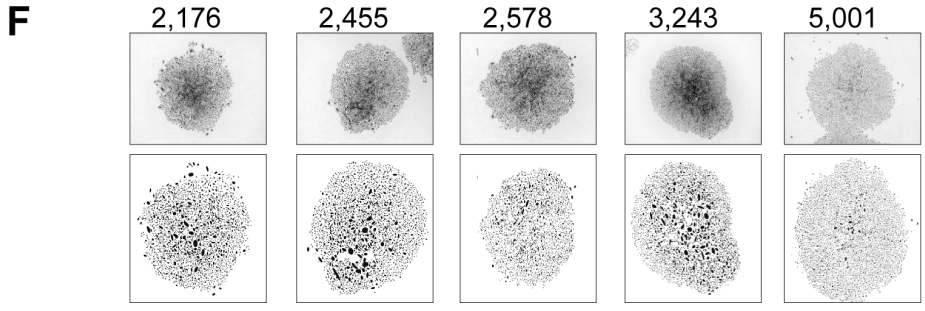
F
2,176
2,455
2,578
3,243
5,001

Figure 13. ECFC clonogenicity and precise cell enumeration of EFCF colonies.

ECFCs after large-scale expansion (LSE) representing ≥20 population doublings of the colony-initiating cells were subjected to an endothelial colony assay in triplicates in a seeding density of 10 ECFCs/cm^2 in EGM/10% pHPL. **(A)** Colony assays were performed with ECFCs from three different donors each for ten (light grey bars) or 14 days (dark grey bars). Colony plates were then fixed and stained before photo documentation. Precise cell numbers of all imaged colonies were counted in ImageJ software (Reinisch and Strunk, 2009). Examples of stereomicroscopic images (upper-row photographs) and resulting translated images of countable cells after using the ImageJ software particle analysis tool (lower-row pictures). Colonies of different sizes representing the entire range of the four categories are shown. **(B)** 51-250 and **(C)** 251-500 were summarized as low proliferative potential ECFC (LPP-ECFC) whereas **(D)** 501-2,000 and **(E)** >2,000 cells per colony were defined as high proliferative potential ECFC (HPP-ECFC), respectively. Exact numbers under each photograph/transformed image pair indicate results of automated colony cell counts.

Karyotyping of early cultures showed normal chromosome content of ECFC progeny recovered from female and male volunteers **(Figure 14A)**. Array CGH profiles of the same two PB derived ECFC samples compared to the corresponding constitutional white blood cell profiles **(Figure 14B,C)** confirmed preservation of the constitutional CGH profile during cell culture and thus genomic stability. This high resolution analysis led to the detection of three copy number variations (CNVs) with a size of 512 kb, 149 kb and 48 kb, respectively, which were not documented in the database of genomic variants (www.projects.tcag.ca/variation). Three additional UCB-ECFC samples after large-scale expansion also reveal genomic stability **(Figure 14D-F)**.

Flow-FISH analysis showed shorter telomere length in PB- and UCB-derived ECFCs compared to mouse 3T3 cells which were used as a positive control. PB ECFCs displayed significantly shorter telomeres than UCB ECFCs. Furthermore a non-significant but measurable decrease in telomere length through passaging compatible with an aging process of progenitor cells was observed **(Figure 15A-D)**. Quantitative telomerase activity measurement using TRAP supported these observations **(Figure 15E)**. TRAP also indicated a higher telomerase activity (mean Ct ± SD) in cells derived from HPP (Ct = 26.8 ± 0.3 cycles) compared to LPP (Ct = 29.9 ± 0.2 cycles) colonies.

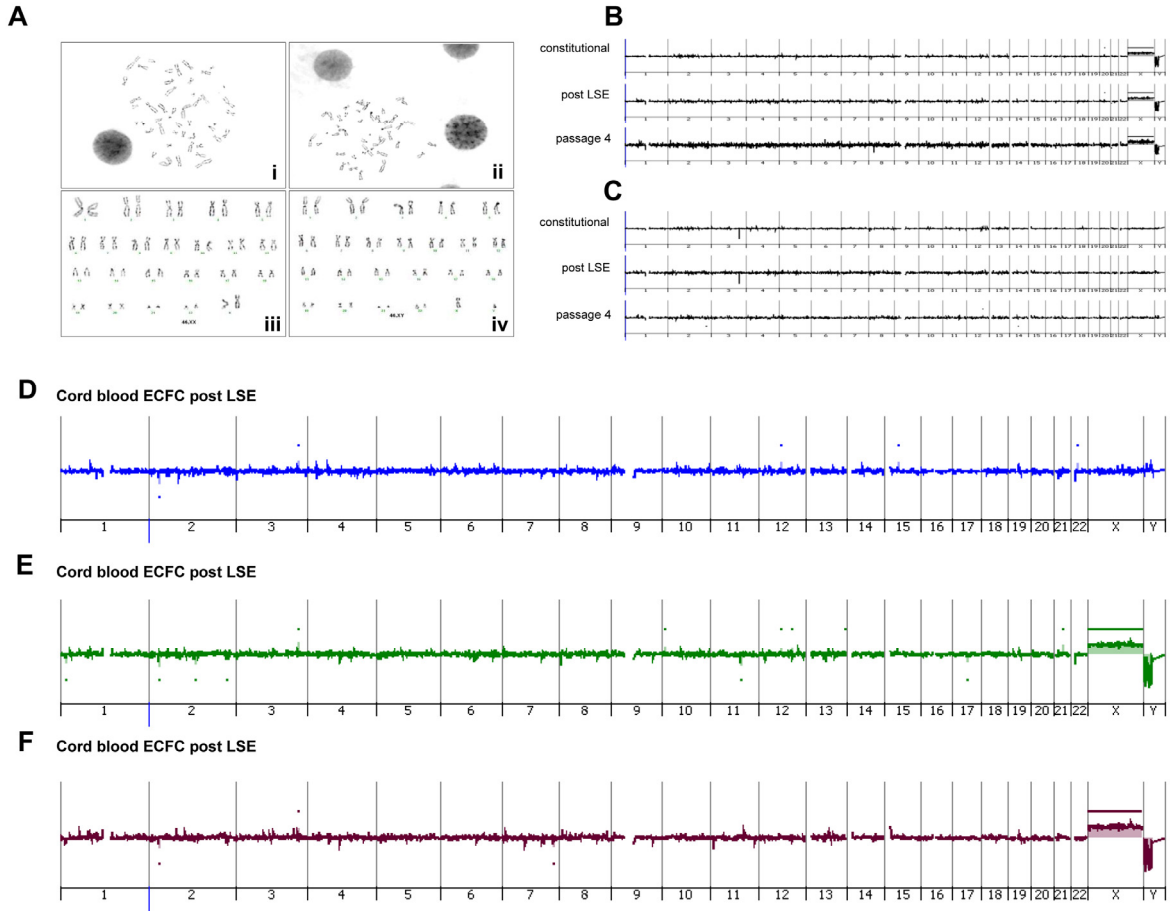

Figure 14. Genomic stability of peripheral blood and umbilical cord blood-derived ECFCs.

Representative chromosome G-banding derived from ECFC nuclei after large-scale expansion of **(Ai)** female and **(Aii)** male ECFCs and corresponding sorted **(Aiii)** female and **(Aiv)** male karyograms are shown. Representative array CGH depiction of constitutional initial white blood cell-derived DNA compared to ECFC-derived DNA post large-scale expansion and after passage four of the same **(B)** female and **(C)** male volunteers as shown in (Ai, Aiii) and (Aii, Aiv), respectively. **(D)** Normal stable high-resolution array CGH profile of a male and **(E,F)** two female cord blood derived ECFC samples. Autosomal chromosomes 1-22 and sex chromosomes in a spatial resolution of 43kb are depicted on the horizontal axis.

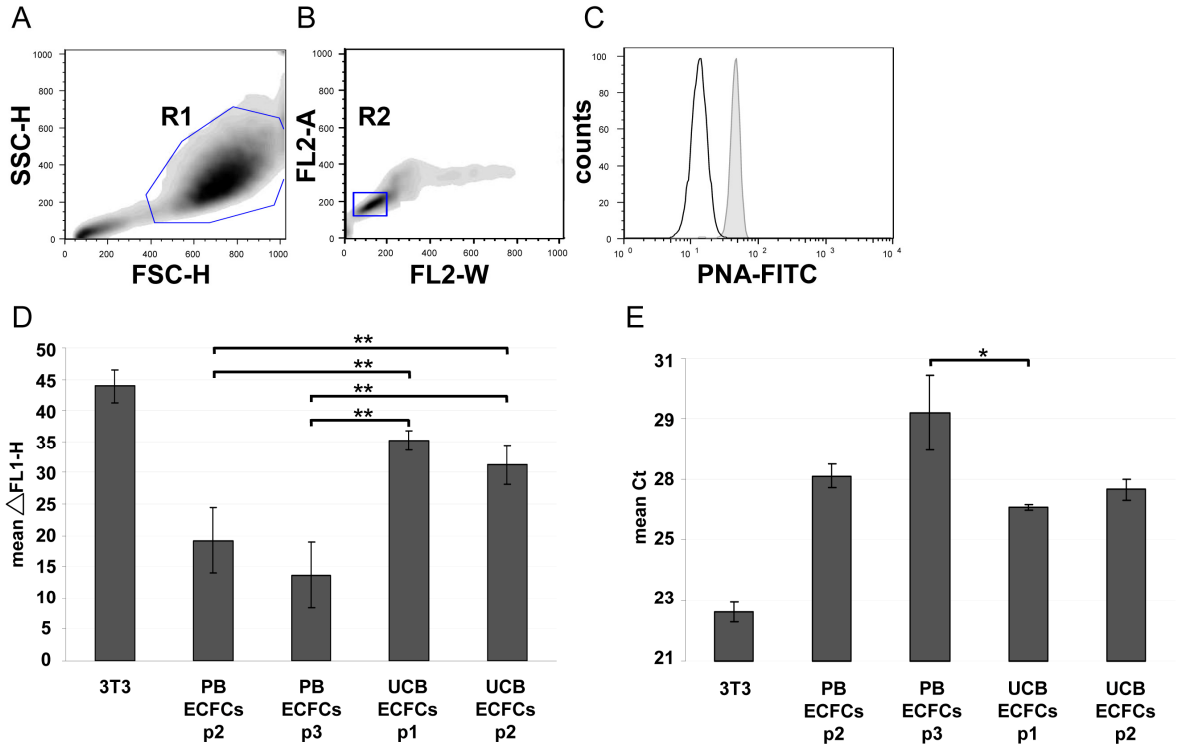

Figure 15. Telomere length and telomerase activity

Human ECFCs derived from peripheral blood (PB ECFCs; n = 4) and umbilical cord blood (UCB ECFC; n = 4) after different culture passages (p1-3) were compared with each other and with mouse 3T3 fibroblasts as a positive control. **(A-D)** Flow cytometry fluorescence in situ hybridization (Flow-FISH) was used to determine telomere length and **(E)** telomere repeat amplification protocol (TRAP) to measure telomerase activity. **(A,B)** Gating strategy of one representative example to select single cells in cell cycle phase $G_{0/1}$ based on size parameters (forward light scatter height, FSC-H; sideward light scatter height, SSC-H; region R1 = 88.6%) and DNA content determined after propidium iodine (PI) staining of hybridized cells (PI fluorescence width vs. area, FL2-W, FL2-A; region R2 = 77.7% of region R1). **(C)** Corresponding histogram showing fluoresceine isothiocyanate-tagged peptide nucleic acid (PNA-FITC) binding to telomeres (grey histogram) compared to background fluorescence after mock hybridization (open histogram). **(D)** Differences between PNA probe specific signal and background fluorescence height (ΔFL1-H; mean ± SD, n = 4 per passage) based on analyses of at least 10,000 single cells in $G_{0/1}$ phase per sample. **(E)** Telomerase activity displayed as cycle of threshold (Ct) in a real time polymerase chain reaction-based TRAP assay. Asterisks denote statistically significant differences (*p < 0.05; **p < 0.01).

MSCs are known to have the capability of regulating immune functions. Since large-scale expanded ECFCs transplanted with or without MSCs constitute possible candidates for treating patients with cardiovascular diseases as well as immune mediated diseased including **t**ype **I** **d**iabetes **m**ellitus (T1DM), Crohn's disease, MS

and others we were interested to compare the immune-regulatory properties of both cell types.

Immune modulation was determined by studying proliferation of allogeneic CFSE-labeled MNCs in the absence or presence of ECFCs as compared to MSCs. MSCs inhibited mitogen induced MNC proliferation in a ratio of one MSC per MNC whereas ECFCs were almost unable to inhibit MNC proliferation. MSCs used as feeder layer were less efficient compared to cells in suspension **(Figure 16).**

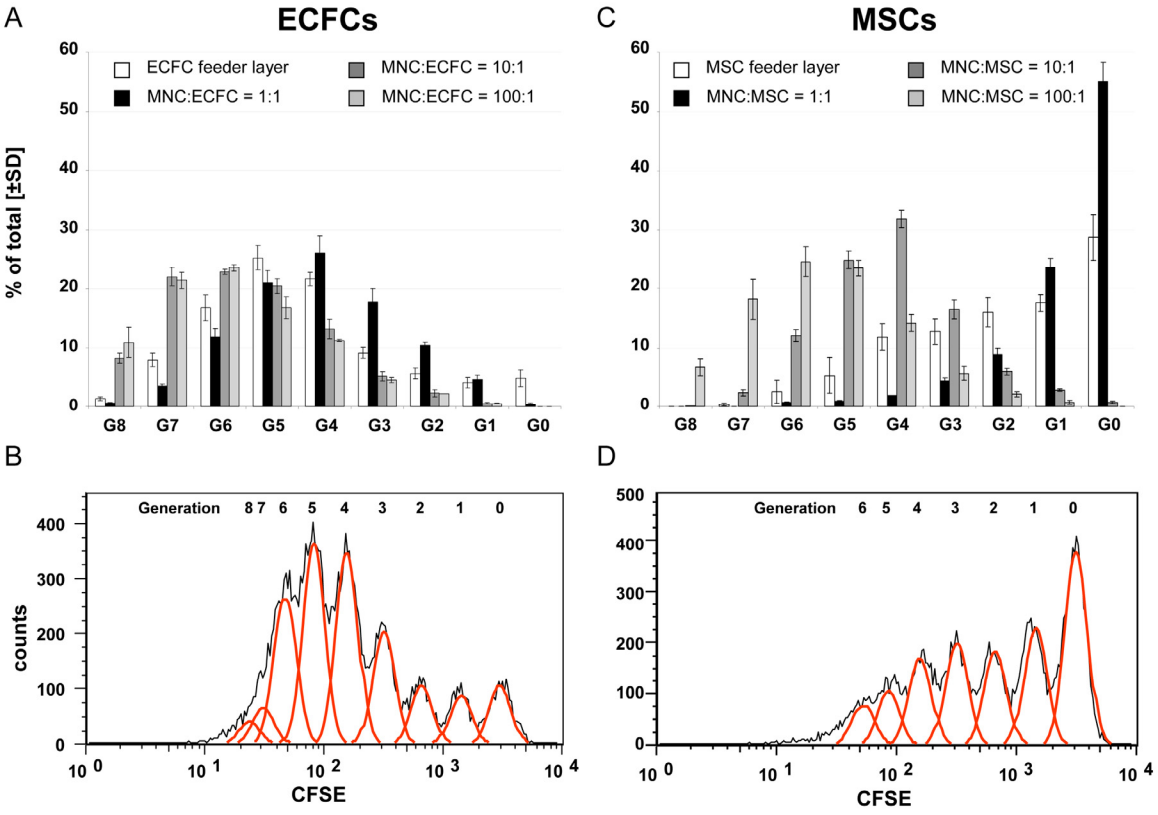

Figure 16. Immunomodulatory properties of UCB-ECFCs

Umbilical cord blood derived ECFCs **(A)** or positive control BM derived MSCs **(B)** were added in a 1:1 (1,5 x 10^5 MNC to 1,5 x 10^5 ECFC/MSC per well, black bars), 1:10 (dark grey bars) or 1:100 (light grey bars) ratio to test their influence on PHA (5 µg/mL) driven proliferation of allogeneic MNC as monitored by CFSE expression. Influence of pre-established, proliferation-inhibited (Mitomycin C) ECFC and MSC feeder layer on PHA stimulated MNC proliferation is depicted in white bars. Proliferation dependent loss of fluorescence intensity in FL-1 was used to calculate MNC generations (G0-G8 in A and B). Representative histograms of PHA driven MNCs cultured on an ECFC **(B)** or MSC feeder layer **(D)** showing several peaks in FL-1 respresenting cell generations (G1-G8) resulting from loss of original CFSE-label (G0) through proliferation. Software (FCS-Express V5) calculated MNC generations (red lines) fitted on the original histogram (black line) are shown.

8.6 ECFC function after humanized large-scale propagation *in vitro* and *in vivo*

The standardized large-scale expansion of ECFCs offers a great opportunity to test human EPCs in various model systems. Vascular network formation *in vitro* using Matrigel® is one of the most simple, rapid and reliable models. By seeding 7,500 oligoclonal or monoclonal blood-derived ECFCs after large-scale culture, we observed complex vascular network formation comparable to that of UCB-derived EPCs **(Figure 17A-F)**. Computer-assisted image composition demonstrated network complexity over the entire 40 mm^2 culture area (one well of a 16-well glass chamber slide; **Figure 17G**). Network formation was found to have resulted from ECFC migration and morphogenesis rather than proliferation when monitored using time lapse video-microscopy (see online supplementary file of reference Reinisch et al., Blood. 2009 Jun 25;113(26):6716-25.,http://bloodjournal.hematologylibrary.org/cgi/content/full/blood-2008-09-181362/DC1)

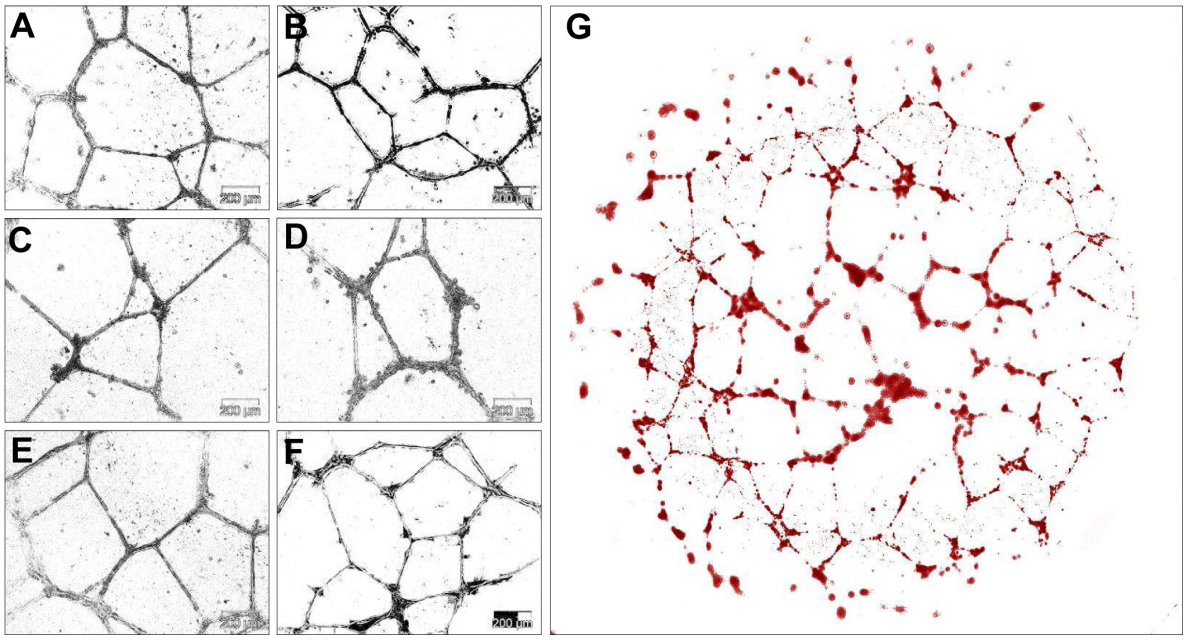

Figure 17. ECFCs function *in vitro* after large-scale humanized expansion.

(A-C) Representative transformed images of vascular network formation from three typical independent oligoclonal cultures and **(D)** one monoclonal ECFC culture compared to **(E,F)** two independent oligoclonal UCB-derived ECFC networks under the same conditions on Matrigel®. **(G)** Serial image reconstruction of one representative complete vascular network created in a 40 mm^2 well of a 16-well glass chamber slide is shown.

To test *in vivo* functionality, 1.2 million large-scale expanded PB-ECFCs representing approximately 20 population doublings since culture initiation were mixed with 0.3 million MSCs into Matrigel® and injected subcutaneously in nude mice. Matrigel® plugs were analyzed after two, five and seven weeks, respectively. After two weeks, there were only sparsely distributed vascular structures detectable in sections of explanted plugs **(Figure 18D.G)**. After five weeks, the implants contained more complex networks of human vasculature **(Figure 18E,H; Figure 19B)**. Durable neo-vessel formation was found in human cell-loaded plugs explanted after five to seven weeks **(Figure 18B, E-F, H-J)**. Immune histochemistry verified human origin of the vessels within plugs **(Figure 19B-E)**. At plug borders, human vasculature appeared in close vicinity to murine vessels **(Figure 19B,C)**. Murine origin of the red blood cells was confirmed by anti-mouse glycophorin A (mTer119) reactivity within the perfused vessels **(Figure 19F)**. The regular red blood cell content in the human vessels, in an amount comparable to that of neighboring mouse vasculature of comparable size, strongly indicates the functional connection of both vascular systems **(Figure 19C-H)**. Subcellular distribution of CD31 and van Willebrand Factor immune reactivity within the human neo-vessels resembled that of human vasculature **(Figure 19D,E)**.

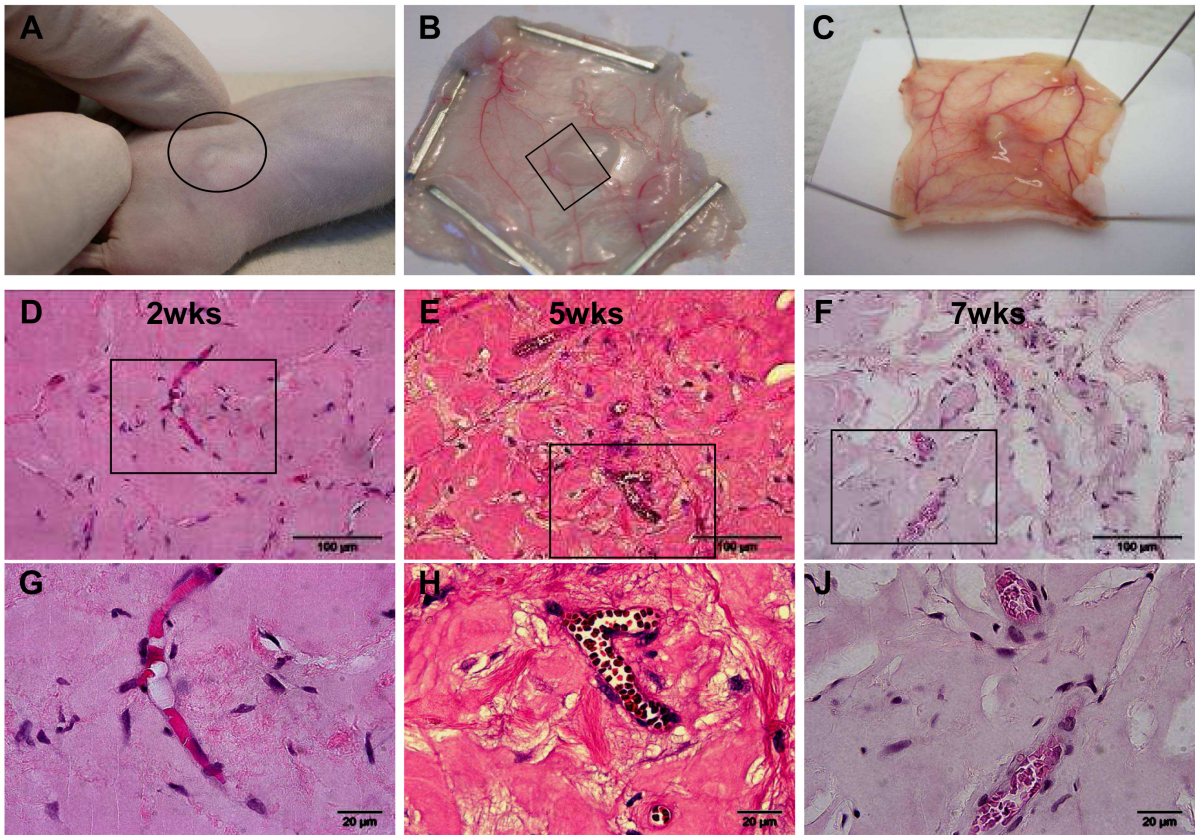

Figure 18. *In vivo* vasculogenesis.

(A,B) 1.2 x 10^6 PB-EPC were admixed with 0.3 x 10^6 BM-MSC in ice cold Matrigel before being implanted into the right flank of immune deficient athymic nude mice**. (A)** Macroscopic detection of the implanted plug before explantation. **(B)** Clearly visible subcutaneous localization of one representative implant with inserting mouse skin vasculature. Plug explantation borders with surrounding mouse tissue to be prepared for fixation as shown in **Figure 19A** are indicated by a box. **(C)** 1 x 10^7 pure ECFCs just resuspended in 0,2 mL phosphate-buffered saline were injected subcutaneously into nude mice and analyzed 7 days post transplantation. Subcutaneous view with clearly visible implant located at the injection site. Dilation and sprouting of mouse vessels into the plug area and reddish opaque coloring of plug surrounding tissue was already detectable macroscopically after extraction. **(D-F)** H&E stained, microscopic overview and **(G-J)** detail pictures as indicated by boxes in D-F of explanted Matrigel® plug sections showing red blood cell-filled vasculature that developed in nude mice *in vivo.* Plugs were loaded with human ECFCs plus MSCs mixed in a 80:20 ratio and analyzed after **(D,G)** two, **(E,H)** five, and **(F,J)** seven weeks.

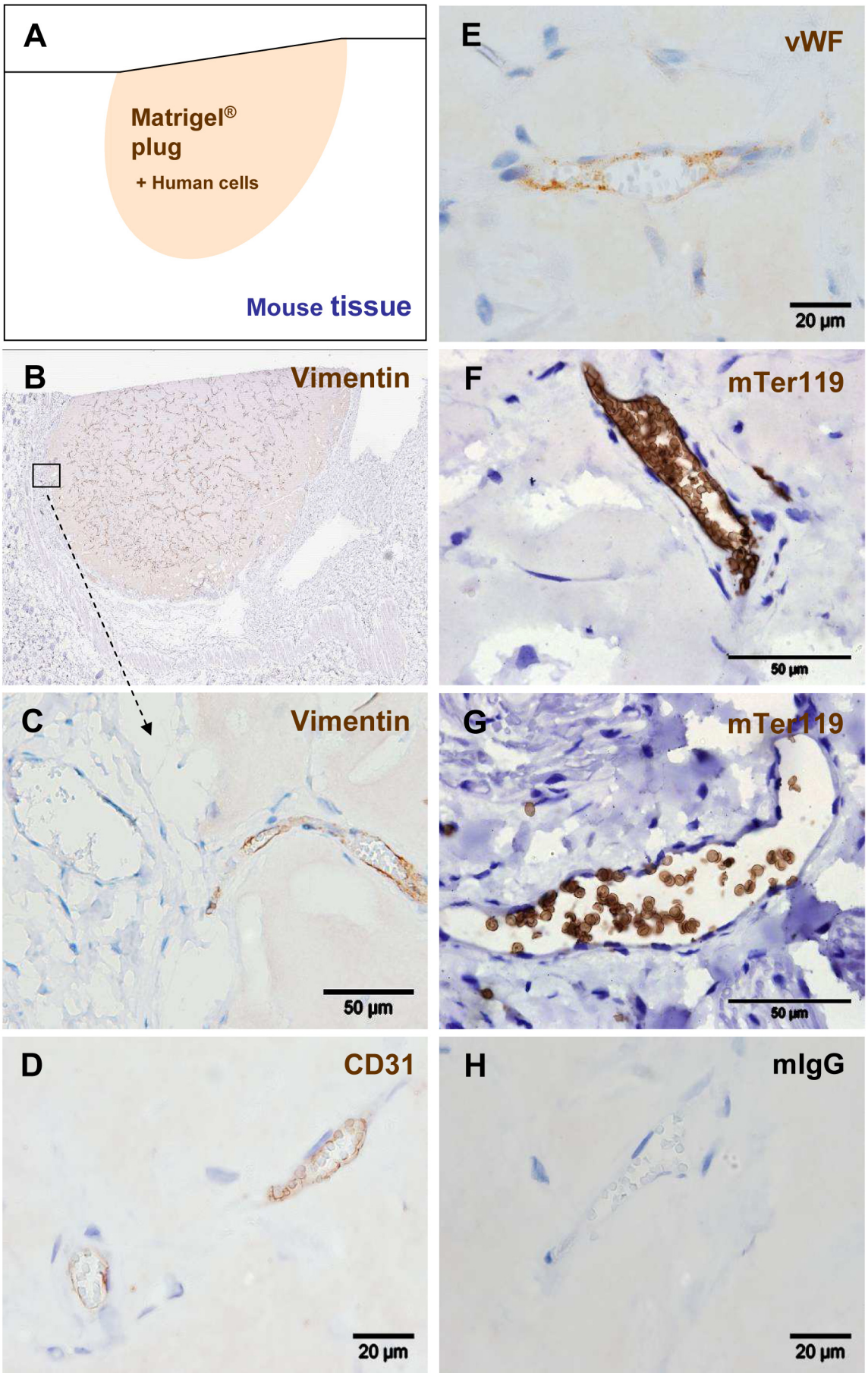
A
Matrigel®
plug
+ Human cells
Mouse tissue
B
Vimentin
C
Vimentin
50 µm
D
CD31
20 µm
E
vWF
20 µm
F
mTer119
50 µm
G
mTer119
50 µm
H
mIgG
20 µm

Figure 19. ECFCs function in vivo after large-scale humanized expansion

For in vivo neo-vasculogenesis, ECFCs from two donors were mixed with MSCs in Matrigel® before injecting 0.2 mL of the composite subcutaneously in four nude mice per group (n = 24; 4 mice per ECFC source analyzed at three time points; a macroscopic view is shown in **Figure 18A,B**). **(A)** Topography of the histology is symbolized and **(B)** shown as a low magnification overview of a Vimentin-labeled vascularized plug part. **(C)** Human vimentin staining in the border area showing negative murine tissue (left half) in the direct vicinity to the human cell-containing area of the Matrigel® plug with positive human vessels as indicated in **(B)**. **(D)** anti-human CD31, **(E)** anti-human vWF, **(F,G)** anti-mouse glycophorin A reactivity detected with antibody mTer119 within **(F)** human and **(G)** mouse vessels and **(H)** representative isotype control reactivity of mouse red blood cell containing vasculature inside the plug.

Such organized vasculature did not develop when pure ECFCs were injected without matrix and without supporting MSCs. Sole ECFC implantation led to the development of disorganized, but still perfused, vasculature in this particular mouse model, reminiscent of the pathologic picture of hemangiomas **(Figure 18C; Figure 20A-C).**

Since co-application of ECFCs and MSCs seems to be necessary for the generation of healthy, stable, long-lasting vessels, we were interested in further elucidating the cell- cell interaction responsible for this stabilizing phenomenon. MSCs and ECFCs are known to produce growth factors that can act in an autocrine as well as paracrine manner. Multiplex growth factor and cytokine analysis revealed that PB-ECFCs consume VEGF during their proliferation but also produce high amounts of PDGF AB/BB **(Figure 21A)**. BM-MSCs may provide their vessel supporing function via the generation of VEGF for the ECFCs. Interestingly, VEGF production by MSCs is inversely correlated to oxygen tension during cell culture **(Figure 21B)**. These data suggest that MSCs and ECFCs may interact via paracrine mechanism and that low oxygen concentrations may have positive influence on vessel formation **(Figure 21C)**.

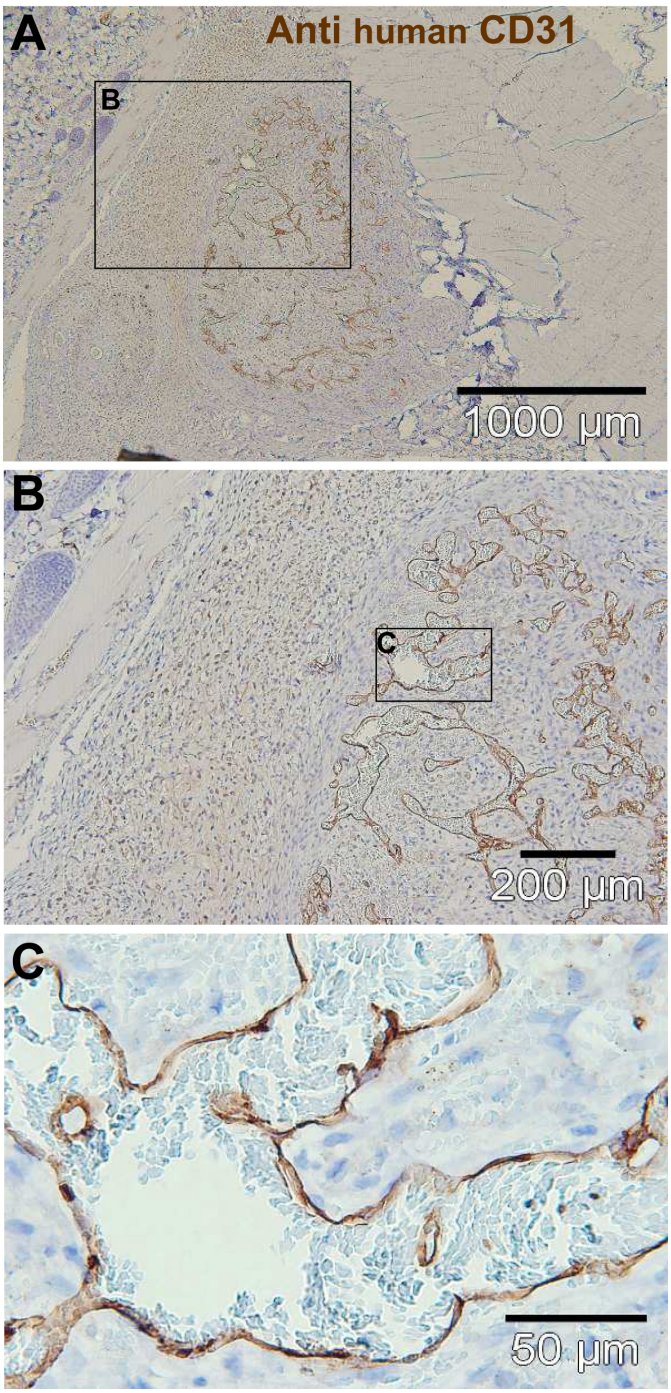

Figure 20. Deranged vessel formation of pure ECFCs in vivo and vascular lineage commitment in vitro.

(A-C) Representative pure ECFCs (1 x 10^7) derived from large-scale single step humanized expansion were resuspended in 0.2 mL phosphate-buffered saline and subcutaneously injected into nude mice. After one week, subcutaneous cell deposits (a macroscopic view is shown in Figure 18C) were processed for human CD31 histochemistry. **(A)** Overview appearance and **(B,C)** higher magnified regional view as indicated by schematic boxes with scale bars documenting magnification.

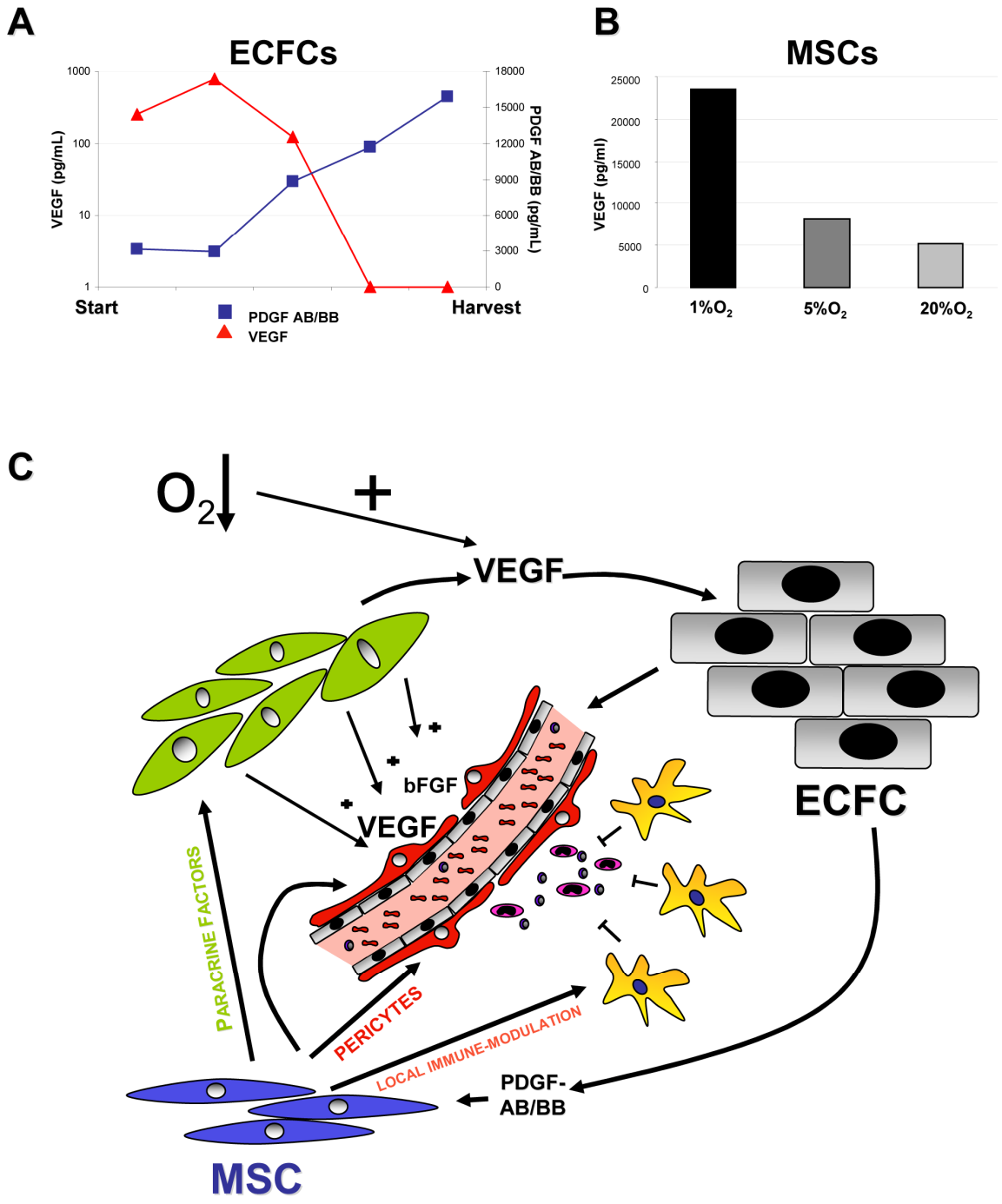

Figure 21. Potential cytokine mediated MSC-ECFC interaction to form stable vessels

(A) VEGF-consumption and PDGF-AB/BB production by ECFCs during *in vitro* culture measured with x-MAP technology. **(B)** Oxygen tension (1%,5% and 20%O2) regulated VEGF secretion by BM-MSC. **(C)** Model for cytokine-mediated interaction between MSC and ECFC to form stable vessel *in vivo*. MSCs produce VEGF in an oxygen dependent manner and may interact with PDGF-AB/BB generating ECFCs. PDGF-AB/BB can stimulate MSC to (1) develop pericyt phenotype, (2) produce further cytokines or (3) locally provide their immune-modulatory properties.

Most research on EPCs has so far investigated different types of hematopoietic CACs (Asahara et al., 1997, Vasa et al., 2001a, Asahara, 2003, Hill et al., 2003), including $CD34^{+}/CD31^{+}/CD45^{low}$ HSPCs. Since the both cell types ECFCs and CACs have several markers in common with HSPCs, e.g. CD31 (PECAM) and the hematopoieitc stem cell marker CD34, it is important to rule out potential HSPC contamination in ECFC cultures. Analyzing a putative hematopoietic differentiation potential of the $CD34^{+}$ vascular ECFCs as compared to $CD34^{+}$ hematopoietic cells is therefore a fundamental question for their characterization. The vascular lineage-restricted differentiation of ECFCs is supported by a complete lack of hematopoietic colony formation when testing 500 and 1,000 ECFCs in standard methyl cellulose assays. In clear contrast, equal numbers of purified hematopoietic progenitor cells produced the estimated mixture of red and different white cell lineage colonies **(Figure 22A-F)**. The complete lack of hematopoietic colonies in ECFC-loaded hematopoietic colony assays further argues against even a minute HSPC contamination of the large-scale expanded PB-ECFCs.

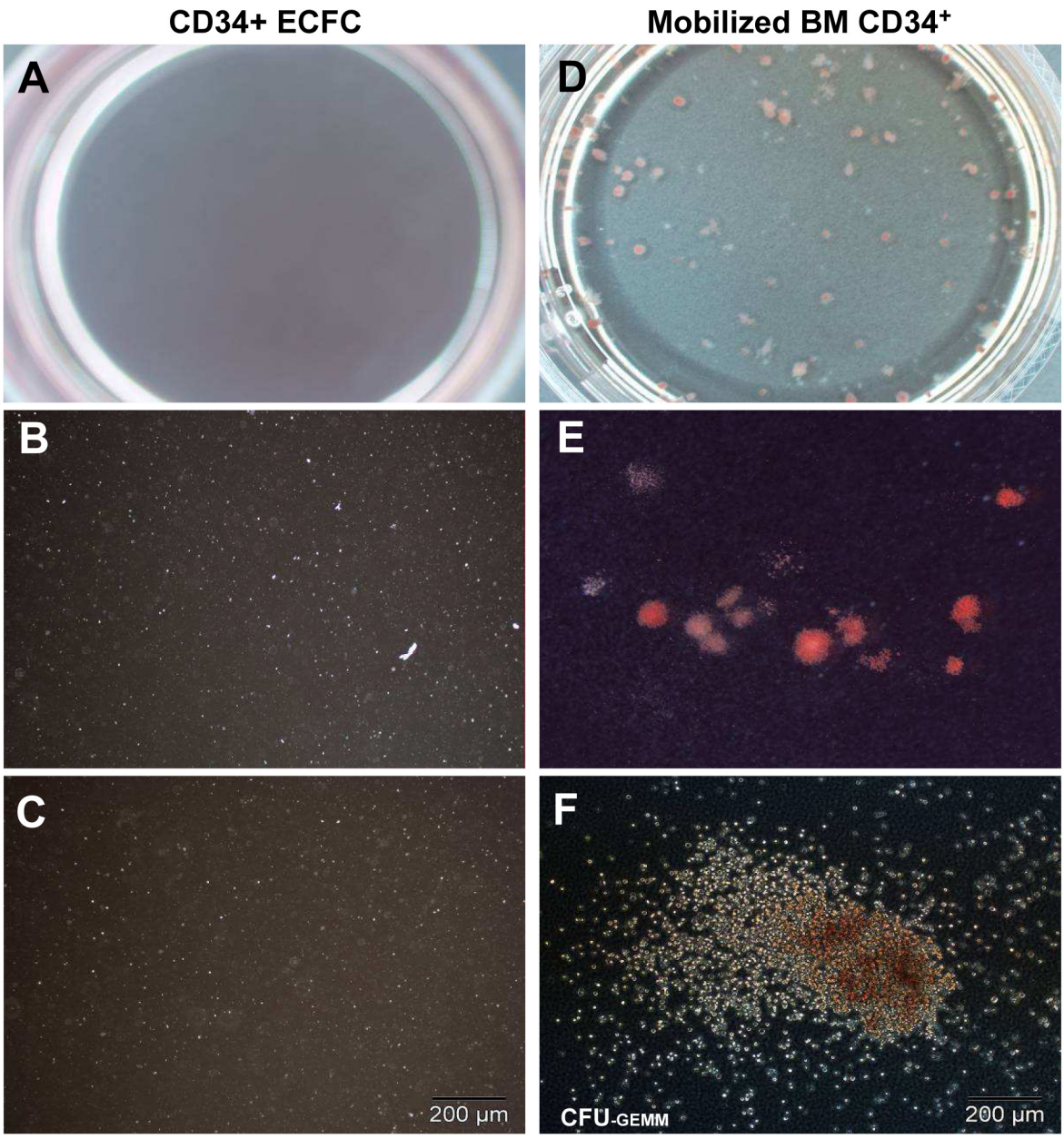

Figure 22. ECFCs do not show hematopoietic lineage commitment in vitro.

ECFCs after large-scale expansion were also evaluated in a hematopoietic colony-forming cell (CFC) assay in methylcellulose. **(A,D)** Pictures show a complete (10 cm^2) assay plate overview, **(B,E)** 10x original magnification view and **(C,F)** high magnification view that documents **(A-C)** complete lack of CFCs derived from ECFCs. In comparison, **(D,E)** regular red blood cell colony formation admixed with a hierarchy of differentially maturating white blood cell colonies and **(F)** <5% colony-forming units of granulocytes, erythrocytes, monocytes and macrophages (CFU-GEMM) was derived from $CD34^+$ hematopoietic progenitors.

8.7 Progenitor cell imaging

Since the beginning of HSCTxs the only reliable way to determine the efficiency of SC therapy is blood drawing and subsequent evaluation of blood cell development and chimerism after 2-7 weeks depending on the graft. These weeks of waiting are a life-threatening period for the patient. Unfortunately recipients that do not engraft also have to await the timepoint that a definive non-engraftment can be assured and retransplantation can be planned. Due to the delayed blood regeneration, in particular after UCB-Tx (for up to 7 weeks), non-engraftment correlates with increased mortality rates. The possibility of tracking applied cells early after SCTx and thereby getting information about their homing to the target organ (e.g. BM) allows for a screening of patients with low SC homing and thus potential non-engraftment. Labeling of cells with SPIOs should allow for detection of applied cells within the target tissue by MRI using iron sensitive T2 or T2*- weighted imaging protocols.

In a first series of experiments endocytotic uptake of two commercially available nanoparticles Resovist® (Bayer-Schering) and Endorem® (Guerbet) **(Table 5)** was quantified.

Different incubation times (2-24 hours) and various concentrations of iron within the culture medium were tested to determine optimal cell labeling conditions.

An optimal cell labeling concentration of 280µg iron/mL medium was defined by quantifying intracellular iron uptake. Iron accumulation could be detected by immunefluorescence microscopy using a SPIO binding FITC-conjugated antibody as well as conventionell Prussian Blue staining **(Figure 23A-C)**. **T**ransmission **e**lectron **m**icroscopy (TEM) confirmed microscopic data and allows for the attribution of iron containing nanoparticles to subcellular structures resembling endocytotic vesicles **(Figure 23D)**. SPIO accumulation within the cytoplasm of ECFCs **(Figure 23F)** and the resulting increase of cellular granularity could be semiquantitatively evaluated at the single cell level by detecting increased side scatter properties using flow cytometry **(Figure 23E)**.

Modifications of the protocols according to recent developments (Janic et al., 2009) were applied to further enhance SPIO uptake with simultaneous reduction of iron content within the medium. By using a polycationic transfection agent, membrane

binding of negatively charged SPIOs and subsequent endocytosis can be increased. Thus lower iron concentrations (only 50 µg/mL final medium) were sufficient to reach comparable labeling.

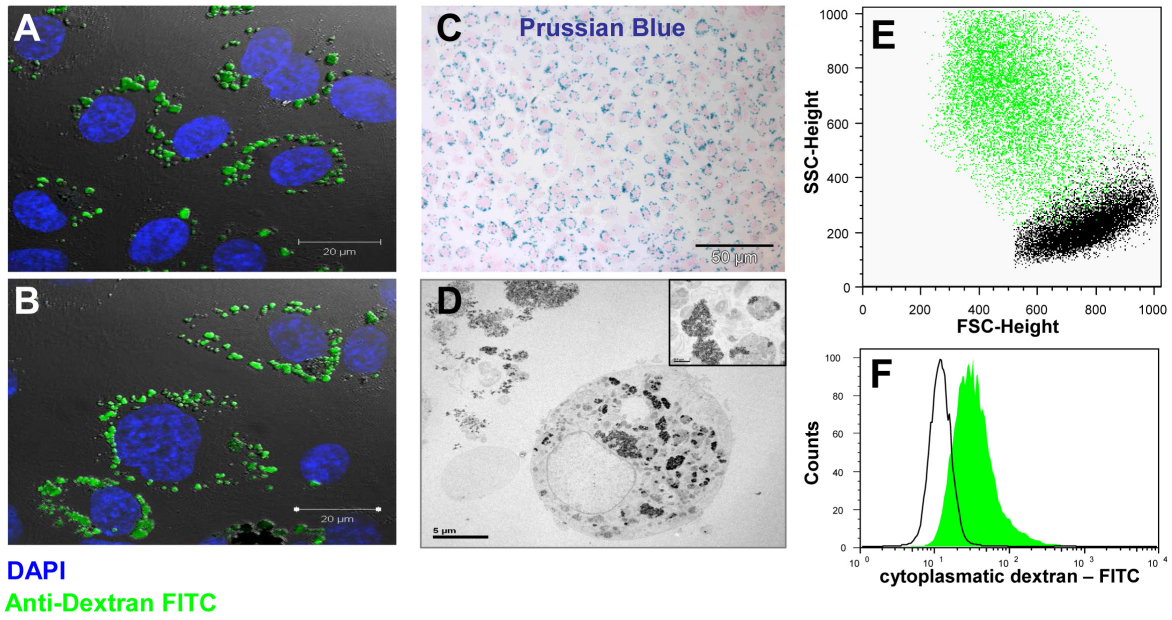

Figure 23. Evaluation of cellular and subcellular SPIO accumulation

Umbilical cord-derived ECFCs were labeled with 50 µg/mL Resovist® and 3 µg/mL protamine sulfate for 24 hours. SPIO uptake was confirmed by intracytoplasmic staining of the nanoparticle dextran sheath. **(A,B)** Intracytoplasmic localized Resovist®-SPIOs (green dots) were visualized through binding of FITC-conjugated anti-dextran antibody (Stem Cells Technologies) and analyzed on a confocal microscope. Cell nuclei (blue) were counterstained with 4',6-diamidino-2-phenylindole (DAPI). **(C)** Microscopic overview of Prussian Blue stained iron accumulation within ECFCs counterstained with nuclear fast red to visualize cell nuclei. **(D)** Subcellular localization of SPIOs within a single ECFC shown by transmission electron microsopy. Insert depicts higher magnification of intravesicular iron accumulation resembling endosmes **(E)** Increased cellular granularity through intracellular localized SPIOs increases side scatter properties (SSC-Height) of ECFCs. FSC-SSC dot plot overlays shows a clearly visible shift of SPIO labeled ECFCs (green dots) in comparison to unlabeled control cell (black dots). **(F)** Flow cytometry histogram overlay after cell fixation and permeabilization showing reactivity of FITC-tagged anti-dextran antibody (green filled curve) with intracytoplamic SPIOs compared to an isotype matched control antibody (black open curve).

To evaluate feasibility of cellular imaging on a 3 Tesla clinical MRI scanner, we developed an agarose-containing phantom, admixed with Gadolinium (Gd^{3+}) to reach human tissue comparable magnetic properties **(Figure 24).** Using this phantom, T1, T2 and T2* imaging sequences were developed (by our collaboration partners at Institute for Medical Engineering, Graz University of Technical) and subsequently improved in order to decrease the cell detection limit and to determine ideal intracellular iron concentrations for optimized cell imaging. Preliminary results showed reproducible visualisation of a minimum of 1,000 cells. Further adaptations of the MRI scanner (use of high resolution surface coils) and improved imaging protocols were made to test single cell imaging. Therefore vascular networks (on Matrigel®) established with SPIO-labeled ECFCs were used in a phantom allowing for single cell detection **(Figure 25).**

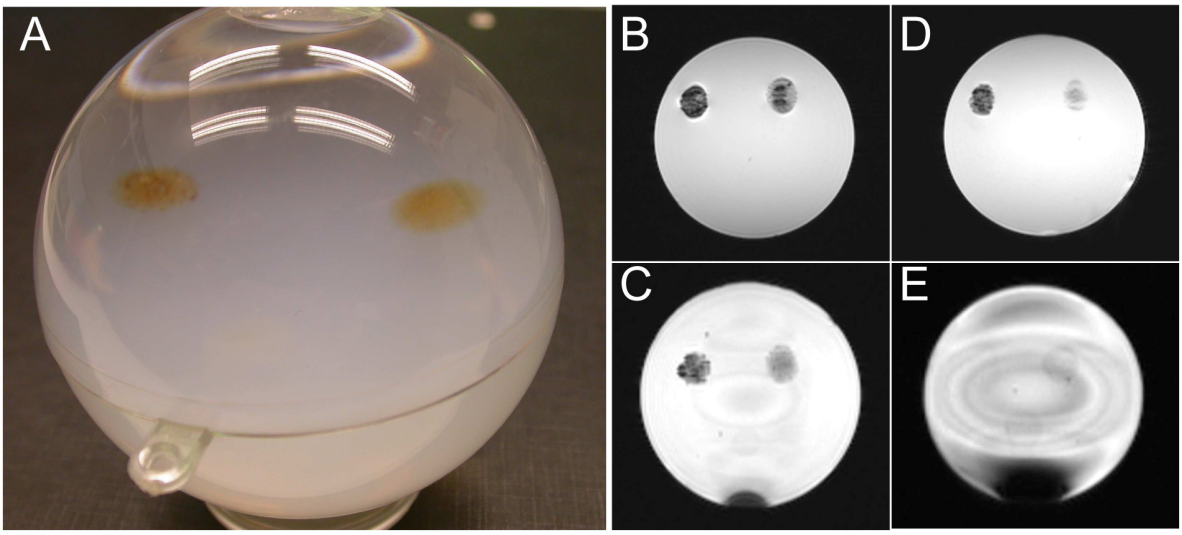

Figure 24. MRI phantom containing SPIO labeled MSCs.

(A) A plastic ball filled with Gadolinium-loaded 1% agarose gel and SPIO-labeled BM-MSCs (brown) was used as aMRI phantom providing human tissue equivalent magnetic properties. Cells were incubated with 280 µg/mL SPIOs in the final medium for 24 hours. Resovist®-(left) and Endorem®-labeled (right) BM-MSCs resuspended in warm agarose were subsequently added to the polymerized agarose gel at decreasing cell numbers of **(B)**$1x10^6$, **(C)**$1x10^5$, **(D)**$1x10^4$, **(E)**$1x10^3$ cells per dot to evaluate the detection limit of the system. Equal numbers of unlabeled cells were used as control.

By combining extented scanning times and the use of surface coils that allow for appropriate high resolution we were able to demonstrate for the first time the detection of structures containing only single cells within vascular networks on a 3 Tesla clinical MRI scanner **(Figure 25 A,B)**.

An increase of magnetic field strength to 7 Tesla further improved the outcome, resulting in an almost complete overlap of the MR-image with the microscopic picture of the cellular networks when superimposing 78µm slices representing the whole imaging volume in a postprocessing step using **m**axium **i**ntensity **p**rojection (MIP) **(Figure 25 C,D)**.

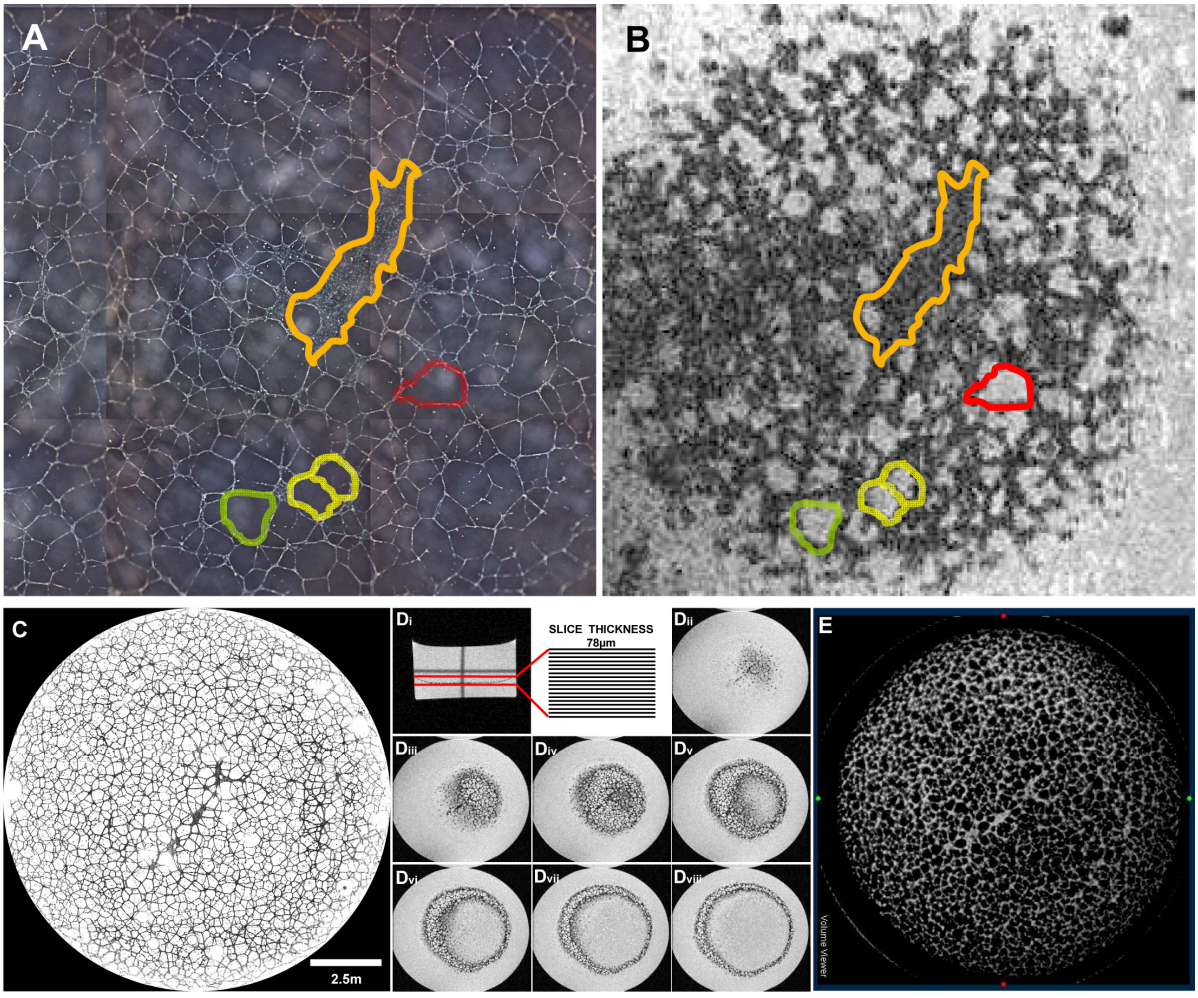

Figure 25. High sensitivity detection of single SPIO labeled cells within vasculare networks formed in extracellular matrix.

3 Tesla MRI. Comparison of network structures visualized first by **(A)** dark field microscopy with the subsequent **(B)** high sensitive gradient echo MR image. Areas surrounded by colored lines show the same structures in (A) and (B). **(C)** Microscopic image reconstruction of a 3.8 cm^2 (22 mm diameter) covering vascular network. Black to white color-inversion was performed using ImageJ software for better visualisation of the network structures

High resolution 7T MRI**. (Di-Dviii)** Serial MRI slices (slice thickness: 78 µm) along the z-axis of the same vascular network as shown in (C). **(E)** Maximum intensity projection (MIP) of the acquired MRI dataset using Image J software.

8.8 Vascular and osteogenic regeneration models

To study contribution of MSCs and ECFCs to tissue regeneration we established subcutaneously localized models for vessel and bone development by injecting MSCs and/or ECFCs into immune-deficient mice. To standardize the model systems independent of the murine immune system, we employed NOG mice as recipients. These mice show a higher degree of immune deficiency compared to nude mice. NOD-SCID background and additional interleukin-2 receptor (IL-2R) deficiency completely abrogates NK-cell development and leads to severe impairment of T and B-cell development and function. Additionally IL-2R γ-chain is a crucial component of several other IL-receptors including receptors for IL-2, IL-4, IL-7, IL-9, IL-15, IL-21 that is required for appropriate cytokine-signaling (Shultz et al., 2007a, Shultz et al., 2007b).

The ideal combination of MSCs:ECFCs of 20:80 resulted in stable vessel formation **(Figure 26 C,D)** whereas transplantation of MSCs:ECFCs at a ration of 80:20 or pure MSC application (100:0) led to the formation of mature human bone **(Figure 26 A,B).**

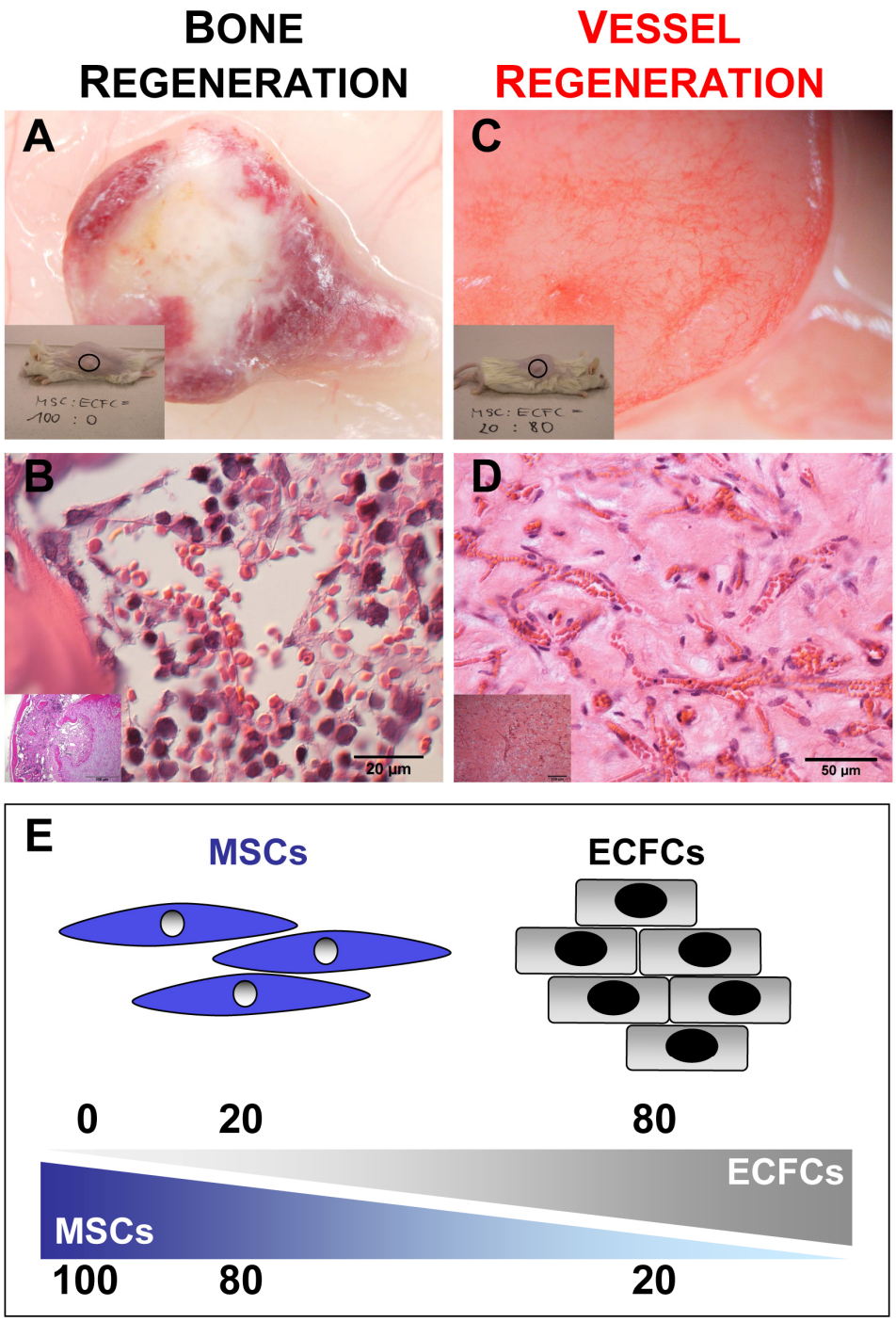

Figure 26. Bone and vessel regeneration by MSCs and ECFCs transplantation

(A-B) Macroscopic images of the excised transplants (A,C) showing bone and vessel formation. Inserts demonstrate exact subcutaneous localization of the implants in immune decficient mice. (B,D) Microscopic pictures of conventional H&E-stains from the same explants. Inserts depict overviews of the sections in lower magnification. (E) Cartoon illustrating combinations of MSCs and ECFCs that lead to regeneration model development.

Micro computed tomography (µCT), flat panel volumen CT (fpVCT) and *in vivo* fluorescence imaging using a bone integrating near infrared dye (Osteosense 750; emission wavelenght 750 nm) were performed to study the time course of bone formation and to find the optimal time points for additional cell tranplantation that enable maximum contribution of transplanted cells to organ development **(Figure 27)**.

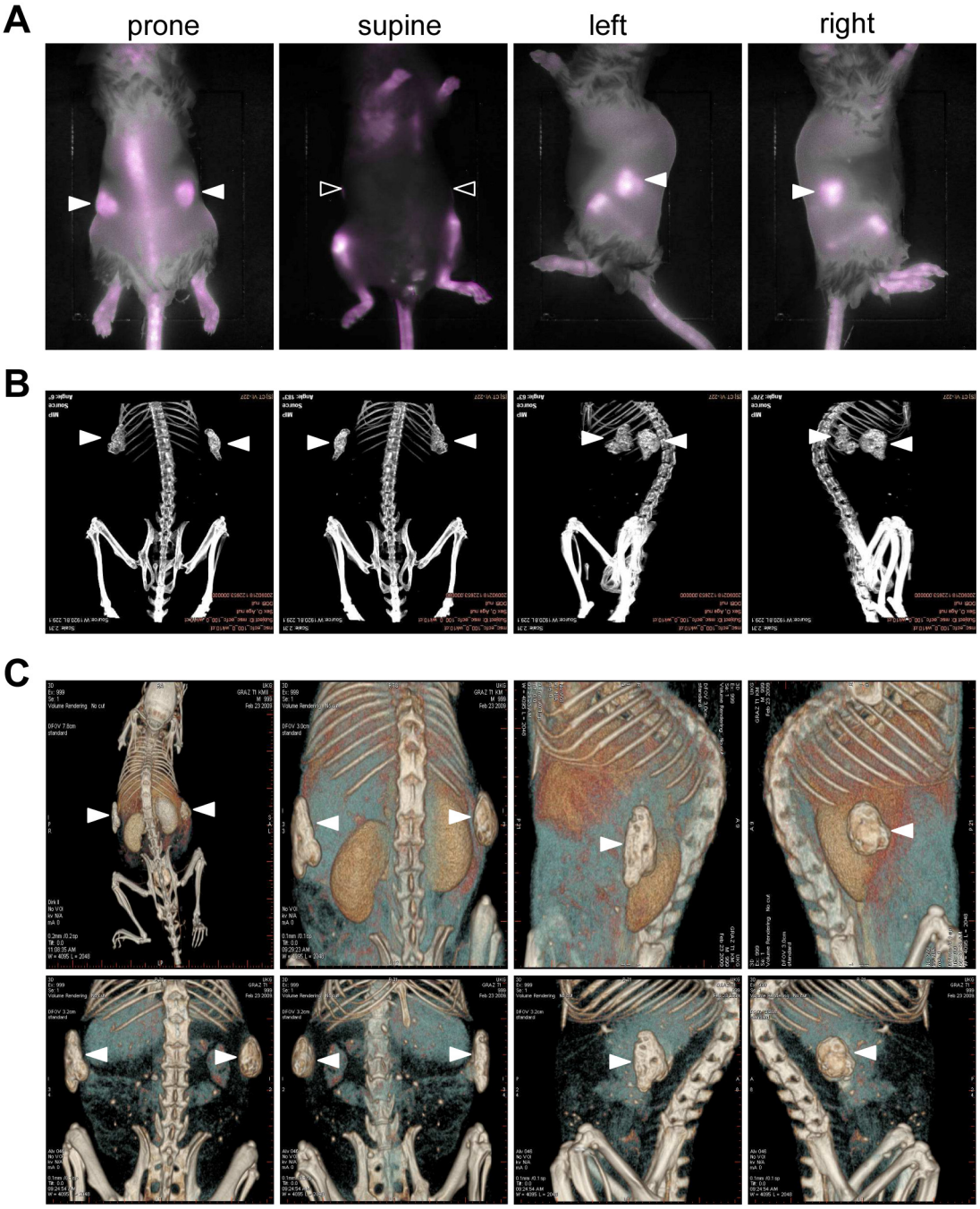

Figure 27. Near infrared fluorescence and computed Tomography based imaging of bone organ development after subcutaneouse application of BM-MSCs.

(A) Near infrared fluorescence imaging using bone integrating Osteosense 750® (Visen Medical). Subcutaneuously formed ossicles in the right and left flank of immune deficient mice are clearly visible as fluorescent light emitting nodules. For better visualisation they were pseudo-colored in purple. Simultanouse detection of physiological bone remodeling processes at proximal tibia, distal femur, small bones of front and hind limb, spine and hip demonstrates high sensitivity of Osteosense 750® **(B)** Micro computed tomography (µCT) and **(C)** contrast agent enhanced flat panel volume computed tomography (fpVCT) can detect dense areas, corresponding to bone formation at the injections sides within the flanks of the animals. Filled triangles indicate generated ossicles. Open triangles in (A) demonstrate that bone formation in the flanks of the animals is not visible in supine imaging position due to limited penetration depth of the emitted light.

9 Discussion

The idea of curing almost every disease, independent of its cause, through transplantation of stem and progenitor cells is one basic concept of regenerative medicine. Unfortunately the transfer of this simple, straightforward idea into regular clinical practice is associated with complex and so far unsolved problems.
This work has been performed to find solutions for several of these problems including (**1**) isolation and expansion of non-hematopoietic progenitor cell populations (MSCs, ECFCs) using an animal-serum free system, by replacing FBS with pHPL, (**2**) employing UCB as an alternative source for the isolation of non-hematopoietic progenitor cells and (**3**) testing functionality of expanded cells *in vitro* as well as *in vivo*. (**4**) Tissue regeneration models and *in vivo* imaging approaches have been developed to address the essential problem of cell traceability after systemic or local administration.

9.1 pHPL can replace FBS during progenitor cell isolation and expansion

Although feasibility and safety of *ex vivo* propagated progenitor cells in cell culture medium containing FBS has been documented in a growing number of studies over the last decade (Lazarus et al., 1995, Horwitz et al., 1999, Koc et al., 2000, Horwitz et al., 2001, Koc et al., 2002, Lee et al., 2002, Le Blanc et al., 2004, Lazarus et al., 2005, Ringden et al., 2006), the use of FBS during MSC propagation carries the immanent risk of pathogen transmission as well as xeno immunization (Selvaggi et al., 1997, Mackensen et al., 2000, Horwitz et al., 2002, Tuschong et al., 2002, Muul et al., 2003, Gregory et al., 2006). Because the ideal MSC transplant would be propagated under defined conditions devoid of animal products pHPL was implemented by us and others (Doucet et al., 2005, Reinisch et al., 2007, Schallmoser et al., 2007a, Reinisch et al., 2009, Schallmoser et al., 2009, Schallmoser and Strunk, 2009) as a source of human growth factors to fully replace FBS. No phenotypic differences have been observed in this study when comparing

cells cultured under either condition by flow cytometry. Both cell types MSCs and ECFCs showed a representative marker profile.

9.2 Umbilical cord blood as a source for non-hematopoietic progenitor cells

MSCs are attractive vehicles for regenerative SC therapy (Prockop, 1997, Prockop et al., 2003). The ability of MSCs to modulate immune reactions in a major histocompatibility complex unrestricted manner has resulted in attractive concepts for the treatment of severe autoimmune diseases and GvHD (Le Blanc, 2003, Le Blanc et al., 2003, Aggarwal and Pittenger, 2005, Le Blanc and Pittenger, 2005). MSC differentiation into bone-forming osteoblasts makes them ideal candidates for treatment of bone fractures, osteoporosis or bone defects related to inborn diseases (Horwitz et al., 2002, Lucarelli et al., 2005, Kitoh et al., 2007) (www.clinicaltrials.gov). Sustained multiplication of functional HSCs in co-cultures with MSCs may even solve many problems associated with the limited SC number in clinical UCB transplantation (Rocha et al., 2004, Arcese et al., 2006, Robinson et al., 2006).

The preferred MSC source should be accessible without invasive harvesting procedures. Because accessibility to BM is associated with great efforts by the investigator and pain as well as risk for the donor, a search for additional MSC sources started.

In our study we investigated human UCB as a potential source of MSC mass-production compared to BM. We have established a reliable procedure for the propagation of UCB-MSCs to transplantable quantities of at least 1 x 10^8 UCB-MSCs within approximately seven weeks. The cells retained osteogenic and chondrogenic differentiation potential. In accordance with published knowledge we observed only minute adipogenic differentiation of UCB-MSC (Bieback et al., 2004, Kern et al., 2006). Compared to a 100% efficiency of BM-MSC culture initiation, the reduced efficiency of establishing UCB-MSC cultures (46% in this and 30-60% in other studies) (Kogler et al., 2004, Kern et al., 2006) may limit the autologous applicability of UCB-MSCs.

A clinical quantity of at least 100 million MSCs can be obtained from BM-MSCs within shorter time compared to UCB-MSCs. This is probably due to significantly lower primary MSC amounts in the UCB samples. We never observed more than four primary CFU-F colonies in our cultures derived from a limited UCB volume. Provided that every colony would be derived from a single precursor cell, at least 18 population doublings of these MSCs are needed to produce a million progeny from four starting cells, if every single cell and its progeny in the system is deviding.

UCB-MSC function was analysed in this study with a particular focus on immune modulation, hematopoiesis support and vascular-like network formation. MSC^{HPL} were at least as efficient as UCB-MSC^{FBS} in inhibiting mitogen-driven lymphocyte proliferation in a 1 : 10 ratio of MSC : MNC. Interestingly, only UCB-MSC^{HPL} significantly inhibited PHA-induced MNC proliferation at a lower MSC : MNC ratio. Neither UCB-MSC^{HPL} nor UCB-MSC^{FBS} induced significant MNC proliferation in 1 : 10 or 1 : 100 ratios in the absence of PHA in our experiments. It may be speculated that immune cell stimulation by MSCs observed under certain conditions displays a specific feature of BM-MSCs (Le Blanc et al., 2003).

The natural role of BM-MSCs during regulation of hematopoiesis relates to a supportive stromal cell function in the hematopoietic SC niche (Dexter et al., 1977, Schofield, 1978, Gutierrez-Rodriguez et al., 2000, Robinson et al., 2006). Interestingly, also UCB-MSCs have been found to support HSC expansion *in vitro* (Ye et al., 1994, Mayani and Lansdorp, 1998). This study was the first to show that UCB-MSC expanded to a clinical quantity under FBS-free conditions can induce a profound multiplication of UCB-derived $CD34^+$ cells. Most interestingly, we observed a mean eight fold increase of immature $CD34^+/CD38^-$ HSC in UCB-MSC^{HPL}-driven cultures (Reinisch et al., 2007). The clinical applicability of such a UCB-HSC multiplication approach is still limited by the fact that the HSPC-expansion cultures worked best in FBS-supplemented RPMI-1640 medium. However, preliminary data already indicate that it may be translated into an FBS-free system (Reinisch A et al., unpublished data). Provided that true HSC expansion can be confirmed by hematopoietic colony and long term culture-initiating cell assays as well as transplantation studies, this would further support the assumption that UCB-MSC^{HPL} may represent an attractive vehicle for regenerative therapies in clinical hematology.

Additionally, the observed vascular-like network formation by UCB-MSCs could argue for a putative role of mesenchymal precursors in vascular regeneration.

9.3 ECFC-based vascular regeneration

Vascular regenerative therapy is a promising new concept to improve diminished organ function through application of stem and progenitor cells after ischemic tissue injury or vascular damage. The disease underlying mechanisms are mainly due to vascular pathologies and subsequent dysfunctional oxygen supply, which leads to local ischemia and tissue damage. Cellular therapy, aiming to improve the vessel density and to increase local oxygen supply, offers a new strategy to overcome disease progression in CVD like acute **m**yocardial **i**nfarction (MI) or stroke. However, up to now, a spectrum of early clinical trials with BM-derived cells or MSCs has shown only limited capacity for long-lasting benefits to the recipients of the transplanted cells (Erbs et al., 2005, Yoder et al., 2007, Matoba et al., 2008, Pompilio et al., 2008, Purhonen et al., 2008). This reflects, at least in part, our currently restricted understanding regarding the physiological mechanisms involved in tissue regeneration and vascular homeostasis (Hirschi et al., 2008, Kovacic et al., 2008).
The selection of cell types with appropriate functions as transplants for vascular regeneration currently presents a major challenge (Hirschi et al., 2008, Purhonen et al., 2008). Growing evidence reinforces traditional knowledge that hematopoietic cells, e.g. CACs or $CD133^+$ HSPCs facilitate vascular and organ regeneration mainly by humoral and cell-mediated support functions and do not directly form vessels (Balsam et al., 2004, Murry et al., 2004, Hirschi et al., 2008, Kovacic et al., 2008). Clinical trials employing hematopoietic CACs appear to be safe but are unfortunately of limited efficacy and mostly lack durable response (Yoder et al., 2007). In sharp contrast, ECFCs, which are blood- or vasculature-derived EPCs characterized by robust proliferative potential, can form perfused long-lasting vessels *in vivo* (Melero-Martin et al., 2007, Yoder et al., 2007, Au et al., 2008, Reinisch et al., 2009). We have developed a novel method that for the first time allows us (1) to efficiently recover human ECFCs from unmanipulated blood under humanized entirely animal protein-free conditions; (2) to propagate these ECFCs to a quantity of mean 1.5 ± 0.5 x 10^8 cells within a single large-scale expansion step after oligoclonal primary culture;

(3) to cryopreserve expanded ECFCs with intact proliferation potential and function after thawing; and (4) to employ human animal serum-free expanded ECFCs in vascular network formation assays *in vitro* and in two different neo-vasculogenesis models *in vivo*.

The vessel-forming capacity and longevity of the ECFC-derived vessels in different mouse models actually increased when the cells were co-transplanted with MSCs. These findings are in accordance with those of previous studies (Melero-Martin et al., 2007, Au et al., 2008, Melero-Martin et al., 2008, Traktuev et al., 2009). Our observations in line with data from Melero-Martin et al. even suggest that the ratio of ECFCs to co-applied cells may influence the degree of vessel formation. Vessel growth supporting cytokines provided by co-applied perivascular cells may play an essential role during *in vivo* vessel formation. The fact that VEGF secretion by MSCs drops with increasing oxygen levels argues for an enhanced vessel forming capacity of transplanted cells under hypoxic conditions within ischemic tissue. ECs themselves also produce many cytokines including PDGF, that are known to recruit mesenchymal cells and stimulate their differentiation towards a pericyte phenotype (Hirschi et al., 1999).

Despite robust proliferation, these ECFCs proved to be genomically stable after clinical large scale as well as long term expansion as indicated by normal karyotype and array CGH profiles. As a proof of principle, ECFCs were also successfully recovered from unmanipulated UCB and PB of patients with CVD using the same optimized animal serum-free procedure. In our experiments there were no significant differences in (1) time to initial colony outgrowth, (2) colony number and (3) capacity of large-scale expansion in patients with stableCVD. In a pig model of induced acute MI, elevated numbers of ECFCs and increased percentage of HPP-ECFCs were observed immediately after balloon catheter-induced coronary damage (Huang et al., 2007). Larger prospective studies would be appropriate to address questions regarding ECFC frequency and function in selected patient populations. Our technology is suited to determine ECFC frequency and functionality in a standardized fashion.

Currently the precise origin of blood-born ECFCs is not clear. We isolated ECFCs directly from small volumes of heparinized whole blood as well as from vessel walls through an initial adhesion step and subsequent selection of proliferating cells in a

specific endothelial growth medium supplemented with human growth factors and pHPL (Hofmann et al., 2009, Reinisch et al., 2009, Reinisch and Strunk, 2009). ECFC phenotype, proliferation potential, maintained progenitor cell hierarchy and vessel formation *in vitro* and *in vivo* clearly meet the criteria established by Ingram and Yoder (Ingram et al., 2004, Ingram et al., 2005a, Ingram et al., 2005b, Yoder et al., 2006). Previous analyses of blood smears by Hebbel and co-workers have already suggested that $CD146^+$ circulating endothelial lineage cells reminiscent of ECFCs by phenotype and profound colony-type proliferation are present in PB as a minute population of 2.6 ± 1.6 cells/mL (Solovey et al., 1997). Consecutive studies by the same authors using blood samples from BM transplant recipients reached the conclusion that most circulating endothelial lineage cells present during the early culture phase originate from vessel walls. Our results, showing an endothelial colony recovery of mean four colonies per milliliter, may strengthen the assumption that the ECFCs first described by Ingram and Yoder (Ingram et al., 2004) and the $CD146^+$ BOECs originally discovered by the Hebbel group (Solovey et al., 1997) are derived from one and the same cell population. Based on the currently published data we favour a view of circulating ECFCs as predominantly vessel wall-derived EPCs that can circulate through the blood stream. Whether ECFCs can really function in an orchestrated interplay with immune cells (including T cells, different activation and differentiation stages of monocytes and other CACs as well as CFU-Hill as a surrogate *in vitro* marker) to maintain vessel integrity and contribute to adult vasculogenesis during organ regeneration and tumor vascularisation needs to be determined prior to planning future clinical trials. Our current technology for the propagation of human ECFCs from PB, UCB and UC builds the basis for such experiments.

We speculate that the higher recovery of ECFCs with our protocol may be due to a diminished cell loss by avoiding density gradient-based cell separation. Human growth factors in the pHPL including PDGF-AA, PDGF-AB/BB, EGF and angiogenin, among others, may further support efficient outgrowth of ECFCs (Kocaoemer et al., 2007, Schallmoser et al., 2007b).

ECFCs can be distinguished from hematopoietic progenitors by their lack of the pan-hematopoietic LCA CD45 and the absence of hematopoietic colony formation (Michaelis et al., 2004, Monasch et al., 2004, Michaelis et al., 2005, Case et al.,

2007, Reinisch et al., 2007, Timmermans et al., 2007, Yoder et al., 2007, Hofmann et al., 2009, Reinisch et al., 2009). The cells described in this study also meet these criteria.

Any efficient vascular regenerative medicine independent, of its mode of action or transplanted cell populations, bears the risk of side effects due to the complex and still poorly understood balance between beneficial and deleterious effects. We observed genomic stability and a normal karyotype of ECFCs expanded for >30 population doublings under humanized culture conditions with preserved functionality. The ECFCs accessible in large quantity and with intact functionality also represent a valuable tool to study pro- and anti-angiogenic therapeutic strategies *in vivo* (Alajati et al., 2008). The ECFC large-scale propagation under humanized culture conditions has the potential to facilitate a wide spectrum of future studies to determine their therapeutic applicability and risk profile during vascular homeostasis and repair.

9.4 Development of novel organ regeneration models

ECFCs and MSCs are known to be highly proliferative cells capable of differentiation and formation of human tissue upon transplantation *in vivo*. This study describes the use of ECFCs together with MSCs for the generation of functional human vasculature in an immune deficient mouse model. Our primary focus was the development of optimal conditions for the generation of durable, patent and perfused vessels. Such vessels could be reproducibly generated if adequate amounts of MSCs were co-transplanted with vessel-forming ECFCs. MSCs constitute the precursor for pericytes and MSC differentiation toward a vessel stabilizing cell phenotype is mediated through cytokines and direct cell contact with ECs (Hirschi et al., 1999).

Currently it is not known if co-applied MSCs actually form pericytes or if they only provide cytokines and growth factors necessary for enhanced vessel development. Co-culture studies *in vitro* with and without direct cell contact and extensive *in vivo* analysis are underway to answer these questions.

Our *in vivo* results favour a MSC:ECFC ratio of 20:80 for optimal vessel generation which is in contrast to results employed by collegues in Boston (Melero-Martin et al.,

2008). Cell ratios of MSC:ECFC = 80:20 for optimal vessel development as described by this group are not applicable in our model because BM-MSCs differentiate to bone rather than functional vasculature. Reasons for these observed differences may include the use of pHPL cultured cells in our study and a different immune compromised mouse model with higher susceptability for human cell engraftment.

Current studies and our observations indicate that subcutaneouse application of pure MSCs leads to bone formation (Crisan et al., 2008). Time course and intensity of bone growth can be evaluated with *in vivo* imaging modalities like CT and fluorescence imaging using a **h**ydroxy**a**ppatite (HA) targeting bone-accumulating near infrared dye. Unfortunately *in vivo* imaging cannot discriminate an intermediate cartilage state that can lead to bone formation via enchondral ossification (Chan et al., 2009). Although serval studies have evaluated the *in vivo* osteogenic potential of human MSCs (Kuznetsov et al., 1997b, Sacchetti et al., 2007), this is the first study to show MSC-driven bone formation without the use of cell pre-conditioning and/or co-application of osteo-inducitve HA/TCP or spongiouse carriers. Bone formation started as early as two weeks after cell application and was stable for the maximum observation periode of 22 weeks. Histological analysis of the explants demonstrated generation of mature bone. Some ossicles even developed a marrow space and could provide a niche for hematopoietic SC engraftment (Figure 24 and Reinisch et al., unpublished observations) similar to recent findings of the Bianco group describing $CD146^+$ MSC-like osteoprogenitors as the putative hematopoietic SC niche forming cell (Sacchetti et al., 2007).

9.5 MRI-based cell tracking

Magnetic labeling of cells with iron oxide containing nanoparitcles and subsequent MRI has been demonstrated to be a non-toxic, non-invasive method that allows for cell tracking early after application and therefore can help to predict possible outcome of the cellular treatments (Bulte et al., 2001, Arbab et al., 2003a, Arbab et al., 2003b, Daldrup-Link et al., 2003, Frank et al., 2003, Arbab et al., 2004, Frank et al., 2004, Arbab et al., 2005, Daldrup-Link et al., 2005, Ittrich et al., 2005, Arbab et

al., 2008). Ferucarbotran (Resovist®), a clinically approved SPIO nanonparticle used in our study has already been shown to be applicable for MSC labeling with high uptake, intracellular accumulation and persistence throughout a periode of several weeks within the cells (Ittrich et al., 2005). We adapted MSC labeling protocols for human blood-derived ECFCs and showed similar uptake kinetics and final intracellular iron content. Cell functionality as demonstrated in vascular network formation assays was unchanged and argues against toxicity resulting from the applied particles. SPIO uptake was proven by several methods including high-throuput single cell analysis based on flow cytometry. Since labeling efficiency has to be determined quickly for cell transplants planned to be applied directly after cell harvesting, this method is optimal suited for preclinical use.

Cell trapping after intravenous application within the lung, liver and spleen diminishes the amount of cells that arrive at target organs like BM or damaged vessels. A recent study was analyzing the percentage of early trapping in the lung of mice with induced MI 15 minutes after i.v. application of MSCs. Their results indicate trapping of more than 80% in the lungs microcirculation. In the same study, less than 1% of applied cells could be found adjacent to the infarcted heart muscle (Lee et al., 2009). Such findings indicate that detection of small cell numbers is a major challenge for cellular imaging approaches and requires methods capable of reaching appropriate high resolution of only several µm voxel size. MRI in combination with iron oxide nanoparticle labeling has the potential to reach this ambiguous goal. We used vascular networks formed *in vitro* by SPIO-labeled ECFCs as a surrogate model resembling the *in vivo* situation of vessel formation. These network branches consisting of only a few cells were detectable for the first time in high resolution with a 7 Tesla preclinical MRI scanner. A comparable recent study did not rearch similar high quality images (Wilhelm et al., 2007) despite using a higher magnetic field strength of 9.4 Tesla. Our study demonstrates the potential of MRI for detection and tracking of progenitor cells. Translation of these promising results into clinically applicable scanning protocols developed for human whole-body scanners and their implementation into SCTx-regimens is the major challenge for the future.

This thesis has shown for the first time the isolation and expansion of UCB and PB derived progenitor cell population under humanized, GMP-compliant culture conditions with conserved *in vitro* and *in vivo* functions. Obtained result can help to develop regenerative medicine towards a safe and efficient clinical routine treatment.

10 Literature

Aggarwal, S. & Pittenger, M. F. 2005. Human mesenchymal stem cells modulate allogeneic immune cell responses. *Blood,* 105**,** 1815-22.

Alajati, A., Laib, A. M., Weber, H., Boos, A. M., Bartol, A., Ikenberg, K., Korff, T., Zentgraf, H., Obodozie, C., Graeser, R., Christian, S., Finkenzeller, G., Stark, G. B., Heroult, M. & Augustin, H. G. 2008. Spheroid-based engineering of a human vasculature in mice. *Nat Methods,* 5**,** 439-45.

Arai, F., Hirao, A., Ohmura, M., Sato, H., Matsuoka, S., Takubo, K., Ito, K., Koh, G. Y. & Suda, T. 2004. Tie2/angiopoietin-1 signaling regulates hematopoietic stem cell quiescence in the bone marrow niche. *Cell,* 118**,** 149-61.

Arbab, A. S., Bashaw, L. A., Miller, B. R., Jordan, E. K., Bulte, J. W. & Frank, J. A. 2003a. Intracytoplasmic tagging of cells with ferumoxides and transfection agent for cellular magnetic resonance imaging after cell transplantation: methods and techniques. *Transplantation,* 76**,** 1123-30.

Arbab, A. S., Bashaw, L. A., Miller, B. R., Jordan, E. K., Lewis, B. K., Kalish, H. & Frank, J. A. 2003b. Characterization of biophysical and metabolic properties of cells labeled with superparamagnetic iron oxide nanoparticles and transfection agent for cellular MR imaging. *Radiology,* 229**,** 838-46.

Arbab, A. S., Janic, B., Knight, R. A., Anderson, S. A., Pawelczyk, E., Rad, A. M., Read, E. J., Pandit, S. D. & Frank, J. A. 2008. Detection of migration of locally implanted AC133+ stem cells by cellular magnetic resonance imaging with histological findings. *FASEB J,* 22**,** 3234-46.

Arbab, A. S., Yocum, G. T., Kalish, H., Jordan, E. K., Anderson, S. A., Khakoo, A. Y., Read, E. J. & Frank, J. A. 2004. Efficient magnetic cell labeling with protamine sulfate complexed to ferumoxides for cellular MRI. *Blood,* 104**,** 1217-23.

Arbab, A. S., Yocum, G. T., Rad, A. M., Khakoo, A. Y., Fellowes, V., Read, E. J. & Frank, J. A. 2005. Labeling of cells with ferumoxides-protamine sulfate complexes does not inhibit function or differentiation capacity of hematopoietic or mesenchymal stem cells. *NMR Biomed,* 18**,** 553-9.

Arcese, W., Rocha, V., Labopin, M., Sanz, G., Iori, A. P., De Lima, M., Sirvent, A., Busca, A., Asano, S., Ionescu, I., Wernet, P. & Gluckman, E. 2006. Unrelated cord blood transplants in adults with hematologic malignancies. *Haematologica,* 91**,** 223-30.

Asahara, T. 2003. Endothelial progenitor cells for neovascularization. *Ernst Schering Res Found Workshop***,** 211-6.

Asahara, T., Masuda, H., Takahashi, T., Kalka, C., Pastore, C., Silver, M., Kearne, M., Magner, M. & Isner, J. M. 1999. Bone marrow origin of endothelial

progenitor cells responsible for postnatal vasculogenesis in physiological and pathological neovascularization. *Circ.Res.,* 85**,** 221.

Asahara, T., Murohara, T., Sullivan, A., Silver, M., Van Der Zee, R., Li, T., Witzenbichler, B., Schatteman, G. & Isner, J. M. 1997. Isolation of putative progenitor endothelial cells for angiogenesis. *Science,* 275**,** 964-7.

Au, P., Daheron, L. M., Duda, D. G., Cohen, K. S., Tyrrell, J. A., Lanning, R. M., Fukumura, D., Scadden, D. T. & Jain, R. K. 2008. Differential in vivo potential of endothelial progenitor cells from human umbilical cord blood and adult peripheral blood to form functional long-lasting vessels. *Blood,* 111**,** 1302-5.

Balsam, L. B., Wagers, A. J., Christensen, J. L., Kofidis, T., Weissman, I. L. & Robbins, R. C. 2004. Haematopoietic stem cells adopt mature haematopoietic fates in ischaemic myocardium. *Nature,* 428**,** 668-73.

Bartmann, C., Rohde, E. & Schallmoser, K., Et Al. 2007a. Two steps to functional MSC for clinical application. *Transfusion*.

Bartmann, C., Rohde, E., Schallmoser, K., Purstner, P., Lanzer, G., Linkesch, W. & Strunk, D. 2007b. Two steps to functional mesenchymal stromal cells for clinical application. *Transfusion,* 47**,** 1426-35.

Bender, J. G., To, L. B., Williams, S. & Schwartzberg, L. S. 1992. Defining a therapeutic dose of peripheral blood stem cells. *J Hematother,* 1**,** 329-41.

Bieback, K., Kern, S., Kluter, H. & Eichler, H. 2004. Critical parameters for the isolation of mesenchymal stem cells from umbilical cord blood. *Stem Cells,* 22**,** 625-34.

Buhring, H. J., Battula, V. L., Treml, S., Schewe, B., Kanz, L. & Vogel, W. 2007. Novel markers for the prospective isolation of human MSC. *Ann N Y Acad Sci,* 1106**,** 262-71.

Bulte, J. W., Douglas, T., Witwer, B., Zhang, S. C., Strable, E., Lewis, B. K., Zywicke, H., Miller, B., Van Gelderen, P., Moskowitz, B. M., Duncan, I. D. & Frank, J. A. 2001. Magnetodendrimers allow endosomal magnetic labeling and in vivo tracking of stem cells. *Nat Biotechnol,* 19**,** 1141-7.

Calvi, L. M., Adams, G. B., Weibrecht, K. W., Weber, J. M., Olson, D. P., Knight, M. C., Martin, R. P., Schipani, E., Divieti, P., Bringhurst, F. R., Milner, L. A., Kronenberg, H. M. & Scadden, D. T. 2003. Osteoblastic cells regulate the haematopoietic stem cell niche. *Nature,* 425**,** 841-6.

Caplan, A. I. 1991. Mesenchymal stem cells. *J Orthop Res,* 9**,** 641-50.

Caplan, A. I. 2005. Review: mesenchymal stem cells: cell-based reconstructive therapy in orthopedics. *Tissue Eng,* 11**,** 1198-211.

Caplan, A. I. 2008. All MSCs are pericytes? *Cell Stem Cell,* 3**,** 229-30.

Carmeliet, P. 2003. Angiogenesis in health and disease. *Nat Med,* 9**,** 653-60.

Case, J., Mead, L. E., Bessler, W. K., Prater, D., White, H. A., Saadatzadeh, M. R., Bhavsar, J. R., Yoder, M. C., Haneline, L. S. & Ingram, D. A. 2007. Human CD34+AC133+VEGFR-2+ cells are not endothelial progenitor cells but distinct, primitive hematopoietic progenitors. *Exp Hematol,* 35**,** 1109-18.

Chan, C. K., Chen, C. C., Luppen, C. A., Kim, J. B., Deboer, A. T., Wei, K., Helms, J. A., Kuo, C. J., Kraft, D. L. & Weissman, I. L. 2009. Endochondral ossification is required for haematopoietic stem-cell niche formation. *Nature,* 457**,** 490-4.

Choi, K., Kennedy, M., Kazarov, A., Papadimitriou, J. C. & Keller, G. 1998. A common precursor for hematopoietic and endothelial cells. *Development,* 125**,** 725-32.

Civin, C. I., Strauss, L. C., Brovall, C., Fackler, M. J., Schwartz, J. F. & Shaper, J. H. 1984. Antigenic analysis of hematopoiesis. III. A hematopoietic progenitor cell surface antigen defined by a monoclonal antibody raised against KG-1a cells. *J Immunol,* 133**,** 157-65.

Crisan, M., Yap, S., Casteilla, L., Chen, C. W., Corselli, M., Park, T. S., Andriolo, G., Sun, B., Zheng, B., Zhang, L., Norotte, C., Teng, P. N., Traas, J., Schugar, R., Deasy, B. M., Badylak, S., Buhring, H. J., Giacobino, J. P., Lazzari, L., Huard, J. & Peault, B. 2008. A perivascular origin for mesenchymal stem cells in multiple human organs. *Cell Stem Cell,* 3**,** 301-13.

D'ippolito, G., Diabira, S., Howard, G. A., Menei, P., Roos, B. A. & Schiller, P. C. 2004. Marrow-isolated adult multilineage inducible (MIAMI) cells, a unique population of postnatal young and old human cells with extensive expansion and differentiation potential. *J Cell Sci,* 117**,** 2971-81.

Daldrup-Link, H. E., Rudelius, M., Oostendorp, R. A., Settles, M., Piontek, G., Metz, S., Rosenbrock, H., Keller, U., Heinzmann, U., Rummeny, E. J., Schlegel, J. & Link, T. M. 2003. Targeting of hematopoietic progenitor cells with MR contrast agents. *Radiology,* 228**,** 760-7.

Daldrup-Link, H. E., Rudelius, M., Piontek, G., Metz, S., Brauer, R., Debus, G., Corot, C., Schlegel, J., Link, T. M., Peschel, C., Rummeny, E. J. & Oostendorp, R. A. 2005. Migration of iron oxide-labeled human hematopoietic progenitor cells in a mouse model: in vivo monitoring with 1.5-T MR imaging equipment. *Radiology,* 234**,** 197-205.

De Bruijn, M. F., Ma, X., Robin, C., Ottersbach, K., Sanchez, M. J. & Dzierzak, E. 2002. Hematopoietic stem cells localize to the endothelial cell layer in the midgestation mouse aorta. *Immunity,* 16**,** 673-83.

Delorme B, Chateauvieux S & Charbord P 2006. The concept of mesenchymal stem cells. *Regen Med,* 1(4)**,** 497-509.

Dexter, T. M., Wright, E. G., Krizsa, F. & Lajtha, L. G. 1977. Regulation of haemopoietic stem cell proliferation in long term bone marrow cultures. *Biomedicine,* 27**,** 344-9.

Dominici, M., Le Blanc, K., Mueller, I., Slaper-Cortenbach, I., Marini, F., Krause, D., Deans, R., Keating, A., Prockop, D. & Horwitz, E. 2006. Minimal criteria for defining multipotent mesenchymal stromal cells. The International Society for Cellular Therapy position statement. *Cytotherapy,* 8**,** 315-7.

Doucet, C., Ernou, I., Zhang, Y. Z., Llense, J. R., Begot, L., Holy, X. & Lataillade, J. J. 2005. Platelet lysates promote mesenchymal stem cell expansion: A safety substitute for animal serum in cell-based therapy applications. *J Cell Physiol,* 205**,** 228-236.

Eilken, H. M., Nishikawa, S. & Schroeder, T. 2009. Continuous single-cell imaging of blood generation from haemogenic endothelium. *Nature,* 457**,** 896-900.

Erbs, S., Linke, A., Adams, V., Lenk, K., Thiele, H., Diederich, K. W., Emmrich, F., Kluge, R., Kendziorra, K., Sabri, O., Schuler, G. & Hambrecht, R. 2005. Transplantation of blood-derived progenitor cells after recanalization of chronic coronary artery occlusion: first randomized and placebo-controlled study. *Circ Res,* 97**,** 756-62.

Erices, A., Conget, P. & Minguell, J. J. 2000. Mesenchymal progenitor cells in human umbilical cord blood. *Br J Haematol,* 109**,** 235-42.

Folkman, J. 2002. Role of angiogenesis in tumor growth and metastasis. *Seminars in Oncology,* 29**,** 15-18.

Frank, J. A., Anderson, S. A., Kalsih, H., Jordan, E. K., Lewis, B. K., Yocum, G. T. & Arbab, A. S. 2004. Methods for magnetically labeling stem and other cells for detection by in vivo magnetic resonance imaging. *Cytotherapy,* 6**,** 621-5.

Frank, J. A., Miller, B. R., Arbab, A. S., Zywicke, H. A., Jordan, E. K., Lewis, B. K., Bryant, L. H., Jr. & Bulte, J. W. 2003. Clinically applicable labeling of mammalian and stem cells by combining superparamagnetic iron oxides and transfection agents. *Radiology,* 228**,** 480-7.

Friedenstein, A. J., Chailakhyan, R. K., Latsinik, N. V., Panasyuk, A. F. & Keiliss-Borok, I. V. 1974. Stromal cells responsible for transferring the microenvironment of the hemopoietic tissues. Cloning in vitro and retransplantation in vivo. *Transplantation,* 17**,** 331-40.

Friedenstein, A. J., Petrakova, K. V., Kurolesova, A. I. & Frolova, G. P. 1968. Heterotopic of bone marrow.Analysis of precursor cells for osteogenic and hematopoietic tissues. *Transplantation,* 6**,** 230-47.

Friedenstein, A. J., Piatetzky, S., Ii & Petrakova, K. V. 1966. Osteogenesis in transplants of bone marrow cells. *J Embryol Exp Morphol,* 16**,** 381-90.

Gao, D., Nolan, D. J., Mellick, A. S., Bambino, K., Mcdonnell, K. & Mittal, V. 2008. Endothelial progenitor cells control the angiogenic switch in mouse lung metastasis. *Science,* 319**,** 195-8.

Geigl, J. B., Langer, S., Barwisch, S., Pfleghaar, K., Lederer, G. & Speicher, M. R. 2004. Analysis of gene expression patterns and chromosomal changes associated with aging. *Cancer Res,* 64**,** 8550-7.

Gong, J. K. 1978. Endosteal marrow: a rich source of hematopoietic stem cells. *Science,* 199**,** 1443-5.

Gregory, C. A., Reyes, E., Whitney, M. J. & Spees, J. L. 2006. Enhanced engraftment of mesenchymal stem cells in a cutaneous wound model by culture in allogenic species-specific serum and administration in fibrin constructs. *Stem Cells,* 24**,** 2232-43.

Gronthos, S., Franklin, D. M., Leddy, H. A., Robey, P. G., Storms, R. W. & Gimble, J. M. 2001. Surface protein characterization of human adipose tissue-derived stromal cells. *J Cell Physiol,* 189**,** 54-63.

Gronthos, S., Zannettino, A. C., Hay, S. J., Shi, S., Graves, S. E., Kortesidis, A. & Simmons, P. J. 2003. Molecular and cellular characterisation of highly purified stromal stem cells derived from human bone marrow. *J Cell Sci,* 116**,** 1827-35.

Grunewald, M., Avraham, I., Dor, Y., Bachar-Lustig, E., Itin, A., Yung, S., Chimenti, S., Landsman, L., Abramovitch, R. & Keshet, E. 2006. VEGF-induced adult neovascularization: recruitment, retention, and role of accessory cells. *Cell,* 124**,** 175-89.

Gulati, R., Jevremovic, D., Peterson, T. E., Chatterjee, S., Shah, V., Vile, R. G. & Simari, R. D. 2003. Diverse origin and function of cells with endothelial phenotype obtained from adult human blood. *Circ Res,* 93**,** 1023-5.

Gutierrez-Rodriguez, M., Reyes-Maldonado, E. & Mayani, H. 2000. Characterization of the adherent cells developed in Dexter-type long-term cultures from human umbilical cord blood. *Stem Cells,* 18**,** 46-52.

Haas, R., Mohle, R., Fruhauf, S., Goldschmidt, H., Witt, B., Flentje, M., Wannenmacher, M. & Hunstein, W. 1994. Patient characteristics associated with successful mobilizing and autografting of peripheral blood progenitor cells in malignant lymphoma. *Blood,* 83**,** 3787-94.

Hill, J. M., Zalos, G., Halcox, J. P., Schenke, W. H., Waclawiw, M. A., Quyyumi, A. A. & Finkel, T. 2003. Circulating endothelial progenitor cells, vascular function, and cardiovascular risk. *N Engl J Med,* 348**,** 593-600.

Hirschi, K. K., Ingram, D. A. & Yoder, M. C. 2008. Assessing identity, phenotype, and fate of endothelial progenitor cells. *Arterioscler Thromb Vasc Biol,* 28**,** 1584-95.

Hirschi, K. K., Rohovsky, S. A., Beck, L. H., Smith, S. R. & D'amore, P. A. 1999. Endothelial cells modulate the proliferation of mural cell precursors via platelet-derived growth factor-BB and heterotypic cell contact. *Circ Res,* 84**,** 298-305.

Hofmann, N. A., Reinisch, A. & Strunk, D. 2009. Isolation and large scale expansion of adult human endothelial colony forming progenitor cells. *J Vis Exp*.

Horwitz, E. M., Gordon, P. L., Koo, W. K., Marx, J. C., Neel, M. D., Mcnall, R. Y., Muul, L. & Hofmann, T. 2002. Isolated allogeneic bone marrow-derived mesenchymal cells engraft and stimulate growth in children with osteogenesis imperfecta: Implications for cell therapy of bone. *Proc Natl Acad Sci U S A,* 99**,** 8932-7.

Horwitz, E. M., Le Blanc, K., Dominici, M., Mueller, I., Slaper-Cortenbach, I., Marini, F. C., Deans, R. J., Krause, D. S. & Keating, A. 2005. Clarification of the nomenclature for MSC: The international society for cellular therapy position statement. *Cytotherapy,* 7**,** 393-395.

Horwitz, E. M., Prockop, D. J., Fitzpatrick, L. A., Koo, W. W., Gordon, P. L., Neel, M., Sussman, M., Orchard, P., Marx, J. C., Pyeritz, R. E. & Brenner, M. K. 1999. Transplantability and therapeutic effects of bone marrow-derived mesenchymal cells in children with osteogenesis imperfecta. *Nat Med,* 5**,** 309-13.

Horwitz, E. M., Prockop, D. J., Gordon, P. L., Koo, W. W., Fitzpatrick, L. A., Neel, M. D., Mccarville, M. E., Orchard, P. J., Pyeritz, R. E. & Brenner, M. K. 2001. Clinical responses to bone marrow transplantation in children with severe osteogenesis imperfecta. *Blood,* 97**,** 1227-31.

Huang, L., Hou, D., Thompson, M. A., Baysden, S. E., Shelley, W. C., Ingram, D. A., March, K. L. & Yoder, M. C. 2007. Acute myocardial infarction in swine rapidly and selectively releases highly proliferative endothelial colony forming cells (ECFCs) into circulation. *Cell Transplant,* 16**,** 887-97.

Hur, J., Yoon, C. H., Kim, H. S., Choi, J. H., Kang, H. J., Hwang, K. K., Oh, B. H., Lee, M. M. & Park, Y. B. 2004. Characterization of two types of endothelial progenitor cells and their different contributions to neovasculogenesis. *Arterioscler Thromb Vasc Biol,* 24**,** 288-93.

In 'T Anker, P. S., Scherjon, S. A., Kleijburg-Van Der Keur, C., Noort, W. A., Claas, F. H., Willemze, R., Fibbe, W. E. & Kanhai, H. H. 2003. Amniotic fluid as a novel source of mesenchymal stem cells for therapeutic transplantation. *Blood,* 102**,** 1548-9.

Ingram, D. A., Caplice, N. M. & Yoder, M. C. 2005a. Unresolved questions, changing definitions, and novel paradigms for defining endothelial progenitor cells. *Blood,* 106**,** 1525-31.

Ingram, D. A., Mead, L. E., Moore, D. B., Woodard, W., Fenoglio, A. & Yoder, M. C. 2005b. Vessel wall-derived endothelial cells rapidly proliferate because they

contain a complete hierarchy of endothelial progenitor cells. *Blood,* 105**,** 2783-6.

Ingram, D. A., Mead, L. E., Tanaka, H., Meade, V., Fenoglio, A., Mortell, K., Pollok, K., Ferkowicz, M. J., Gilley, D. & Yoder, M. C. 2004. Identification of a novel hierarchy of endothelial progenitor cells using human peripheral and umbilical cord blood. *Blood,* 104**,** 2752-60.

Ittrich, H., Lange, C., Dahnke, H., Zander, A. R., Adam, G. & Nolte-Ernsting, C. 2005. [Labeling of mesenchymal stem cells with different superparamagnetic particles of iron oxide and detectability with MRI at 3T]. *Rofo,* 177**,** 1151-63.

Jaffredo, T., Gautier, R., Eichmann, A. & Dieterlen-Lievre, F. 1998. Intraaortic hemopoietic cells are derived from endothelial cells during ontogeny. *Development,* 125**,** 4575-83.

Janic, B., Rad, A. M., Jordan, E. K., Iskander, A. S., Ali, M. M., Varma, N. R., Frank, J. A. & Arbab, A. S. 2009. Optimization and validation of FePro cell labeling method. *PLoS One,* 4**,** e5873.

Jiang, Y. H., Vaessena, B., Lenvik, T., Blackstad, M., Reyes, M. & Verfaillie, C. M. 2002. Multipotent progenitor cells can be isolated from postnatal murine bone marrow, muscle, and brain. *Exp Hematol,* 30**,** 896.

Jin, D. K., Shido, K., Kopp, H. G., Petit, I., Shmelkov, S. V., Young, L. M., Hooper, A. T., Amano, H., Avecilla, S. T., Heissig, B., Hattori, K., Zhang, F., Hicklin, D. J., Wu, Y., Zhu, Z., Dunn, A., Salari, H., Werb, Z., Hackett, N. R., Crystal, R. G., Lyden, D. & Rafii, S. 2006. Cytokine-mediated deployment of SDF-1 induces revascularization through recruitment of CXCR4+ hemangiocytes. *Nat Med,* 12**,** 557-67.

Kern, S., Eichler, H., Stoeve, J., Kluter, H. & Bieback, K. 2006. Comparative analysis of mesenchymal stem cells from bone marrow, umbilical cord blood, or adipose tissue. *Stem Cells,* 24**,** 1294-301.

Khakoo, A. Y. & Finkel, T. 2005. Endothelial progenitor cells. *Annu Rev Med,* 56**,** 79-101.

Kiel, M. J., Radice, G. L. & Morrison, S. J. 2007. Lack of evidence that hematopoietic stem cells depend on N-cadherin-mediated adhesion to osteoblasts for their maintenance. *Cell Stem Cell,* 1**,** 204-17.

Kiel, M. J., Yilmaz, O. H., Iwashita, T., Terhorst, C. & Morrison, S. J. 2005. SLAM family receptors distinguish hematopoietic stem and progenitor cells and reveal endothelial niches for stem cells. *Cell,* 121**,** 1109-21.

Kitoh, H., Kitakoji, T., Tsuchiya, H., Katoh, M. & Ishiguro, N. 2007. Transplantation of culture expanded bone marrow cells and platelet rich plasma in distraction osteogenesis of the long bones. *Bone,* 40**,** 522-8.

Koc, O. N., Day, J., Nieder, M., Gerson, S. L., Lazarus, H. M. & Krivit, W. 2002. Allogeneic mesenchymal stem cell infusion for treatment of metachromatic leukodystrophy (MLD) and Hurler syndrome (MPS-IH). *Bone Marrow Transplant,* 30**,** 215-22.

Koc, O. N., Gerson, S. L., Cooper, B. W., Dyhouse, S. M., Haynesworth, S. E., Caplan, A. I. & Lazarus, H. M. 2000. Rapid hematopoietic recovery after coinfusion of autologous-blood stem cells and culture-expanded marrow mesenchymal stem cells in advanced breast cancer patients receiving high-dose chemotherapy. *J Clin Oncol,* 18**,** 307-16.

Kocaoemer, A., Kern, S., Klueter, H. & Bieback, K. 2007. Human AB-Serum as well as Thrombin-activated Platelet-Rich-Plasma are suitable Alternatives to Fetal Calf Serum for the Expansion of Mesenchymal Stem Cells from Adipose Tissue. *Stem Cells*.

Kogler, G., Sensken, S., Airey, J. A., Trapp, T., Muschen, M., Feldhahn, N., Liedtke, S., Sorg, R. V., Fischer, J., Rosenbaum, C., Greschat, S., Knipper, A., Bender, J., Degistirici, O., Gao, J., Caplan, A. I., Colletti, E. J., Almeida-Porada, G., Muller, H. W., Zanjani, E. & Wernet, P. 2004. A new human somatic stem cell from placental cord blood with intrinsic pluripotent differentiation potential. *J.Exp.Med.,* 200**,** 123.

Kovacic, J. C., Moore, J., Herbert, A., Ma, D., Boehm, M. & Graham, R. M. 2008. Endothelial progenitor cells, angioblasts, and angiogenesis--old terms reconsidered from a current perspective. *Trends Cardiovasc Med,* 18**,** 45-51.

Kucia, M., Reca, R., Campbell, F. R., Zuba-Surma, E., Majka, M., Ratajczak, J. & Ratajczak, M. Z. 2006. A population of very small embryonic-like (VSEL) CXCR4(+)SSEA-1(+)Oct-4+ stem cells identified in adult bone marrow. *Leukemia,* 20**,** 857-69.

Kuznetsov, S. A., Friedenstein, A. J. & Robey, P. G. 1997a. Factors required for bone marrow stromal fibroblast colony formation in vitro. *Br J Haematol,* 97**,** 561-70.

Kuznetsov, S. A., Krebsbach, P. H., Satomura, K., Kerr, J., Riminucci, M., Benayahu, D. & Robey, P. G. 1997b. Single-colony derived strains of human marrow stromal fibroblasts form bone after transplantation in vivo. *J Bone Miner Res,* 12**,** 1335-47.

Kuznetsov, S. A., Mankani, M. H. & Robey, P. G. 2000. Effect of serum on human bone marrow stromal cells: ex vivo expansion and in vivo bone formation. *Transplantation,* 70**,** 1780-7.

Lange, C., Cakiroglu, F., Spiess, A. N., Cappallo-Obermann, H., Dierlamm, J. & Zander, A. R. 2007. Accelerated and safe expansion of human mesenchymal stromal cells in animal serum-free medium for transplantation and regenerative medicine. *J Cell Physiol,* 213**,** 18-26.

Lazarus, H. M., Haynesworth, S. E., Gerson, S. L., Rosenthal, N. S. & Caplan, A. I. 1995. Ex vivo expansion and subsequent infusion of human bone marrow-derived stromal progenitor cells (mesenchymal progenitor cells): implications for therapeutic use. *Bone Marrow Transplant,* 16**,** 557-64.

Lazarus, H. M., Koc, O. N., Devine, S. M., Curtin, P., Maziarz, R. T., Holland, H. K., Shpall, E. J., Mccarthy, P., Atkinson, K., Cooper, B. W., Gerson, S. L., Laughlin, M. J., Loberiza, F. R., Jr., Moseley, A. B. & Bacigalupo, A. 2005. Cotransplantation of HLA-identical sibling culture-expanded mesenchymal stem cells and hematopoietic stem cells in hematologic malignancy patients. *Biol Blood Marrow Transplant,* 11**,** 389-98.

Le Blanc, K. 2003. Immunomodulatory effects of fetal and adult mesenchymal stem cells. *Cytotherapy,* 5**,** 485-9.

Le Blanc, K., Frassoni, F., Ball, L., Locatelli, F., Roelofs, H., Lewis, I., Lanino, E., Sundberg, B., Bernardo, M. E., Remberger, M., Dini, G., Egeler, R. M., Bacigalupo, A., Fibbe, W. & Ringden, O. 2008. Mesenchymal stem cells for treatment of steroid-resistant, severe, acute graft-versus-host disease: a phase II study. *Lancet,* 371**,** 1579-86.

Le Blanc, K. & Pittenger, M. 2005. Mesenchymal stem cells: progress toward promise. *Cytotherapy,* 7**,** 36-45.

Le Blanc, K., Rasmusson, I., Sundberg, B., Gotherstrom, C., Hassan, M., Uzunel, M. & Ringden, O. 2004. Treatment of severe acute graft-versus-host disease with third party haploidentical mesenchymal stem cells. *Lancet,* 363**,** 1439-41.

Le Blanc, K., Tammik, L., Sundberg, B., Haynesworth, S. E. & Ringden, O. 2003. Mesenchymal stem cells inhibit and stimulate mixed lymphocyte cultures and mitogenic responses independently of the major histocompatibility complex. *Scand J Immunol,* 57**,** 11-20.

Lee, R. H., Pulin, A. A., Seo, M. J., Kota, D. J., Ylostalo, J., Larson, B. L., Semprun-Prieto, L., Delafontaine, P. & Prockop, D. J. 2009. Intravenous hMSCs improve myocardial infarction in mice because cells embolized in lung are activated to secrete the anti-inflammatory protein TSG-6. *Cell Stem Cell,* 5**,** 54-63.

Lee, S. T., Jang, J. H., Cheong, J. W., Kim, J. S., Maemg, H. Y., Hahn, J. S., Ko, Y. W. & Min, Y. H. 2002. Treatment of high-risk acute myelogenous leukaemia by myeloablative chemoradiotherapy followed by co-infusion of T cell-depleted haematopoietic stem cells and culture-expanded marrow mesenchymal stem cells from a related donor with one fully mismatched human leucocyte antigen haplotype. *Br J Haematol,* 118**,** 1128-31.

Lin, Y., Weisdorf, D. J., Solovey, A. & Hebbel, R. P. 2000. Origins of circulating endothelial cells and endothelial outgrowth from blood. *J Clin Invest,* 105**,** 71-7.

Lu, L. L., Liu, Y. J., Yang, S. G., Zhao, Q. J., Wang, X., Gong, W., Han, Z. B., Xu, Z. S., Lu, Y. X., Liu, D., Chen, Z. Z. & Han, Z. C. 2006. Isolation and characterization of human umbilical cord mesenchymal stem cells with hematopoiesis-supportive function and other potentials. *Haematologica,* 91**,** 1017-26.

Lucarelli, E., Fini, M., Beccheroni, A., Giavaresi, G., Di Bella, C., Aldini, N. N., Guzzardella, G., Martini, L., Cenacchi, A., Di Maggio, N., Sangiorgi, L., Fornasari, P. M., Mercuri, M., Giardino, R. & Donati, D. 2005. Stromal stem cells and platelet-rich plasma improve bone allograft integration. *Clin Orthop Relat Res***,** 62-8.

Lyden, D., Hattori, K., Dias, S., Costa, C., Blaikie, P., Butros, L., Chadburn, A., Heissig, B., Marks, W., Witte, L., Wu, Y., Hicklin, D., Zhu, Z., Hackett, N. R., Crystal, R. G., Moore, M. A., Hajjar, K. A., Manova, K., Benezra, R. & Rafii, S. 2001. Impaired recruitment of bone-marrow-derived endothelial and hematopoietic precursor cells blocks tumor angiogenesis and growth. *Nat Med,* 7**,** 1194-201.

Mackensen, A., Drager, R., Schlesier, M., Mertelsmann, R. & Lindemann, A. 2000. Presence of IgE antibodies to bovine serum albumin in a patient developing anaphylaxis after vaccination with human peptide-pulsed dendritic cells. *Cancer Immunol Immunother,* 49**,** 152-6.

Majdic, O., Stockl, J., Pickl, W. F., Bohuslav, J., Strobl, H., Scheinecker, C., Stockinger, H. & Knapp, W. 1994. Signaling and induction of enhanced cytoadhesiveness via the hematopoietic progenitor cell surface molecule CD34. *Blood,* 83**,** 1226-34.

Majeti, R., Park, C. Y. & Weissman, I. L. 2007. Identification of a hierarchy of multipotent hematopoietic progenitors in human cord blood. *Cell Stem Cell,* 1**,** 635-45.

Mannello, F. & Tonti, G. A. 2007. Concise review: no breakthroughs for human mesenchymal and embryonic stem cell culture: conditioned medium, feeder layer, or feeder-free; medium with fetal calf serum, human serum, or enriched plasma; serum-free, serum replacement nonconditioned medium, or ad hoc formula? All that glitters is not gold! *Stem Cells,* 25**,** 1603-9.

Mareschi, K., Biasin, E., Piacibello, W., Aglietta, M., Madon, E. & Fagioli, F. 2001. Isolation of human mesenchymal stem cells: bone marrow versus umbilical cord blood. *Haematologica,* 86**,** 1099-100.

Matoba, S., Tatsumi, T., Murohara, T., Imaizumi, T., Katsuda, Y., Ito, M., Saito, Y., Uemura, S., Suzuki, H., Fukumoto, S., Yamamoto, Y., Onodera, R., Teramukai, S., Fukushima, M. & Matsubara, H. 2008. Long-term clinical outcome after intramuscular implantation of bone marrow mononuclear cells (Therapeutic Angiogenesis by Cell Transplantation [TACT] trial) in patients with chronic limb ischemia. *Am Heart J,* 156**,** 1010-8.

Mayani, H. & Lansdorp, P. M. 1998. Biology of human umbilical cord blood-derived hematopoietic stem/progenitor cells. *Stem Cells,* 16**,** 153-65.

Melero-Martin, J. M., De Obaldia, M. E., Kang, S. Y., Khan, Z. A., Yuan, L., Oettgen, P. & Bischoff, J. 2008. Engineering robust and functional vascular networks in vivo with human adult and cord blood-derived progenitor cells. *Circ Res,* 103**,** 194-202.

Melero-Martin, J. M., Khan, Z. A., Picard, A., Wu, X., Paruchuri, S. & Bischoff, J. 2007. In vivo vasculogenic potential of human blood-derived endothelial progenitor cells. *Blood,* 109**,** 4761-8.

Miao, Z., Jin, J., Chen, L., Zhu, J., Huang, W., Zhao, J., Qian, H. & Zhang, X. 2006. Isolation of mesenchymal stem cells from human placenta: comparison with human bone marrow mesenchymal stem cells. *Cell Biol Int,* 30**,** 681-7.

Michaelis, M., Kohler, N., Reinisch, A., Eikel, D., Gravemann, U., Doerr, H. W., Nau, H. & Cinatl, J., Jr. 2004. Increased human cytomegalovirus replication in fibroblasts after treatment with therapeutical plasma concentrations of valproic acid. *Biochem Pharmacol,* 68**,** 531-8.

Michaelis, M., Suhan, T., Reinisch, A., Reisenauer, A., Fleckenstein, C., Eikel, D., Gumbel, H., Doerr, H. W., Nau, H. & Cinatl, J., Jr. 2005. Increased replication of human cytomegalovirus in retinal pigment epithelial cells by valproic acid depends on histone deacetylase inhibition. *Invest Ophthalmol Vis Sci,* 46**,** 3451-7.

Monasch, R., Reinisch, A., Steketee, R. W., Korenromp, E. L., Alnwick, D. & Bergevin, Y. 2004. Child coverage with mosquito nets and malaria treatment from population-based surveys in african countries: a baseline for monitoring progress in roll back malaria. *Am J Trop Med Hyg,* 71**,** 232-8.

Muller, I., Kordowich, S., Holzwarth, C., Spano, C., Isensee, G., Staiber, A., Viebahn, S., Gieseke, F., Langer, H., Gawaz, M., Horwitz, E., Conte, P., Handgretinger, R. & Dominici, M. 2006. Animal serum-free culture conditions for isolation and expansion of multipotent mesenchymal stromal cells from human BM. *Cytotherapy,* 8**,** 437-44.

Murray, L., Chen, B., Galy, A., Chen, S., Tushinski, R., Uchida, N., Negrin, R., Tricot, G., Jagannath, S., Vesole, D. & Et Al. 1995. Enrichment of human hematopoietic stem cell activity in the CD34+Thy-1+Lin- subpopulation from mobilized peripheral blood. *Blood,* 85**,** 368-78.

Murry, C. E., Soonpaa, M. H., Reinecke, H., Nakajima, H., Nakajima, H. O., Rubart, M., Pasumarthi, K. B., Virag, J. I., Bartelmez, S. H., Poppa, V., Bradford, G., Dowell, J. D., Williams, D. A. & Field, L. J. 2004. Haematopoietic stem cells do not transdifferentiate into cardiac myocytes in myocardial infarcts. *Nature,* 428**,** 664-8.

Muul, L. M., Tuschong, L. M., Soenen, S. L., Jagadeesh, G. J., Ramsey, W. J., Long, Z., Carter, C. S., Garabedian, E. K., Alleyne, M., Brown, M., Bernstein, W.,

Schurman, S. H., Fleisher, T. A., Leitman, S. F., Dunbar, C. E., Blaese, R. M. & Candotti, F. 2003. Persistence and expression of the adenosine deaminase gene for 12 years and immune reaction to gene transfer components: long-term results of the first clinical gene therapy trial. *Blood,* 101**,** 2563-9.

Pittenger, M. F., Mackay, A. M., Beck, S. C., Jaiswal, R. K., Douglas, R., Mosca, J. D., Moorman, M. A., Simonetti, D. W., Craig, S. & Marshak, D. R. 1999. Multilineage potential of adult human mesenchymal stem cells. *Science,* 284**,** 143-47.

Pompilio, G., Steinhoff, G., Liebold, A., Pesce, M., Alamanni, F., Capogrossi, M. C. & Biglioli, P. 2008. Direct minimally invasive intramyocardial injection of bone marrow-derived AC133+ stem cells in patients with refractory ischemia: preliminary results. *Thorac Cardiovasc Surg,* 56**,** 71-6.

Prockop, D. J. 1997. Marrow stromal cells as stem cells for nonhematopoietic tissues. *Science,* 276**,** 71-4.

Prockop, D. J., Gregory, C. A. & Spees, J. L. 2003. One strategy for cell and gene therapy: harnessing the power of adult stem cells to repair tissues. *Proc.Natl.Acad.Sci.U.S.A,* 100 Suppl 1**,** 11917.

Purhonen, S., Palm, J., Rossi, D., Kaskenpaa, N., Rajantie, I., Yla-Herttuala, S., Alitalo, K., Weissman, I. L. & Salven, P. 2008. Bone marrow-derived circulating endothelial precursors do not contribute to vascular endothelium and are not needed for tumor growth. *Proc Natl Acad Sci U S A,* 105**,** 6620-5.

Rafii, S. & Lyden, D. 2003. Therapeutic stem and progenitor cell transplantation for organ vascularization and regeneration. *Nat Med,* 9**,** 702-12.

Rafii, S., Shapiro, F., Rimarachin, J., Nachman, R. L., Ferris, B., Weksler, B., Moore, M. A. & Asch, A. S. 1994. Isolation and characterization of human bone marrow microvascular endothelial cells: hematopoietic progenitor cell adhesion 102. *Blood,* 84**,** 10-19.

Reinisch, A., Bartmann, C., Rohde, E., Schallmoser, K., Bjelic-Radisic, V., Lanzer, G., Linkesch, W. & Strunk, D. 2007. Humanized system to propagate cord blood-derived multipotent mesenchymal stromal cells for clinical application. *Regen Med,* 2**,** 371-82.

Reinisch, A., Hofmann, N. A., Obenauf, A. C., Kashofer, K., Rohde, E., Schallmoser, K., Flicker, K., Lanzer, G., Linkesch, W., Speicher, M. R. & Strunk, D. 2009. Humanized large-scale expanded endothelial colony-forming cells function in vitro and in vivo. *Blood,* 113**,** 6716-25.

Reinisch, A. & Strunk, D. 2009. Isolation and animal serum free expansion of human umbilical cord derived mesenchymal stromal cells (MSCs) and endothelial colony forming progenitor cells (ECFCs). *J Vis Exp*.

Reyes, M., Lund, T., Lenvik, T., Aguiar, D., Koodie, L. & Verfaillie, C. M. 2001. Purification and ex vivo expansion of postnatal human marrow mesodermal progenitor cells. *Blood,* 98**,** 2615.

Ringden, O., Uzunel, M., Rasmusson, I., Remberger, M., Sundberg, B., Lonnies, H., Marschall, H. U., Dlugosz, A., Szakos, A., Hassan, Z., Omazic, B., Aschan, J., Barkholt, L. & Le Blanc, K. 2006. Mesenchymal stem cells for treatment of therapy-resistant graft-versus-host disease. *Transplantation,* 81**,** 1390-7.

Robinson, S. N., Ng, J., Niu, T., Yang, H., Mcmannis, J. D., Karandish, S., Kaur, I., Fu, P., Del Angel, M., Messinger, R., Flagge, F., De Lima, M., Decker, W., Xing, D., Champlin, R. & Shpall, E. J. 2006. Superior ex vivo cord blood expansion following co-culture with bone marrow-derived mesenchymal stem cells. *Bone Marrow Transplant,* 37**,** 359-66.

Rocha, V., Labopin, M., Sanz, G., Arcese, W., Schwerdtfeger, R., Bosi, A., Jacobsen, N., Ruutu, T., De Lima, M., Finke, J., Frassoni, F. & Gluckman, E. 2004. Transplants of umbilical-cord blood or bone marrow from unrelated donors in adults with acute leukemia. *N Engl J Med,* 351**,** 2276-85.

Rohde E, Schallmoser K , Bartmann C, Reinisch A & D, S. 2008a. GMP-Compliant Propagation of Human Multipotent Mesenchymal Stromal Cells. *In:* GAD, S. C. (ed.) *Pharmaceutical Manufacturing Handbook: Regulations and Quality.* John Wiley & Sons, Inc.

Rohde E, Schallmoser K , Bartmann C, Reinisch A & D, S. 2008b. *GMP Compliant Propagation of Human Multipotent Mesenchymal Stromal Cells (MSC)*, The pharmaceutical development handbook.

Rohde, E., Bartmann, C., Schallmoser, K., Reinisch, A., Lanzer, G., Linkesch, W., Guelly, C. & Strunk, D. 2007. Immune cells mimic the morphology of endothelial progenitor colonies in vitro. *Stem Cells,* 25**,** 1746-52.

Rohde, E., Malischnik, C., Thaler, D., Maierhofer, T., Linkesch, W., Lanzer, G., Guelly, C. & Strunk, D. 2006. Blood monocytes mimic endothelial progenitor cells. *Stem Cells,* 24**,** 357-67.

Romanov, Y. A., Svintsitskaya, V. A. & Smirnov, V. N. 2003. Searching for alternative sources of postnatal human mesenchymal stem cells: candidate MSC-like cells from umbilical cord. *Stem Cells,* 21**,** 105-10.

Ruiz De Almodovar, C., Luttun, A. & Carmeliet, P. 2006. An SDF-1 trap for myeloid cells stimulates angiogenesis. *Cell,* 124**,** 18-21.

Sacchetti, B., Funari, A., Michienzi, S., Di Cesare, S., Piersanti, S., Saggio, I., Tagliafico, E., Ferrari, S., Robey, P. G., Riminucci, M. & Bianco, P. 2007. Self-renewing osteoprogenitors in bone marrow sinusoids can organize a hematopoietic microenvironment. *Cell,* 131**,** 324-36.

Sakamoto, N., Tsuji, K., Muul, L. M., Lawler, A. M., Petricoin, E. F., Candotti, F., Metcalf, J. A., Tavel, J. A., Lane, H. C., Urba, W. J., Fox, B. A., Varki, A.,

Lunney, J. K. & Rosenberg, A. S. 2007. Bovine apolipoprotein B-100 is a dominant immunogen in therapeutic cell populations cultured in fetal calf serum in mice and humans. *Blood,* 110**,** 501-8.

Sarugaser, R., Lickorish, D., Baksh, D., Hosseini, M. M. & Davies, J. E. 2005. Human umbilical cord perivascular (HUCPV) cells: a source of mesenchymal progenitors. *Stem Cells,* 23**,** 220-9.

Schallmoser, K., Bartmann, C. & Rohde, E., Et Al. 2007a. Human platelet lysate can replace fetal bovine serum for clinical scale expansion of functional MSC. *Transfusion*.

Schallmoser, K., Bartmann, C., Rohde, E., Reinisch, A., Kashofer, K., Stadelmeyer, E., Drexler, C., Lanzer, G., Linkesch, W. & Strunk, D. 2007b. Human platelet lysate can replace fetal bovine serum for clinical-scale expansion of functional mesenchymal stromal cells. *Transfusion,* 47**,** 1436-46.

Schallmoser, K., Rohde, E., Bartmann, C., Obenauf, A. C., Reinisch, A. & Strunk, D. 2009. Platelet-derived growth factors for GMP-compliant propagation of mesenchymal stromal cells. *Biomed Mater Eng,* 19**,** 271-6.

Schallmoser, K., Rohde, E., Reinisch, A., Bartmann, C., Thaler, D., Drexler, C., Obenauf, A., Lanzer, G., Linkesch, W. & Strunk, D. 2008. Rapid large-scale expansion of functional mesenchymal stem cells from unmanipulated bone marrow without animal serum *Tissue Eng Part C Methods,* 14**,** 185-196.

Schallmoser, K. & Strunk, D. 2009. Preparation of pooled human platelet lysate (pHPL) as an efficient supplement for animal serum-free human stem cell cultures. *J Vis Exp*.

Schatteman, G. C., Dunnwald, M. & Jiao, C. 2007. Biology of bone marrow-derived endothelial cell precursors. *Am J Physiol Heart Circ Physiol,* 292**,** H1-18.

Schofield, R. 1978. The relationship between the spleen colony-forming cell and the haemopoietic stem cell. *Blood Cells,* 4**,** 7-25.

Selvaggi, T. A., Walker, R. E. & Fleisher, T. A. 1997. Development of antibodies to fetal calf serum with arthus-like reactions in human immunodeficiency virus-infected patients given syngeneic lymphocyte infusions. *Blood,* 89**,** 776-9.

Serke, S. & Johnsen, H. E. 2001. A European reference protocol for quality assessment and clinical validation of autologous haematopoietic blood progenitor and stem cell grafts. *Bone Marrow Transplant,* 27**,** 463-70.

Shpall, E. J., Champlin, R. & Glaspy, J. A. 1998. Effect of CD34+ peripheral blood progenitor cell dose on hematopoietic recovery. *Biol Blood Marrow Transplant,* 4**,** 84-92.

Shultz, L. D., Ishikawa, F. & Greiner, D. L. 2007a. Humanized mice in translational biomedical research. *Nat Rev Immunol,* 7**,** 118-30.

Shultz, L. D., Pearson, T., King, M., Giassi, L., Carney, L., Gott, B., Lyons, B., Rossini, A. A. & Greiner, D. L. 2007b. Humanized NOD/LtSz-scid IL2 receptor common gamma chain knockout mice in diabetes research. *Ann N Y Acad Sci,* 1103**,** 77-89.

Simmons, P. J. & Torok-Storb, B. 1991. Identification of stromal cell precursors in human bone marrow by a novel monoclonal antibody, STRO-1. *Blood,* 78**,** 55-62.

Solovey, A., Lin, Y., Browne, P., Choong, S., Wayner, E. & Hebbel, R. P. 1997. Circulating activated endothelial cells in sickle cell anemia. *N Engl J Med,* 337**,** 1584-90.

Spangrude, G. J., Heimfeld, S. & Weissman, I. L. 1988. Purification and characterization of mouse hematopoietic stem cells. *Science,* 241**,** 58-62.

Spees, J. L., Gregory, C. A., Singh, H., Tucker, H. A., Peister, A., Lynch, P. J., Hsu, S. C., Smith, J. & Prockop, D. J. 2004. Internalized antigens must be removed to prepare hypoimmunogenic mesenchymal stem cells for cell and gene therapy. *Mol Ther,* 9**,** 747-56.

Stier, S., Ko, Y., Forkert, R., Lutz, C., Neuhaus, T., Grunewald, E., Cheng, T., Dombkowski, D., Calvi, L. M., Rittling, S. R. & Scadden, D. T. 2005. Osteopontin is a hematopoietic stem cell niche component that negatively regulates stem cell pool size. *J Exp Med,* 201**,** 1781-91.

Sugiyama, T., Kohara, H., Noda, M. & Nagasawa, T. 2006. Maintenance of the hematopoietic stem cell pool by CXCL12-CXCR4 chemokine signaling in bone marrow stromal cell niches. *Immunity,* 25**,** 977-88.

Sundin, M., Ringden, O., Sundberg, B., Nava, S., Gotherstromm, C. & Le Blanc, K. 2007. No alloantibodies against mesenchymal stromal cells, but presence of anti-fetal calf serum antibodies, after transplantation in allogeneic hematopoietic stem cell recipients. *Haematologica,* 92**,** 1208-15.

Tavassoli, M. & Crosby, W. H. 1968. Transplantation of marrow to extramedullary sites. *Science,* 161**,** 54-6.

Thomas, E. D., Lochte, H. L., Jr., Lu, W. C. & Ferrebee, J. W. 1957. Intravenous infusion of bone marrow in patients receiving radiation and chemotherapy. *N Engl J Med,* 257**,** 491-6.

Till, J. E. & Mc, C. E. 1961. A direct measurement of the radiation sensitivity of normal mouse bone marrow cells. *Radiat Res,* 14**,** 213-22.

Timmermans, F., Van Hauwermeiren, F., De Smedt, M., Raedt, R., Plasschaert, F., De Buyzere, M. L., Gillebert, T. C., Plum, J. & Vandekerckhove, B. 2007. Endothelial outgrowth cells are not derived from CD133+ cells or CD45+ hematopoietic precursors. *Arterioscler Thromb Vasc Biol,* 27**,** 1572-9.

Traktuev, D. O., Prater, D. N., Merfeld-Clauss, S., Sanjeevaiah, A. R., Saadatzadeh, M. R., Murphy, M., Johnstone, B. H., Ingram, D. A. & March, K. L. 2009. Robust functional vascular network formation in vivo by cooperation of adipose progenitor and endothelial cells. *Circ Res,* 104**,** 1410-20.

Tuschong, L., Soenen, S. L., Blaese, R. M., Candotti, F. & Muul, L. M. 2002. Immune response to fetal calf serum by two adenosine deaminase-deficient patients after T cell gene therapy. *Hum Gene Ther,* 13**,** 1605-10.

Uccelli, A., Moretta, L. & Pistoia, V. 2008. Mesenchymal stem cells in health and disease. *Nat Rev Immunol,* 8**,** 726-36.

Vasa, M., Fichtlscherer, S., Adler, K., Aicher, A., Martin, H., Zeiher, A. M. & Dimmeler, S. 2001a. Increase in circulating endothelial progenitor cells by statin therapy in patients with stable coronary artery disease. *Circulation,* 103**,** 2885.

Vasa, M., Fichtlscherer, S., Aicher, A., Adler, K., Urbich, C., Martin, H., Zeiher, A. M. & Dimmeler, S. 2001b. Number and migratory activity of circulating endothelial progenitor cells inversely correlate with risk factors for coronary artery disease. *Circ Res,* 89**,** E1-7.

Wang, H. S., Hung, S. C., Peng, S. T., Huang, C. C., Wei, H. M., Guo, Y. J., Fu, Y. S., Lai, M. C. & Chen, C. C. 2004. Mesenchymal stem cells in the Wharton's jelly of the human umbilical cord. *Stem Cells,* 22**,** 1330-7.

Wilhelm, C., Bal, L., Smirnov, P., Galy-Fauroux, I., Clement, O., Gazeau, F. & Emmerich, J. 2007. Magnetic control of vascular network formation with magnetically labeled endothelial progenitor cells. *Biomaterials,* 28**,** 3797-806.

Ye, Z. Q., Burkholder, J. K., Qiu, P., Schultz, J. C., Shahidi, N. T. & Yang, N. S. 1994. Establishment of an adherent cell feeder layer from human umbilical cord blood for support of long-term hematopoietic progenitor cell growth. *Proc Natl Acad Sci U S A,* 91**,** 12140-4.

Yin, A. H., Miraglia, S., Zanjani, E. D., Almeida-Porada, G., Ogawa, M., Leary, A. G., Olweus, J., Kearney, J. & Buck, D. W. 1997. AC133, a novel marker for human hematopoietic stem and progenitor cells. *Blood,* 90**,** 5002-12.

Yoder, M. C., Mead, L. E., Prater, D., Krier, T. R., Mroueh, K. N., Li, F., Krasich, R., Temm, C. J., Prchal, J. T. & Ingram, D. A. 2006. Re-defining endothelial progenitor cells via clonal analysis and hematopoietic stem/progenitor cell principals. *Blood,* 109**,** 1801-1809.

Yoder, M. C., Mead, L. E., Prater, D., Krier, T. R., Mroueh, K. N., Li, F., Krasich, R., Temm, C. J., Prchal, J. T. & Ingram, D. A. 2007. Redefining endothelial progenitor cells via clonal analysis and hematopoietic stem/progenitor cell principals. *Blood,* 109**,** 1801-9.

Yoon, C. H., Hur, J., Park, K. W., Kim, J. H., Lee, C. S., Oh, I. Y., Kim, T. Y., Cho, H. J., Kang, H. J., Chae, I. H., Yang, H. K., Oh, B. H., Park, Y. B. & Kim, H. S.

2005. Synergistic neovascularization by mixed transplantation of early endothelial progenitor cells and late outgrowth endothelial cells: the role of angiogenic cytokines and matrix metalloproteinases. *Circulation,* 112**,** 1618-27.

Zhang, J., Niu, C., Ye, L., Huang, H., He, X., Tong, W. G., Ross, J., Haug, J., Johnson, T., Feng, J. Q., Harris, S., Wiedemann, L. M., Mishina, Y. & Li, L. 2003. Identification of the haematopoietic stem cell niche and control of the niche size. *Nature,* 425**,** 836-41.

Ziegler, B. L., Valtieri, M., Porada, G. A., De Maria, R., Muller, R., Masella, B., Gabbianelli, M., Casella, I., Pelosi, E., Bock, T., Zanjani, E. D. & Peschle, C. 1999. KDR receptor: a key marker defining hematopoietic stem cells. *Science,* 285**,** 1553-8.

Zuk, P. A., Zhu, M., Ashjian, P., De Ugarte, D. A., Huang, J. I., Mizuno, H., Alfonso, Z. C., Fraser, J. K., Benhaim, P. & Hedrick, M. H. 2002. Human adipose tissue is a source of multipotent stem cells. *Mol Biol Cell,* 13**,** 4279-95.

11 Declaration

I hereby declare that this thesis is my own original work and that I have fully acknowledged by name all of those individuals and organisations that have contributed to the research for this thesis. Throughout this thesis and in all related publications I followed the guidelines of “Good Scientific Practice”.

Date Signature

12 Appendix I

Humanized system to propagate cord blood-derived multipotent mesenchymal stromal cells for clinical application.

Reinisch A, Bartmann C, Rohde E, Schallmoser K, Bjelic-Radisic V, Lanzer G, Linkesch W, Strunk D.

Regen Med. 2007 Jul;2(4):371-82.

13 Appendix II

Humanized large-scale expanded endothelial colony-forming cells function in vitro and in vivo.

Reinisch A, Hofmann NA, Obenauf AC, Kashofer K, Rohde E, Schallmoser K, Flicker K, Lanzer G, Linkesch W, Speicher MR, Strunk D.

Blood. 2009 Jun 25;113(26):6716-25. Epub 2009 Mar 25.

14 Appendix III

Isolation and animal serum free expansion of human umbilical cord derived mesenchymal stromal cells (MSCs) and endothelial colony forming progenitor cells (ECFCs).

Reinisch A, Strunk D.

J Vis Exp. 2009 Oct 8;(32). pii: 1525. doi: 10.3791/1525.

15 Appendix IV

Immune cells mimic the morphology of endothelial progenitor colonies in vitro.
Rohde E, Bartmann C, Schallmoser K**, Reinisch A**, Lanzer G, Linkesch W, Guelly C, Strunk D.
Stem Cells. 2007 Jul;25(7):1746-52. Epub 2007 Mar 29.

Human platelet lysate can replace fetal bovine serum for clinical-scale expansion of functional mesenchymal stromal cells.
Schallmoser K, Bartmann C, Rohde E, **Reinisch A**, Kashofer K, Stadelmeyer E, Drexler C, Lanzer G, Linkesch W, Strunk D.
Transfusion. 2007 Aug;47(8):1436-46.

Rapid large-scale expansion of functional mesenchymal stem cells from unmanipulated bone marrow without animal serum.
Schallmoser K, Rohde E, **Reinisch A**, Bartmann C, Thaler D, Drexler C, Obenauf AC, Lanzer G, Linkesch W, Strunk D.
Tissue Eng Part C Methods. 2008 Sep;14(3):185-96.

Isolation and large scale expansion of adult human endothelial colony forming progenitor cells.
Hofmann NA, **Reinisch A**, Strunk D.
J Vis Exp. 2009 Oct 28;(32). pii: 1524. doi: 10.3791/1524.

Platelet-derived growth factors for GMP-compliant propagation of mesenchymal stromal cells.
Schallmoser K, Rohde E, Bartmann C, Obenauf AC, **Reinisch A**, Strunk D.
Biomed Mater Eng. 2009;19(4-5):271-6.

Replicative senescence-associated gene expression changes in mesenchymal stromal cells are similar under different culture conditions.
Schallmoser K, Bartmann C, Rohde E, Bork S, Guelly C, Obenauf AC, **Reinisch A**, Horn P, Ho AD, Strunk D, Wagner W.
Haematologica. 2010 Jan 6. [Epub ahead of print]